AN EMPIRICAL STUDY OF THE DRAG FORCE AND THE POWER CONSUMPTION FOR THE VORTEX RING GENERATOR IN AQUEOUS $CaCO_3$ SLURRY

By:

ALEKSANDAR KOJOVIC, B.ENG.

A Thesis
Submitted to the School of Graduate Studies
in Partial Fulfillment of the Requirements
for the Degree
Master of Engineering

McMaster University

November, 1999.

MASTER OF ENGINEERING (1999) McMaster University

(Mechanical Engineering) Hamilton, Ontario

TITLE: An Empirical Study of the Drag Force and the Power Consumption for the Vortex Ring Generator in Aqueous $CaCO_3$ Slurry

AUTHOR: Aleksandar Kojovic, B.Eng.

SUPERVISOR: Dr. Brian Latto

NUMBER OF PAGES: xviii, 112

ABSTRACT

The objective of this research was to investigate the affects of various generator plate size, D/d ratio, stroke frequency and slurry concentration, for a plate type vortex ring mixer, on the drag force and power consumption. In this case $CaCO_3$ aqueous slurry was used for the investigation.

The generator plate was driven using an AC induction motor with gear type speed reducer which was controlled using a frequency inverter and a mechanism for converting rotational into translational motion. This drive system resulted in sinusoidal motion of the generator plate.

The applied force, the displacement of the generator plate and the input power were measured using measurement cell developed for this purpose. The viscosity was also measured. The data were analyzed, organized and presented using appropriate graphs.

The force measurement data showed that drag force was mainly affected by the size of generator plate and its oscillating frequency. Larger generator plates had greater drag force acting on them and, therefore, required more power for running. Oscillating frequency had similar effect on drag force and power consumption. However, tested $CaCO_3$ slurry concentrations showed to have no significant affect on these two parameters.

Drag force results obtained during this study are considered to be reasonably representative, while power consumption data, although representative for this system, will probably be different for different drive systems employed.

ACKNOWLEDGMENTS

I would like to thank Dr. B. Latto for giving me the opportunity to work on this project and for all the assistance that I received throughout this study.

Special thanks goes to the technicians in the Department of Mechanical Engineering: J. Verhaeghe, D. Schick, R. Lodewyks and Y. Kitamura from machine shop for preparing and assisting in building equipment required for this research. I would also like to thank M. Behr for help in laboratory.

The research was supported by a grant from NSERC to whom grateful acknowledgment is made.

Finally, I would like to thank my wife Milica and sons Lazar and Stefan for the support, care and patience.

TABLE OF CONTENTS

LIST OF FIGURES

LIST OF GRAPHS

LIST OF TABLES

NOMENCLATURE

A- Area of the generator plate

C_D- Drag coefficient

D- Outside diameter of generating plate

Dvr- Diameter of the fully formed vortex ring

d- Inside diameter of generating plate (orifice)

Fd- Drag force

Fr- Froude number

f- Oscillating frequency of the generator plate

G_1, G_2- Geometrical ratios

g- Gravitational acceleration

h- Displacement of the vortex ring

K- Consistency index of power law

Kp- Coefficient of the impeller geometry

k_s- Shear Rate constant

Le- Length of the cylindrical volume of fluid during vortex ring formation

m_T- Mass of a slurry in a sample volume

N- Impeller speed

N_P- Dimensioneless power number

P- Power

Δp- Pressure across an impeller

r- Radius

R- Core radius of vortex ring

Re- Reynolds number

s- Stroke length

Tp- Injection period

Ts- Surface shear stress

U, Uv- Traverse velocity of the vortex ring

u- x component of fluid velocity

Vj- Theoretical jet velocity

Vin(it)- Injection velocity history

Vr- Translational velocity of the vortex ring

V_T- Sample volume

V*- Average injection velocity

v- Velocity of the generator plate

v_j- Mean jet velocity

x- Concentration of water in slurry

y- Concentration of $CaCO_3$ in slurry

Greek Variables

δ- Displacement

ρ- Density

ρ_T- Density of a slurry

μ- Viscosity

μ_a- Apparent viscosity

μ'- Plastic viscosity

α- Entrainment rate, dR/dX

Γ- Circulation = $\int$ Uds

γ- Shear rate

τ- Shear stress

τ_o- Yield stress

ξ- Le/d ratio

CHAPTER 1

INTRODUCTION

The mixing and agitation of liquids and slurries is one of the most common industrial processes and in particularly municipal waste water treatment. It eliminates discontinuities or gradients of physical or chemical properties in a mass of liquid by the circulation and transfer of material from one location to another within the mass of the liquid.

Three factors which determine the efficiency of any particular method of mixing are: the mixing time, power consumption and the homogeneity of the liquid or slurry being agitated. Numerous methods for mixing and agitation of fluids have been developed, from standard rotating or oscillating impellers to the oscillation of perforated plates, static mixers and many complex agitator configurations.

The majority of mixers used in industry are rotary mixers and while these have proven useful, they are often relatively inefficient and limited in their use and control. Some rotary mixers require strong shafts which must be dynamically balanced and have massive structure. Rotary mixers are often not able to create

complete homogeneous mixing of the fluid being agitated and may easily create solid body rotation of the fluid. Virtually all rotary mixers require vessel baffles to avoid liquid solid body rotation or surface free vortices. Ahmad et al. (1985) discussed the problem associated with the mixing of stratified liquids using rotating marine type propeller mixers. The majority of these type of rotary mixers are very poor for mixing of stratified fluids and sedimentary materials. If the impeller is located near the liquid surface a free vortex may be created which usually results in the ingestion of air and generation of surface foam, while if the impeller is located much deeper in the liquid the mixing can be poor due to the relatively poor fluid convection.

A primary objective of mixing is the agitation and mixing of liquids or solid suspensions efficiently to create a homogeneous distribution of the fluid with minimal energy consumption and mixing time, using the simplest of equipment. Furthermore, there is a primary interest by industries in easy maintenance, low maintenance costs, and low capital costs.

An innovative method of mixing liquids has been developed by Brian Latto[1] which appears to avoid many of the application and operation problems associated with conventional mixers, while being very energy conservative with low mixing times. This mixer involves the propagation of vortex rings to create mass transfer and circulation in a fluid media.

---

[1] Department of Mechanical Engineering at McMaster University and MIXIS Corporation Dundas Ontario Canada

A vortex ring is a toroidal ring of rotating fluid which has an overall oblate spheroidal shape. The internal structure of a vortex ring can be laminar or turbulent depending on the generation conditions and the elapsed time. However, it may be questioned as to whether vortex ring is ever truly turbulent. A vortex ring is one of the most interesting phenomena in fluid dynamics. Several properties of vortex rings are quite remarkable. Of particular interest from a practical point of view is that they are capable of transporting a parcel of fluid a considerable distance through an ambient fluid with only slight decrease in their translational velocities. This is primarily due to the fact that the fluid within the vortex ring is rotating such that at its periphery the velocity of the fluid inside relative to the velocity of the fluid outside of the ring approaches zero. Hence, the shear rate at the periphery of the vortex ring is very low and in essence the vortex ring basically rolls through an ambient fluid. Since the viscous shear is a function of the product of the fluid viscosity and the shear rate, and the shear rate is very low, the viscous drag is therefore very low, i.e. $\tau = \mu(du/dr)$, and therefore if $du/dr \rightarrow 0$ then $\tau \rightarrow 0$. As a consequence of this the fluid viscosity has very little effect on the viscous drag for laminar vortex ring. Another remarkable feature of vortex rings is that they are directionally stable and normally travel in relatively straight lines, although their trajectories can be affected by adjacent vortex rings and solid boundaries under certain conditions.

Latto (1987, 1989, 1992) has developed two novel forms of vortex ring mixers (VRM's), which he has patented. These are: an oscillating orifice plate

mixer and a tube (chimney) type mixer. These units are being used in industrial sites in Canada and the USA.

A very large number of quantitative and qualitative experiments, and numerical studies using finite difference analysis of the flow equation have been done over a twenty year period. Latto's studies indicate quite clearly that eventhough vortex ring mixers are a novel approach to the mixing of fluids, are a very effective and efficient for a very wide range of mixing applications. These VRM's are often capable of being used in processes that current rotary mixers fail to fulfill.

Although there has been a great deal of research and publications on vortex rings, the majority of the work has been done on fundamental aspects of vortex rings. Obviously the prior studies are useful in the analysis of the behavior of individual vortex rings, but they are not really very useful for analyzing or designing practical mixing systems which employ the continuous generation of vortex rings. Latto has devoted a great deal of time and effort to the study of VRM's and has made considerable progress in this area of interest. However, it is also apparent that in order to maximize the efficiency and use of these novel mixers/agitators more research has to be done on various aspects of the mixers.

The experiments described in this thesis were intended to investigate effects of different disc diameter D, disk orifice diameter d, (D/d) ratio, slurry concentrations, and oscillating frequencies of an impeller plate on the force in

the drive shaft, and thereby the drag coefficient and the power consumption. The data were analyzed in order to determine how combination of parameters affects the force, the drag coefficient and the power consumption.

CHAPTER 2

LITERATURE REVIEW

2.1 VORTEX RINGS

Vortex rings have been the subject of much attention in the last century, which has resulted in numerous publications. The first reported investigations were mainly on flow visualization or theoretical ideal flow (inviscid) models. Later a mathematical model referred to as "Hill's Spherical Vortex" (1894) was developed. This model assumed that an inviscid fluid occupies a spherical fluidic envelope. Later, a model was developed by Lamb (1933), whose premise was that the primary vorticity is contained in a torus whose core is smaller than that of the circumscribing torus. More recently, the research has been more specialized, such as the stages of vortex ring development; boundary conditions or energetics, as well as the properties of vortex rings under varying conditions by Irdmusa and Garris (1984, 1987); impact of vortex rings on a wall Walker (1987) , vortex rings traversing a fluid with a step change in density Linden (1973) and Hecht (1987) ; and fluid mixing using vortex rings Baird (1979, 1992) and Latto (1987, 1989, 1990, 1992, 1994).

2.2 FORMATION OF VORTEX RINGS

At the most basic level, vortex rings consist of a moving mass of fluid rotating about toroidal axis. The formation of a vortex ring is the most important stage for generation of a vortex ring for vortex ring mixing and was investigated in a numerical study by Stapleton (1995) and empirical study by Perrons (1995). A sketch of a vortex ring being generated through an orifice plate is shown in Figure 2.2.1. The diagram indicates that fluid is ejected, through an orifice of diameter d with outside plate diameter D. The fluid motion can be either created by the motion of the orifice plate moved through a defined stroke length s, for defined duration (T_p) with a mean jet velocity (v_j) or by ejecting a quantity of fluid through the orifice. During this period of time a certain volume of fluid is forced through the orifice. The fluid that comes adjacent to the inner edge of the orifice is retarded causing it to curl over the upper surface. This causes a low pressure region directly above the plate area and a higher pressure region in the volume of displaced fluid. The higher pressure displaced fluid curls over to "fill" the low pressure region which creates vorticity. At the end of the stroke, this process stops and fluid with high vorticity is trapped by the fluid at the centre of the orifice. The resulting self-encapsulated toroidal (donut-shaped) volume of fluid creates a circumscribing volume of rotating fluid which propagates through the fluid as a fully formed vortex ring (Figure 2.2.2).

The important parameters of fully formed vortex rings are the diameter D_{vr}, circulation Γ and its translational velocity V_r, which were considered by

Irdmusa and Garris (1987). It is generally agreed that vortex ring properties depend on mainly (a) the type of generator and its geometric configuration; (b) initial conditions: the stroke s and the fluid injection velocity-history Vin(t).

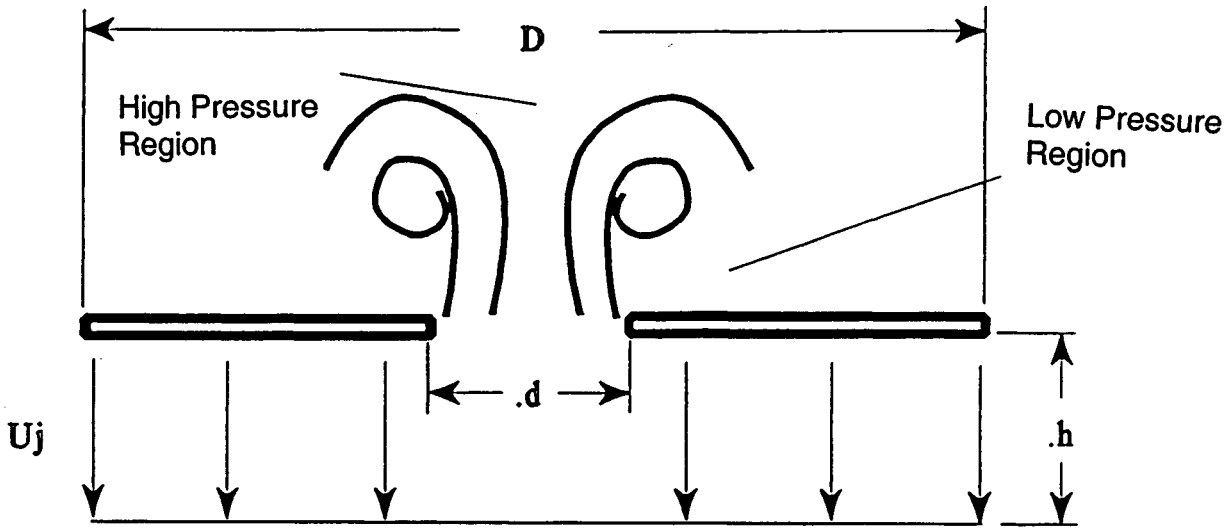

Figure 2.2.1. Vortex Ring Formation

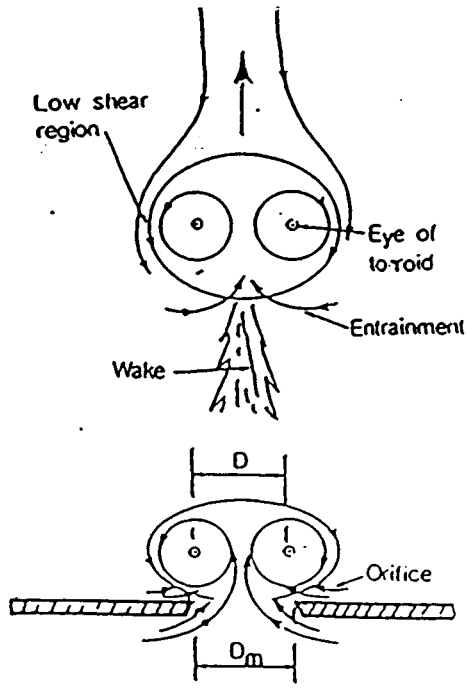

Figure 2.2.2. Generation of a Vortex Ring Through an Orifice (Latto 1987)

Some of these parameters can be combined into a Reynolds number for identifying generation and flow conditions. However, no satisfactory theory quantitatively relates specific parameters to generation conditions for a vortex ring. Many studies have been directed at this problem, some of the more pertinent are cited here.

Maxworthy (1977) obtained the following results for vortex rings: (*i*) formation is strongly Reynolds Number dependent, (ii) the amount of vorticity that appears downstream is close to that predicted by a simple slug model, and (iii) a bimodal form of vortex-core instability occurs at moderate Reynolds numbers. Maxworthy found that vortex rings generated using an orifice plate generates a secondary ring that travels in the opposite direction back through the orifice. This is shown in Figure 2.2.3.

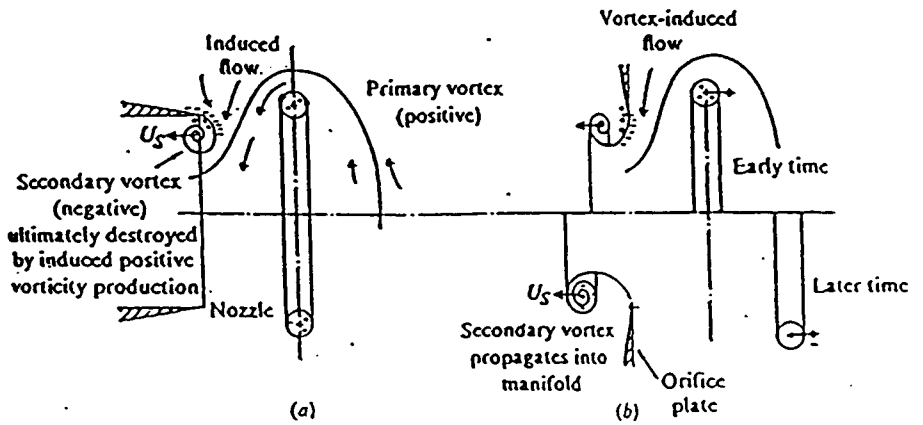

Figure 2.2.3. Rolling up process for tube-generator (a) and orifice generator (b) Maxworthy (1977)

To obtain more detailed information on fluid velocity near the exit of vortex ring generator orifice, Didden (1979) used laser Doppler anemometry to measure the unsteady velocity field in a nozzle-exit plane during the roll-up process shown in Figure 2.2.4. His study revealed that the diameter of the formed vortex ring and circulation near a vortex ring generator nozzle wall depend on the parameter ξ=Le/d and are independent of the average injection velocity V* for certain Reynolds number range.

Further work showed that the ξ parameter is indeed important in vortex ring formation. Baird et al (1979) suggested that for the most efficient generation of laminar vortex rings the ξ should be $0.7<\xi<2.8$. More recently Latto (1987) recommended this range should be $0.5<\xi<3.5$ with an optimal value of 2.8. However, more recent experiments by Latto have indicated that the optimal value may be a function of the generator plate motion.

Wang (1999) studied various aspects of vortex ring propagation using a commercial CFD program FLUENT. She found that the velocity of a vortex ring is directly proportional to the injection velocity and it can be correlated with a specific Le/d ratio. Using the software three different injection profiles were investigated, namely sinusoidal, trapezoidal and rectangular. Although all three input profiles had the same average velocity Wang found that both triangular and sinusoidal profiles appeared to give a higher vortex ring axial traveling velocity than the rectangular profile.

As previously mentioned, the characteristics of a vortex ring depend strongly on geometric boundary conditions. Vorticity is an essential element in the formation of vortex rings, and since it is generated in the boundary layer, various geometries produce different amounts of vorticity. Two common geometries of vortex ring generation are shown in Figure 2.2.5. A comparison of results from the two geometries was completed by Irdmusa and Garris (1987) and are shown in Figure 2.2.6. These experiments showed that tube-generated vortex rings tend to have a slower translational velocity and larger volume than orifice generated vortices. Irdmusa and Garris also pointed out that vortex rings with minimal amounts of kinetic energy of rotation can be generated by proper attention to boundary conditions and by using pulses of very short duration.

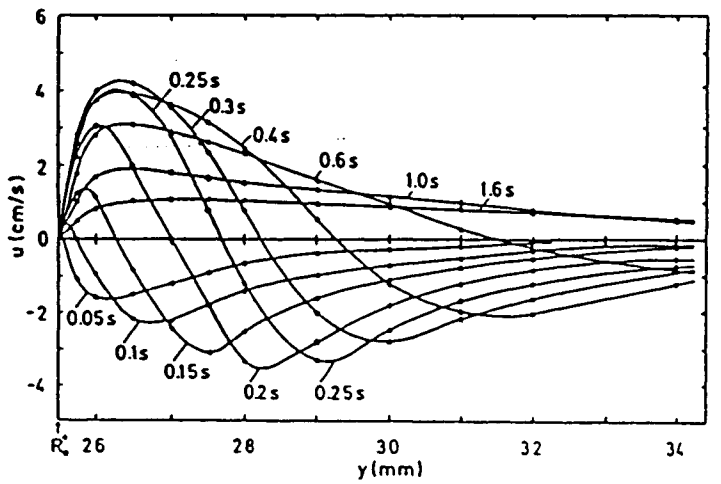

Figure 2.2.4. Axial Velocity u versus radial distance y in the nozzle-exit plane x=0. U_0=4.6 cms^{-1}, R_0^*=25.5 mm: outer nozzle wall (Didden 1979)

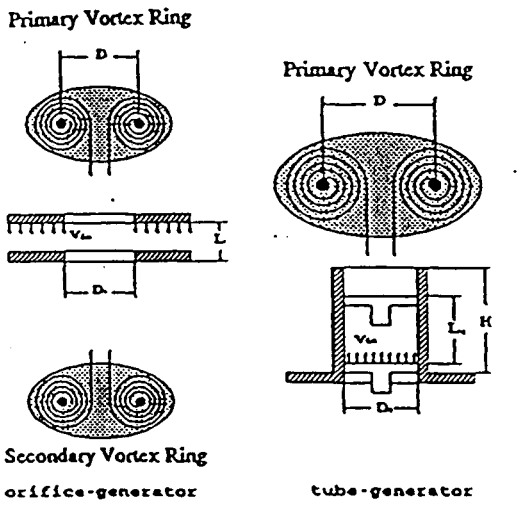

Figure 2.2.5. Two Types of Vortex Ring Generator (Latto 1987)

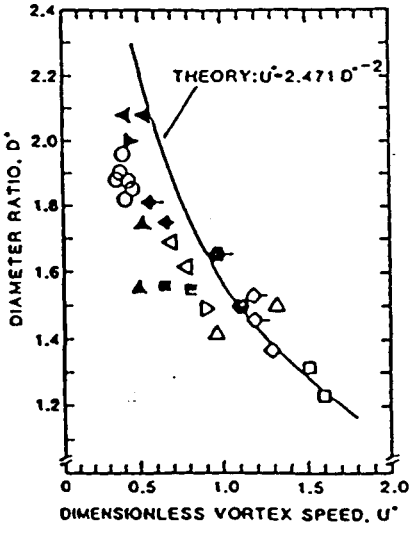

Figure 2.2.6. Ratio of Vortex Diameter to Exit Diameter vs. Dimensionless Vortex Speed U*. Filled - chimneys, unfilled - orifices. (Irdmusa and Garris)

Finally, another critical effect on formation and development of vortex rings is the injection velocity history Vin(t). Didden (1977) considered various injection velocity conditions. Figure 2.2.7 shows his results, which illustrate that

any departure from constant-velocity program increases the circulation of a vortex ring, even when using identical average injection velocity V*.

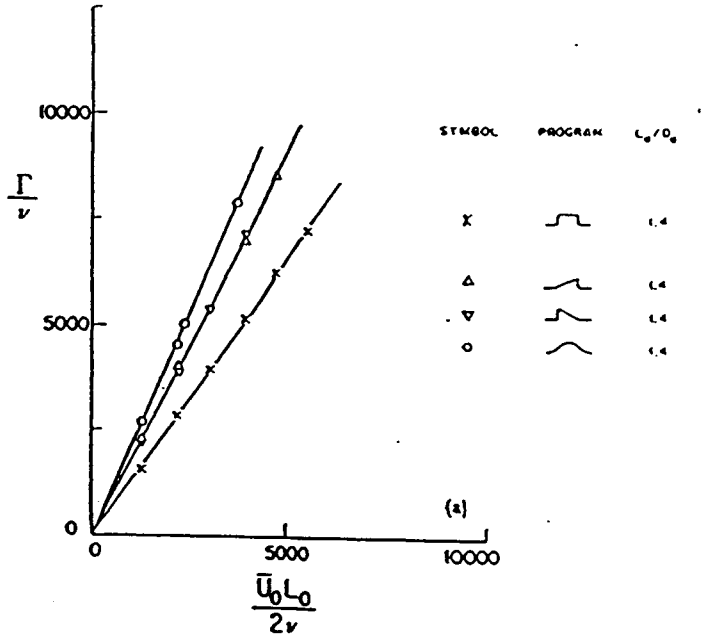

Figure 2.2.7. Circulation for the laminar vortex rings produced with various injection velocity programs (Glezer)

2.3. PROPAGATION OF VORTEX RINGS

In general, vortex rings travel in the direction of the axis of its toroidal geometry. When full stroke is achieved and the volume of fluid is ejected through an orifice, it is said that vortex ring is fully formed. Once it reaches this phase it is considered as part of the laminar propagation stage. Characteristics of a vortex ring include low energy dissipation during travel and relatively low fluid exchange between itself and the fluid through which it is moving. This is particularly the case when the vortex ring is laminar.

Basically, one underlying assumption has been used in vortex rings theory and experimentation in recent history: a vortex ring is considered to have

negligible shear/viscous effects from the ambient fluid acting on it. It is quite difficult to make quantitative empirical measurements and consequently no such data appear to have been published. For instance, the type of sensor to use would play a key role in results, but what is more important, the orientation of this sensing equipment would be paramount. The reason for this being, the periphery of the vortex ring, being the ideal sensor placement, cannot be predicted with sufficient accuracy. Therefore, it is necessary to justify this assumption of negligible shear indirectly.

Firstly, the physical nature of a laminar vortex ring causes it to be unaffected by shear. This is because the internal rotation of the fluid in a ring is basically solid body rotation and has relative velocity that is almost zero at its outer surface. This can be visualized as equivalent to a tire rolling along a surface as opposed to a non-rotating tire sliding over a surface. Since the viscous shear at the outer surface is given by $\tau=\mu\gamma$, where τ is the surface shear stress, μ is the viscosity of the fluid and γ is the shear rate, du/dr is the radial velocity gradient. Consequently, if the relative velocity approaches zero, τ approaches zero and is basically independent of μ. This is very important since once a vortex ring is generated the transport of a laminar vortex ring is relatively insensitive to the viscosity of the fluid involved.

Secondly, Irdmusa and Garris (1987) using the conservation of linear momentum principle, which supposes the insignificance of drag forces on a

vortex ring basically justified by flow of the external fluid about the vortex ring, derived the relationship:

$$U^*=2.4711D^{-2} \tag{2.3.1}$$

where

$$U^* = \frac{U}{\Gamma/D} = \frac{\text{Translational Speed}}{\text{Rotational Speed}} = \text{dimensionless speed} \tag{2.3.2}$$

and

$$D^* = \frac{D_v}{D_e} = \frac{\text{Vortex Diameter}}{\text{Exit Diameter}} = \text{diameter ratio} \tag{2.3.3}$$

Figure 2.3.1 shows the ratio of translational kinetic enegy of the vortex to the initial kinetic energy of the jet vs. U*.

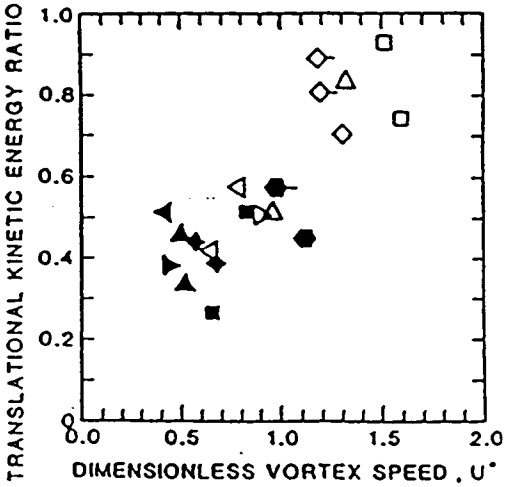

Figure 2.3.1. Ratio of translational kinetic energy of a vortex to the initial kinetic energy of the pulse vs. dimensionless vortex speed U*. (Filled - chimneys, unfilled - orifices). (Irdmusa and Garris)

Their experiment suggests that the chimney generated vortex ring has proportionally more kinetic energy of rotation then one generated on the orifice plate. This observation is consistent with physical interpretation of equation 2.3.2.

Continuing with a similar type of argument Papple and Latto (1991) using numerical simulation, found that traversing motion of a laminar vortex ring in non-Newtonian fluids is basically the same as those for a laminar vortex ring in Newtonian fluids. Later Hua (1994) obtained similar results using an improved form of the Papple et al numerical simulation model for non-Newtonian power law fluids. In these simulations, vortex rings were generated in shear thinning and shear thickening fluids and compared with those for Newtonian fluids. The vortex rings were observed to travel the same distance for a given time irrespective of the type of fluid considered. Therefore, the same vortex ring velocities were observed with different shear conditions.

2.4 POWER CONSUMPTION

The power consumption or preferably the power density is a very important mixing parameter. For rotary mixers, measurements can be made of shaft torque using conventional torque transducers although, with small mixing equipment, there may be problems, due to the very small values of torque and the relatively high losses in the equipment. Very small scale measurements can be made in modified rotational viscometers. In most cases measurements of

electrical power consumption are not sufficiently closely related to torque to provide an alternative to torque measurements.

Although the characteristic of power consumption is simple, the information is quite valuable. In addition to the obvious value in motor selection, it is perhaps even more useful for gearbox and shaft design for high viscosity mixing equipment, where torques are usually much higher than those encountered with the higher speed impellers used for low viscosity mixing. Power consumption also provides a useful basis for comparison in the evaluation of different mixer designs for mixing rate and efficiency and in some cases the heating of a fluid being mixed.

2.4.1 NEWTONIAN FLUIDS

Because of the complex motion in any mixing process, dimensional analysis is widely used to establish simple relationships between power consumption and the controlling variables. The majority of published research refer to the rotary mixers and for these the dimensionless power number N_P is defined as follows (Harnaby et al.):

$$N_P=P/(\rho N^3D^5) \text{ or } N_P=f[R_e,F_r] \qquad (2.4.1.1)$$

since: $R_e=ND^2\rho/\mu$ and $F_r=N^2D/g$

For laminar mixing conditions the relationship is of the same general form for large and small impellers:

$$N_P=K_pR_e^{-1} \qquad (2.4.1.2)$$

This is identical in form to the well-known relationship for propellers and turbines with K_p being specific to the impeller geometry tested but independent of scale. For small variations in geometry for a particular impeller design, equation 2.4.1.2 can be expanded by including various geometric ratios and exponents:

$$N_P = K_p' R_e^{-1} (G_1)^a (G_2)^b \qquad (2.4.1.3)$$

This form of relationship has been successfully demonstrated and it appears that the values of K_p', a,... are independent of equipment size. It is important to note that: $K_p = K_p'(G_1)^a(G_2)^b$ and therefore K_p and K_p' are not equal.

2.4.2 NON-NEWTONIAN FLUIDS

Metzner and Otto (1957) showed that a simple relationship exist between Newtonian and much non-Newtonian power consumption data in the laminar regime, using their correlation based on calculation of apparent viscosities for rotary mixers. The basis of the method is the assumption that there is an average shear rate for a mixer which describes power consumption and that this shear rate is directly proportional to impeller speed:

$$\gamma = k_s N \qquad (2.4.2.1)$$

where k_s is the mixer shear rate constant. The average shear rate γ defines an apparent viscosity for power prediction for non-Newtonian fluids. The apparent viscosity is determined from viscometric data at the appropriate shear rate and used directly in the usual Newtonian power number vs. Reynolds number

correlation. To test this hypothesis, measurements were made of the power number vs. Reynolds number characteristics of Newtonian and power number vs. impeller speed characteristics for non-Newtonian fluids. For a measured value of power consumption for a non-Newtonian fluid a power number and corresponding Reynolds number were calculated. From the Reynolds number:

$$R_e=ND^2\rho/\mu, \qquad (2.4.2.2)$$

μ can be determined. The shear rate corresponding to this apparent viscosity was found from the apparent viscosity vs. shear rate for a non-Newtonian fluid, see Figure 2.4.2.1. The mixer shear rate constant, k_s can than be determined from the equation 2.4.2.1. The values of k_s, determined by Metzner and Otto were relatively constant for a range of impeller speeds and fluid properties, and an average value could be used in the prediction of non-Newtonian power consumption data.

For power law fluids k_s, may be incorporated into a power number-Reynolds number equation. For a power law fluid:

$$\tau=K(\gamma)^n \qquad (2.4.2.3)$$

and apparent viscosity is: $\mu_a = \tau / \gamma = K(\gamma)^{n-1}$.

If $\gamma=k_sN$, than:

$$\mu_a = K(k_sN)^{n-1} \qquad (2.4.2.4)$$

This value of μ_a may be incorporated in the Reynolds number:

$$R_e=ND^2\rho/\mu_a=N^{2-n}\, D^2\rho/K(k_s)^{n-1} \qquad (2.4.2.5)$$

The power number equation may be rewritten as:

$$N_P = K_p[N^{2-n} D^2\rho/K(k_s)^{n-1}]^{-1} \qquad (2.4.2.6)$$

where the value of K_p is valid for Newtonian and non-Newtonian fluids. It is important to note that the presence of the mixer shear rate constant in the power number equation 2.4.2.6 and correlations which do not include this constant or some equivalent, should be carefully checked before application.

The simple concept of an average mixer shear rate has been widely used in laboratory and industrial work and in most applications it has been assumed that the shear rate constant, k_s, is only a function of impeller type. Research is continuing on a possible influence of flow behavior index and elastic properties and also on procedures necessary to describe power consumption for dilatant fluids. It should be noted that in all aspects of power prediction and data analysis, power law models should only be used with caution.

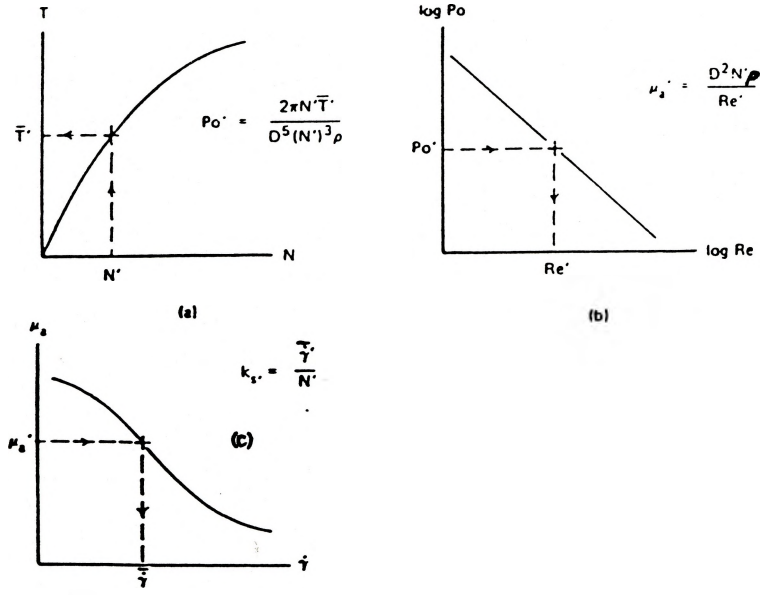

Figure 2.4.2.1. Determination of shear rate constant k_s from experimental data. (a) Non-Newtonian power consumption; (b) Newtonian power consumption; (c) Non-Newtonian (riscometry). (Metzner and Otto)

2.5 DRAG COEFFICIENT

Drag may be due to surface viscous shear (skin-friction) drag, pressure or profile drag, gravity effects (wave drag), or compressibility effects (high-speed flow). In any case, a dimensional analysis will indicate that drag coefficient is a function of the Reynolds number, the Froude number, or the Mach number. For dynamically similar flow, the appropriate one of these numbers will be the same for model and prototype, and thus the drag coefficient will also be the same for both. This may be expressed as:

$$C_D = \frac{F_d}{(\rho V^2 / 2)A} \qquad (2.5.1)$$

Maxworthy (1974) presented a special feature of turbulent vortex rings that makes them very desirable for mixing processes. Turbulent vortex rings have a low drag coefficient and are able to travel much longer distances than turbulent eddies. In his paper, he described the growth of a ring by an entrainment coefficient and the loss of linear momentum by a drag force acting on the ring. By equating these two quantities and eliminating the dependence on time, Maxworthy obtained the following relationships;

$$R = \alpha x + 1 \qquad (2.5.2)$$

and

$$U = \{ \alpha x + 1 \}^{-(Cd+3)} \qquad (2.5.3)$$

From the measurements of the core radius of the ring and the distance traveled or displacement of the ring x, the entrainment rate of the ring α, can be determined. The drag coefficient Cd can be evaluating by substituting the entrainment rate into the velocity equation. Maxworthy (1974) found that for a turbulent vortex ring with the same cross sectional area as a solid sphere, the drag coefficient for the ring was 0.04 as compared with 0.23 for the sphere.

With a thin core of highly concentrated vorticity and a relatively low drag coefficient, turbulent vortex rings are able to travel much longer distances than other types of turbulent eddies.

CHAPTER 3

EQUIPMENT DESIGN

3.1. INTRODUCTION

When designing the equipment for a mixing system a number of things require special attention and represent constraints for a designer. An important aspect is the manufacturing cost. The mixers patented by Latto are very simple yet ingenious in their simplicity. An orifice plate generator is easy to manufacture and generally not expensive. The mixer is easy to assemble. The generator plate is connected to the drive system by one central drive or several peripheral drive rods. Furthermore, unlike rotary mixers a VRM does not require dynamic balancing.

Another important aspect of mixing system components must be interchangeable with readily available or inexpensive parts. The system must be designed in a way that it is compatible with other different systems, simple to use and to transport. In the past, an important problem with the actuation systems was that they were not very durable. Various problems occurred when running

the systems for a prolonged period of time and bearing and seal failure were not uncommon.

The operation of the system is easily understood, so it requires a minimum amount of operational training. The equipment is expected to be used in both large and medium scale mixing systems.

3.2. MECHANICAL DRIVE

The first decision to make in the design of a VRM mixing system is what mechanical drive is to be used. Several of the more obvious basic linear drive systems are briefly discussed below.

1) Hydraulic systems

Hydraulic systems can provide the necessary power transfer required for vortex ring agitation. Some of the advantages of the system are that depending on the actual fluid used, heat dissipation is very good, there is very little deterioration of the seals and the hydraulic fluids are usually fire and contamination resistant. However, they have a few major drawbacks. The major shortfall is in attaining the required dynamics characteristics. This cannot be accomplished without an extremely elaborate and expensive hydraulic system. Also, due to the need to move the fluid through the various components, energy losses can be large. Furthermore, care is needed for storage and handling of the

working fluid, a separate pumping system to meet the demands, and the system components are not easily interchangeable. If the system is not properly sealed, the leaks can be expensive in terms of spillage and clean up costs. In general, hydraulic systems are characteristically heavy and usually require expensive components to withstand the forces and avoid friction losses in the pistons.

2) DC Motor

A DC drive motor unit could be used and was used in laboratory experimental vortex ring mixing systems. Any rotary drive system requires some type of mechanism to convert the sinusoidal motion into linear motion. Since this type of mechanism would be common for any rotary electrical motor drive it will be discussed later.

The biggest advantage of the system is the ease at which speed and torque can be varied and they can also be easily controlled using a computer or a simple electronic circuit. However, these motors can be expensive and relatively large for the application of fluid agitation. A cam/follower mechanism can have numerous problems associated with them. The biggest disadvantage of this mechanism is sinusoidal motion. However compared with hydraulic systems this type of linear mechanical drive is inexpensive.

3) Stepper Motor

These unique motors are a relatively new method of actuation being used in industrial applications. The name of the device describes its principal functions. "Motor" means that electrical input energy is converted to mechanical output energy, and "stepper" means that energy conversion process is performed in discrete steps. This type of motor can be easily adapted to open loop computer control. Another advantage is that the motor can be stalled without damage. Maximum pulse excitation are more than 1000 pulses per second which allows it to simulate continuous movement. Stepper motors are also bi-directional. Unfortunately they have major drawbacks: they are not very efficient, friction loads tend to increase their error, they cannot handle very large inertia loads, and are quite expensive thus rendering these motors infeasible.

4) Pneumatics

Referring to the basic requirements of the system, which are cost and versatility, a pneumatic drive system is an effective solution for this type of agitator. Air is often readily available. The majority of the components needed for such a system are also readily available. Pneumatic systems are very versatile and interchangeable. Leakage of fluid is not a problem and capital costs are relatively low. Power consumption is much lower than that for hydraulics systems but considerably higher than for electrical drive systems. However, they have

durability problems of relatively quick deterioration of seals and piston rings and compressed air is relatively costly.

5) Induction Motor Drives

Induction motors have many of the advantages and disadvantages of DC motors, but are much less expensive and more readily available than DC motors. Furthermore, they offer more variability in specifications.

An induction motor with a frequency inverter is the most efficient, readily available in industry. It was decided to use an induction motor for this work.

3.3. MECHANISMS

As mentioned before, the drive mechanism is required to convert rotational motion of the drive shaft into a linear motion which in turn is used to generate vortex rings. The motion of the orifice plate is important. The production of a vortex ring is very sensitive to the motion of the orifice plate. If the displacement of the plate is too large, two vortex rings may form per stroke, and the second vortex ring may overtake and destroy the first vortex ring. If the displacement is too small, a vortex ring may not fully form and thus only localized mixing will occur. There are generation criteria for the efficient production of a vortex ring. Depending on the required velocity profile there may be three stages for the generation velocity profile: an initial rapid increase in the velocity of the plate to initiate the formation of the ring; followed by a period of

constant velocity while the vortex ring is gaining energy and finally a rapid drop in velocity to zero to allow the vortex ring to break free of the plate while retaining as much energy as possible.

The following are some possible suitable mechanisms for the required motion of the generator plate to create the desired profile and their advantages and disadvantages.

1) Cam with linear follower movement (Figure 3.3.1)

This mechanism translates rotational motion into linear motion by means of a cam and four bar linkage. As the cam rotates, the follower E moves along straight line path G. It has a gradual forward motion and a quick return motion.

Advantages:

- operates well at both high and low speeds and
- quick return allows vortex ring to break free with more energy.

Disadvantages:

- the motion obtained does not fit the velocity profile required for the most efficient vortex ring generation due to gradual forward movement,
- high wear characteristics on the cam and roller, especially on the return stroke,

- complex mechanism and

- expensive to build and difficult to maintain.

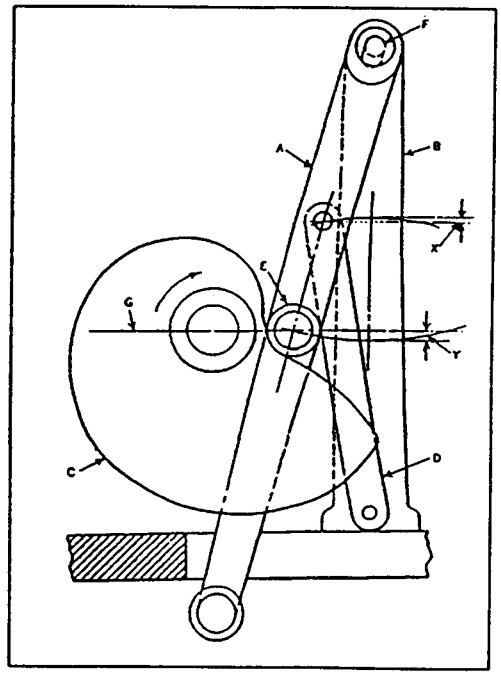

Figure 3.3.1. Cam with linear follower movement (Kamerman et al.)

2) Trigger cam (Figure 3.3.2)

This mechanism uses a cam, linkages and a spring to transform rotational motion into linear motion of a lever arm. While the cam rotates the spring maintains contact between the follower and cam. When the cam reaches point G on the cam there is rapid drop of the linkage. As the cam continues to rotate the linkage moves up slowly relative to downward drop. Linear motion is achieved through lever arm A.

The resulting velocity profile begins as sinusoidal with a period of dwell and a sharp downward return. The slope of the return motion can be changed by changing the spring stiffness.

Advantages:

- simple device to manufacture and
- adjustable dwell time and return velocity.

Disadvantages:

- may be noisy due to the follower leaving the cam during the downward motion,
- the cam and follower are prone to wear and high maintenance cost may result,
- response depends on spring strength compared to inertia forces and hydrodynamic drag on system and
- the motion obtained does not fit the velocity profile required for the most efficient vortex ring generation.

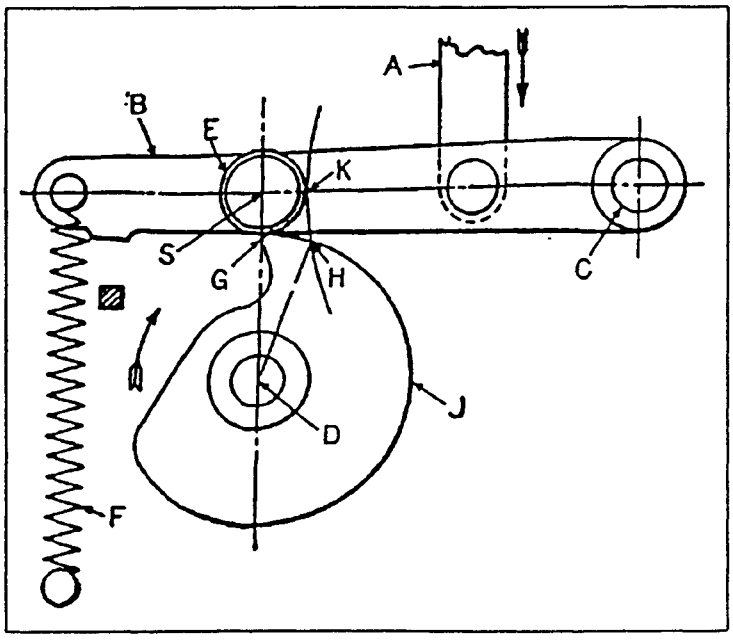

Figure 3.3.2. Trigger Cam (Kamerman et al.)

3) Cylindrical Cam (Figure 3.3.3)

This mechanism is designed to provide the follower with relatively long and powerful stroke. It is designed around a cylindrical cam. The cam A rotates while the follower D causes the linear motion. When the follower reaches section F on the cam it rolls off and the counterweight on cable H returns the follower to its starting position.

Advantages:

- can be operated at various speeds.

Disadvantages:

- expensive to manufacture and maintain,

- complex design with many parts,

- possibility of malfunction with respect to the counterweight mechanism at high speeds and

- the motion obtained does not fit the velocity profile required for the most efficient vortex ring generation.

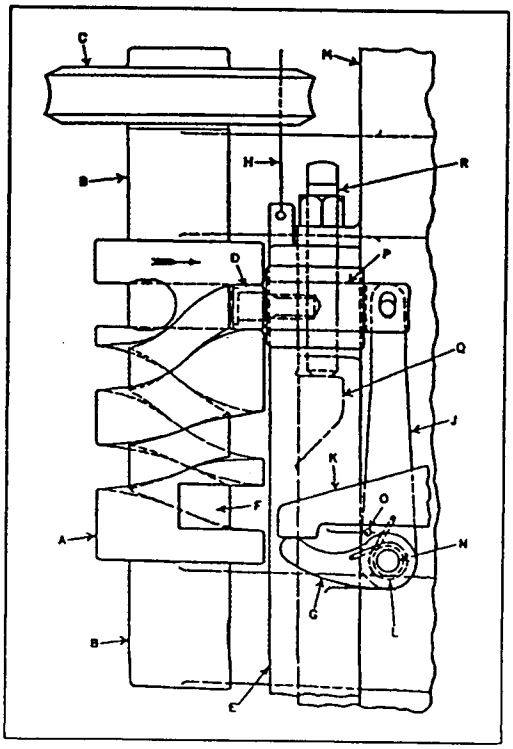

Figure 3.3.3. Cylindrical Cam (Kamerman et al.)

4) The Barrel Cam (Figure 3.3.4)

This device consists of a shaft with a groove cut out in the form of a cam profile. A follower is seated in this groove, and as cam rotates the follower is moved through linear motion.

Advantages:

- relatively inexpensive to manufacture and
- it can be operated at various speeds.

Disadvantages:

- it must have a large diameter due to the fact that the pressure angle must be low in order to decrease wear,
- high inertial forces are created due to weight and size and
- the motion obtained does not fit the velocity profile required for the most efficient vortex ring generation.

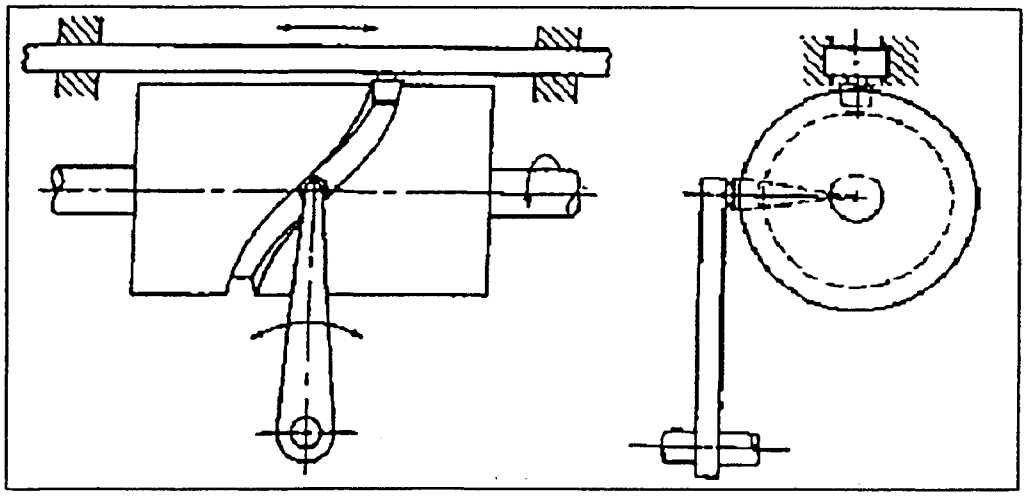

Figure 3.3.4. The Barrel Cam (Kamerman et al.)

5) Single Stroke Toggle Mechanism (Figure 3.3.5)

The follower of the cam is directly connected to the first link of the device. This link is then in turn connected to two other linkages as shown in Figure 3.3.5. The cyclical motion of the cam follower causes linkage to move up and down creating a displacement at the end of the slider linkage. This displacement has one cycle every time the cam makes one rotation.

Advantages:

- simple to construct and easy to maintain and
- ideal when utilizing its powerful squeezing action.

Disadvantages:

- requires large space and
- the conversion from angular to linear motion is not direct so the linear motion may not be suitable for certain types of cams.

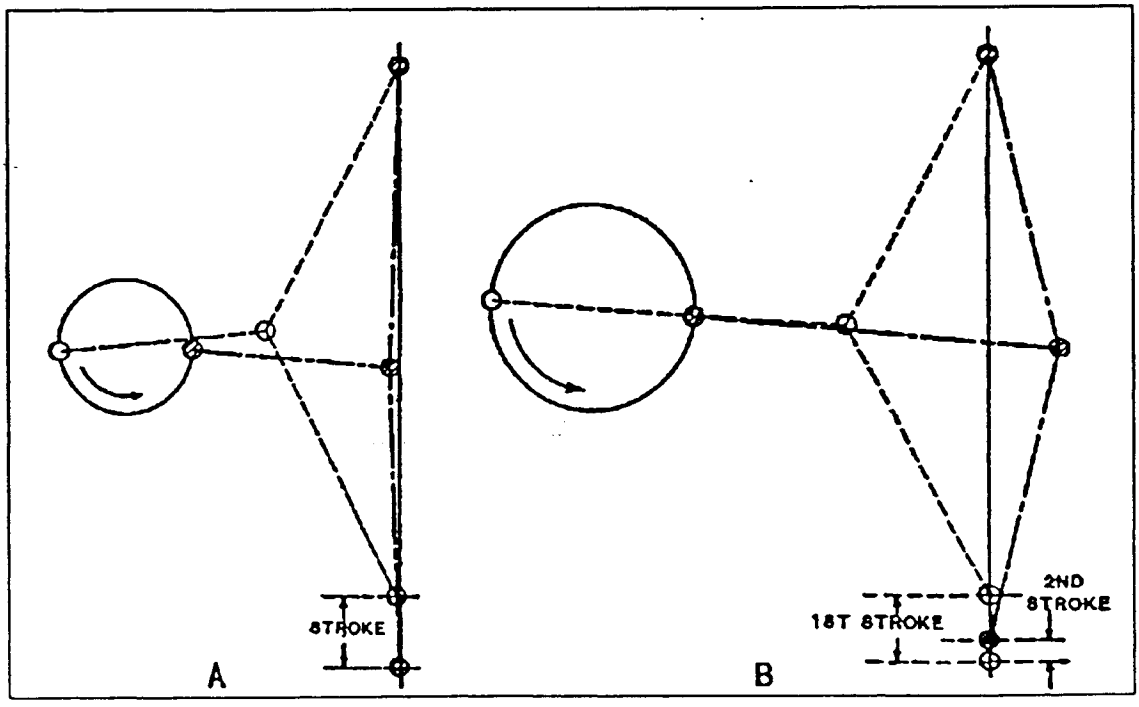

Figure 3.3.5 Single Stroke Toggle Mechanism (Kamerman et al.)

6) Tschudi Cam (Figure 3.3.6)

It consists of a cam profile cut out on a lobe with two followers. These two followers are attached together via a connecting arm. The cam and connecting arm lie off centre of each other. As the cam rotates at constant angular velocity the followers have a variable angular velocity. Therefore, this mechanism translates constant rotational motion into intermittent rotational motion.

Advantages:

- capable of exactly producing the required profile as for the efficient generation of vortex rings,

- easily maintained and

- the cam can be operated at various speeds and has high wear resistance as evidenced by its historical application in rotary engines.

Disadvantages:

- possible patent difficulties and

- requires additional mechanism to produce linear translational motion.

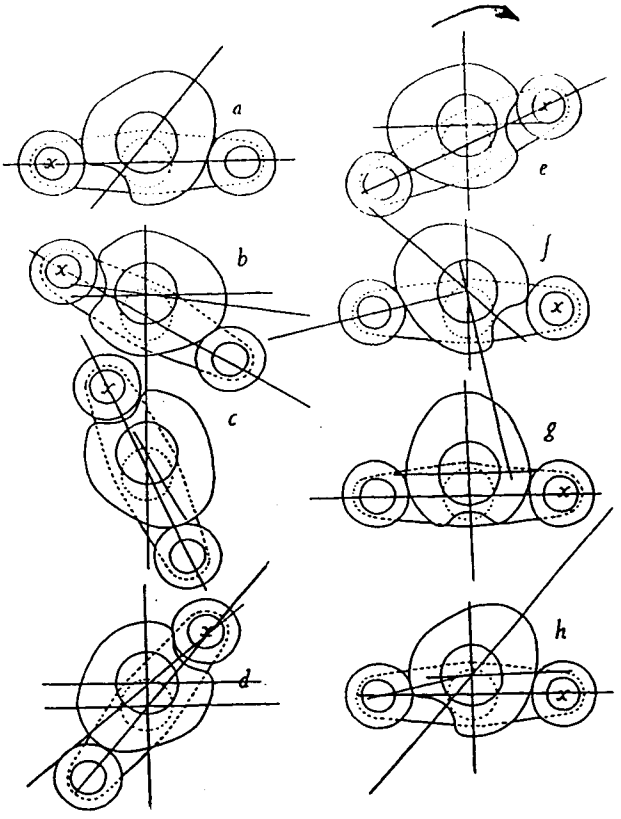

Figure 3.3.6 Tschudi Cam (Series Depicting Motion of the System) (Kamerman et al.)

6) Scotch Yoke (Figure 3.3.7)

The Scotch Yoke mechanism shown in Figure 3.3.7 consists of a fixed frame (1), a disk (2), rotating about a fixed axis on (1), a block (3) pin connected to (2) at point C and a yoke (4) having a slot for pin (3) to slide in. This mechanism gives a reciprocating motion in form of a sinusoidal wave pattern. The continuous elliptical drive, applied between the uniform speed input and Scotch Yoke as shown in Figure 3.3.8, has the effect of reducing the peak of the sinusoidal output so that it gives near to a uniform value for a large section of its cycle.

Advantages:

- easy to manufacture and it is one of the simplest mechanisms for converting rotary motion to translating motion.

Disadvantages:

- excessive wear in the slot
- needs constant lubrication and
- produces a modified sinusoidal motion of the follower.

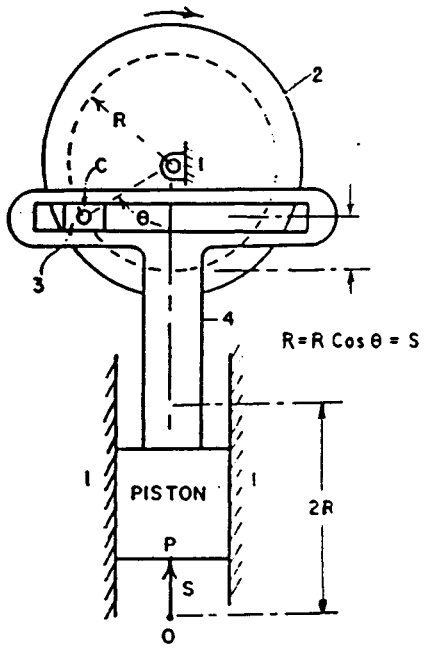

Figure 3.3.7 Scotch Yoke (Jensen)

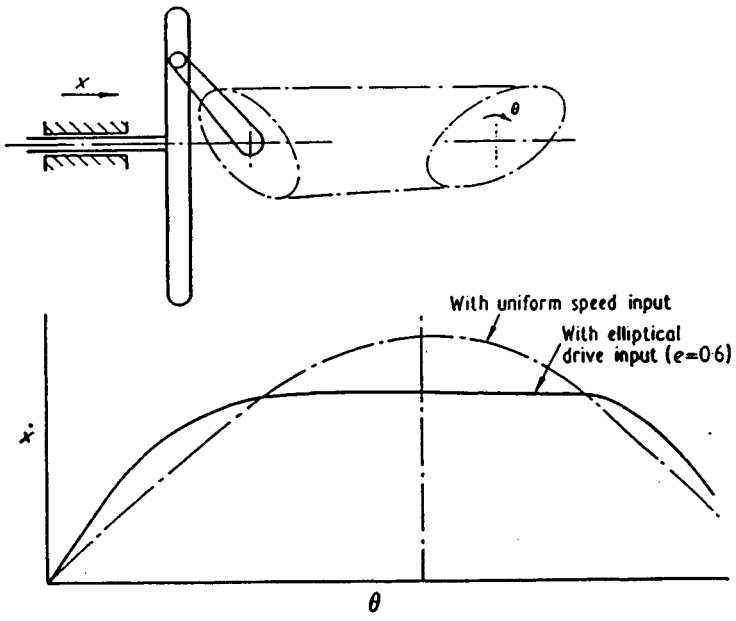

Figure 3.3.8 Effect of the application of the drive to a Scotch Yoke (Peters)

3.4. EQUIPMENT SELECTION

An AC induction motor is currently being used to drive the mixing system. Therefore a mechanism that converts rotational to translational motion is required. The actual VRM's already produced use an AC motor with frequency inverter with disk toggle mechanism. Therefore, it was appropriate to obtain data for this type of drive system. The disk toggle mechanism (Figure 3.4.1) consisted of aluminum disk (1) - (11" (27.94 cm) in diameter) with machined slot (2). The disk was mounted on a reducer output shaft using a coupler (3). A crank lever (4) was positioned in a slot with connecting shaft (5). This design permitted an adjustable stroke, while variable speed was provided by using an AC motor controlled using a frequency inverter.

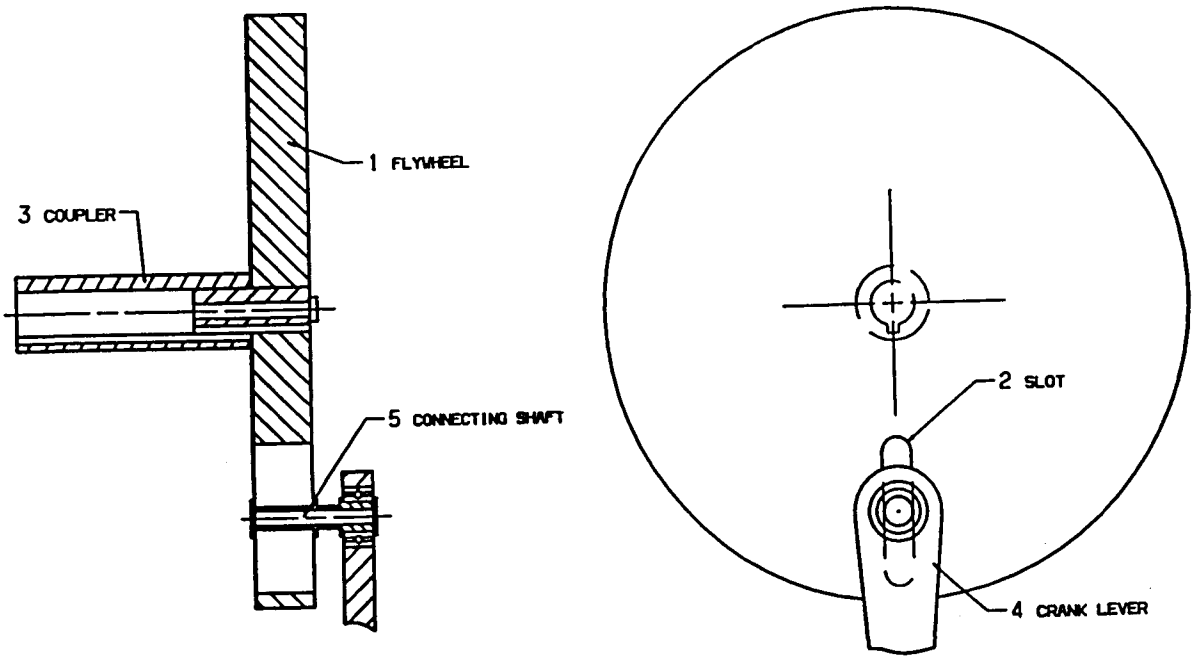

Figure 3.4.1 Disk Toggle Mechanism

3.4.1 Control System

3.4.1.1 AC Drive Motor Operation

The following equation gives the relation between synchronous speed, frequency, and the number of poles:

$$S_s = 120\ f/p$$

where: S_s = synchronous speed (rpm), f = frequency (Hz), p = number of poles.

In three phase induction motors the actual shaft speed differs from the synchronous speed as load is applied. This difference is known as "slip". Slip is commonly expressed as a percentage of synchronous speed. A typical value for the slip is three percent at full load.

The strength of the magnetic field in the gap between the rotor and the stator is proportional to the amplitude of the voltage at given frequency. The output torque capability of the motor is, therefore, a function of the applied voltage amplitude at a given frequency. When operated below base (rated) speed, AC motors are commonly run in a mode known as "constant torque". Constant torque output is obtained by maintaining a constant ratio between voltage amplitude and frequency. Operating at the ratio generally yields optimum torque capability. Operating at lower ratio values lowers torque and power capability. Operating at higher ratio values will cause the motor to overheat.

A typical motor derating curve is shown below.

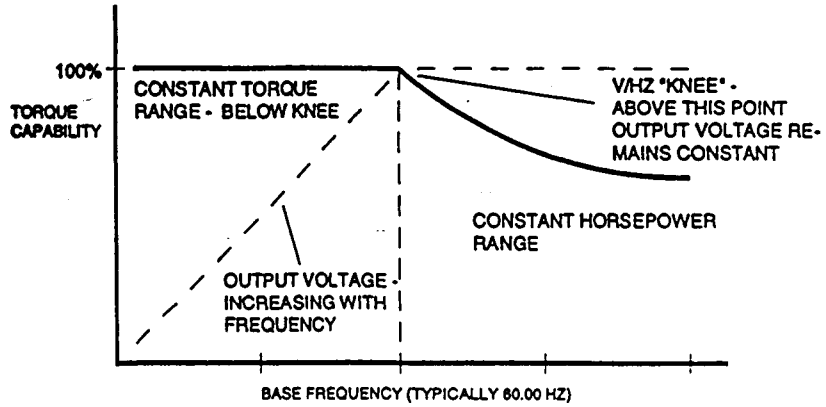

Figure 3.4.1.1.1 AC Motor Operating Ranges

If the applied frequency to the motor is increased while voltage remains constant, the torque capability will decrease as speed increases. This will cause energy capability of the motor to remain approximately constant. Motors are commonly run in this mode when operated above the base speed, where drive output voltage is limited by the input line voltage. This operating range is known as the "constant horsepower" range.

3.4.1.2 Drive Function and Operation Description

A frequency inverter is a 16 bit microprocessor based, keypad programmable, variable speed AC motor drive. There are four major sections: an

input diode bridge and filter, a power board, a control board, and an output intelligent power module.

The supply AC line voltage is converted to a pulsating DC voltage by the input diode bridge. The DC voltage is supplied to the bus filter capacitors through a charge circuit which limits inrush current to the capacitors during power-up. The oscillating DC voltage is filtered by the bus capacitors which reduces the ripple level. The filtered DC voltage enters the inverter section of the drive, composed of six output intelligent insulated gate bi-polar transistors (IGBT's) which make up the three output legs of the drive. Each leg has one intelligent IGBT at a very high frequency (known as the carrier frequency) for varying time intervals, the inverter is able to produce a smooth three phase, sinusoidal current wave which optimizes motor performance.

During these experiments a SQUARE D Adjustable Speed Drive Controller VSD 17 was used. This unit can support motors with fractional output HP rating up to 7.5 HP and 200-575 VAC.

3.4.2 Measurement Cell Design

In order to measure the force, displacement and velocity of the drive shaft a measurement cell was used. The measurement cell is schematically shown in Figure 3.4.2.1. It consists of two plates, top (1) and bottom plate (2), four supporting rods (3), one antirotational rod (4), two linear Thompson bearings (5), a linear displacement transducer (6) and a load cell (7).

The load cell is attached to the drive mechanism shaft (8) and to the impeller drive shaft (9) and measures the force exerted on the shaft by the vortex ring generator. A linear displacement potentiometer gives a measurement of displacement versus time. A flat plate (10) is attached at the bottom of the load cell, and is connected to one side of the linear displacement potentiometer while the other end is held by the top plate (1).

The mechanism (3 - Figure 3.5.1.) drives the shaft through the linear bearing, which in turn drives the vortex ring generator plate or impeller. The transducers transmit analog signals to the 2805 A/D Data translation board that converts analog signal to digital for the 486DX66 processor. A data acquisition system, LabTech Notebook software is then used to present resulting data.

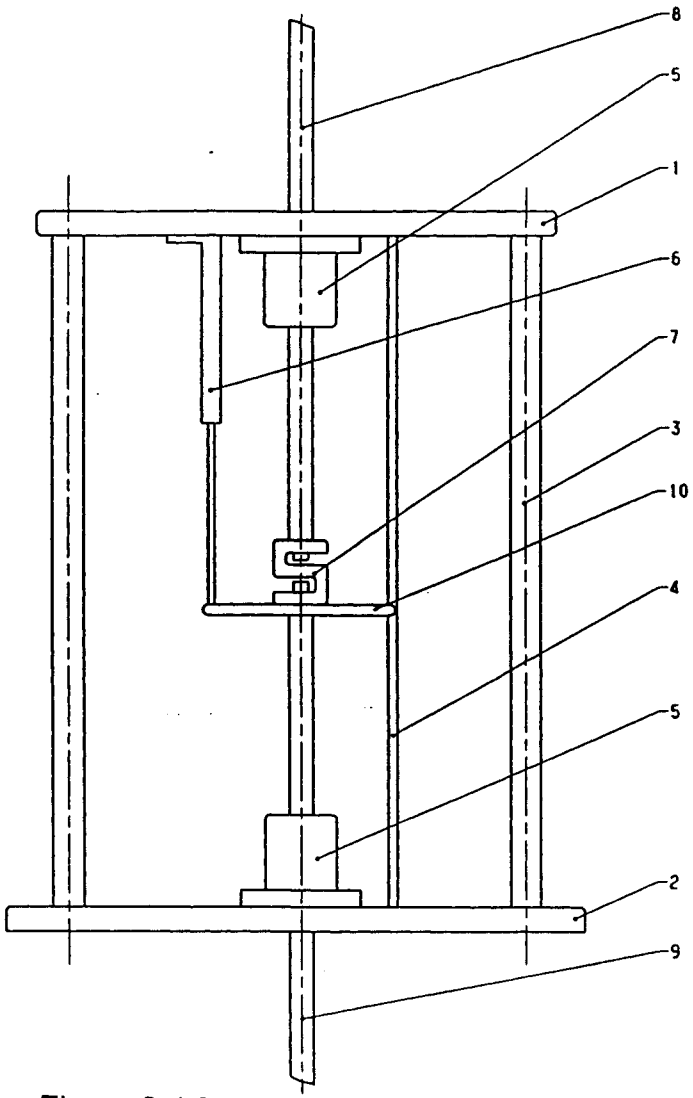

Figure 3.4.2.1 Measurement Cell Design

3.5 SYSTEM SETUP

The mixing experiments were conducted in a 190 litre capacity cylindrical tank having a diameter of 560 mm and a height of 762 mm. The measurements were made using a stratified aqueous $CaCO_3$ slurry.

The system setup is schematically shown in figure 3.5.1.

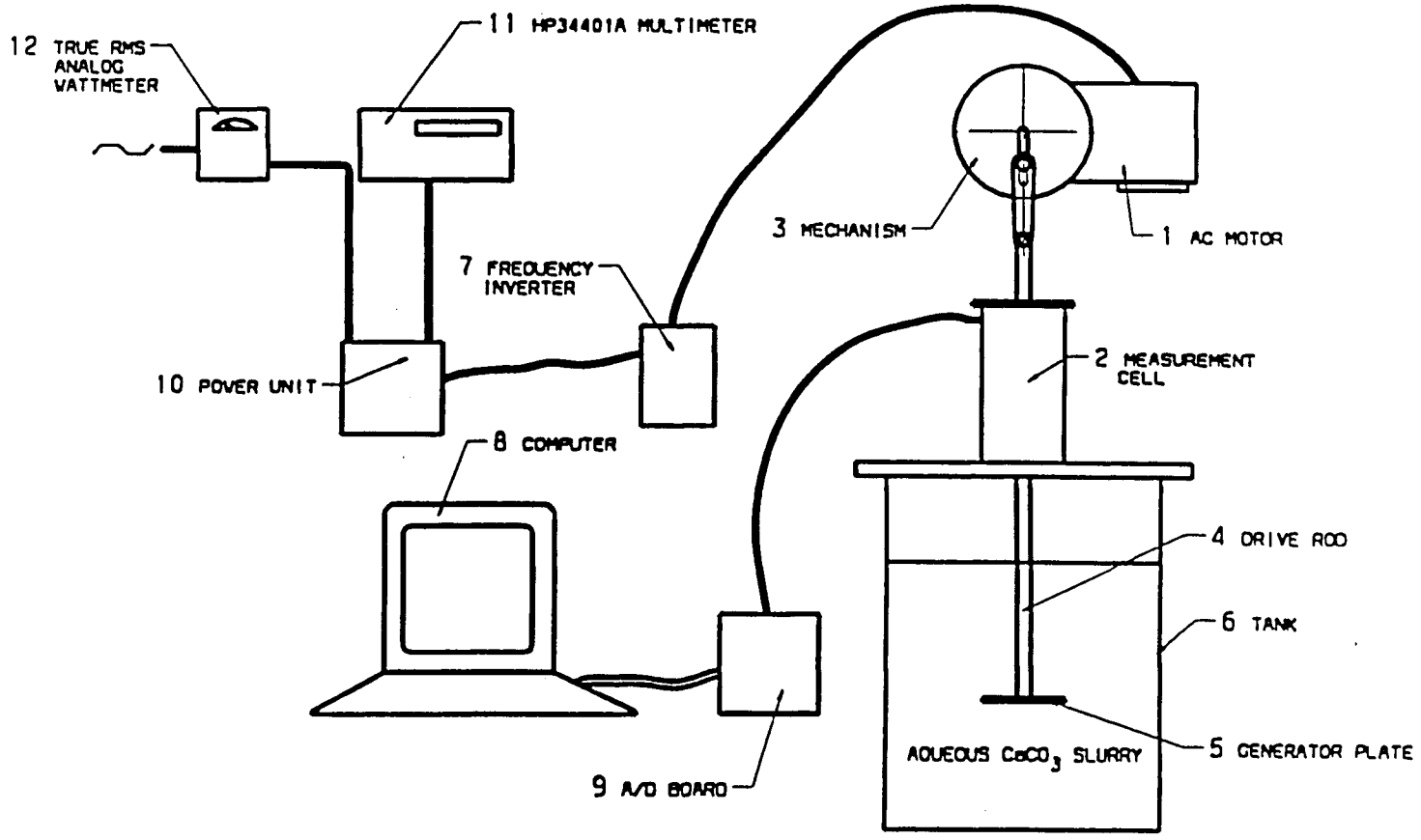

Figure 3.5.1 System Setup

An AC motor (1) was mounted on the top of the measurement cell (2). A disk mechanism (3) provided connection between a motor shaft and measurement cell shaft which was connected to the drive rod (4) of the generator plate (5) via load cell (see Figure 3.4.2.1). The generator plate was submerged in the aqueous $CaCO_3$ slurry in the holding tank (6). An adjustable drive speed controller (inverter) (7) was connected to AC motor and mounted on the support frame. The computer (8) was used to process, store and display the measured data. The signal from measurement cell was sent to the Data Translation 2805 A/D board (9) which converted the analog signals to digital ones for 486DX66 processor. LabTech Notebook software is then used to process the data.

A signal from the frequency inverter was used to record power in the initial set of test runs. However, after reviewing the data and consulting the manufacturer, it was decided that the signal was not valid for accurate measurement of power. A true RMS Wattmeter (item 12 Figure 3.5.1) was the next choice for power measurement, but the fluctuation of the power signal was too large for simple readings and "visual" averaging of consumed power. It was decided to build a power measurement system (Figure 3.5.2., item 10 Figure 3.5.1) in order to accurately record power fluctuation and consumption. Signals from voltage and current were recorded and than processed using a spreadsheet to determine the power.

The next set of tests, however, showed that the frequency inverter generated a noise signal that distorted the readings of the power unit (10) to the extent that calibration linear scale factor for current readings (3V/amp) became nonlinear. This was confirmed in separate experiment using thermocouples, where the noise signal from frequency inverter corrupted the signal such that it was necessary to use shielded thermocouples in order to obtain meaningful data.

Another problem was that current signal contained very high peaks, which were observed and analyzed using an oscilloscope. The peaks lasted 5 milliseconds, and the acquisition system could not sample faster than 300 Hz. This limitation resulted in insufficient number of points for analysis.

A "Hewlett Packard" multimeter HP34401A (item 11 Figure 3.5.1) was also used in an attempt to obtain true RMS current readings. It has the capability to sample up to 50,000 samples for a given period of time (maximum 10 sec), but even it was affected by the noise signal from the frequency inverter.

Finally, it was decided to use "visual" averaging from an analog RMS Wattmeter. It appeared that the inertia of the analog wattmeter significantly "filtered" noise. The results are presented in Appendix A. Readings from the multimeter were consistent with "visual" averaging obtained from the Wattmeter in a way that the consistency of the readings from the Wattmeter were observed throughout the entire experiment.

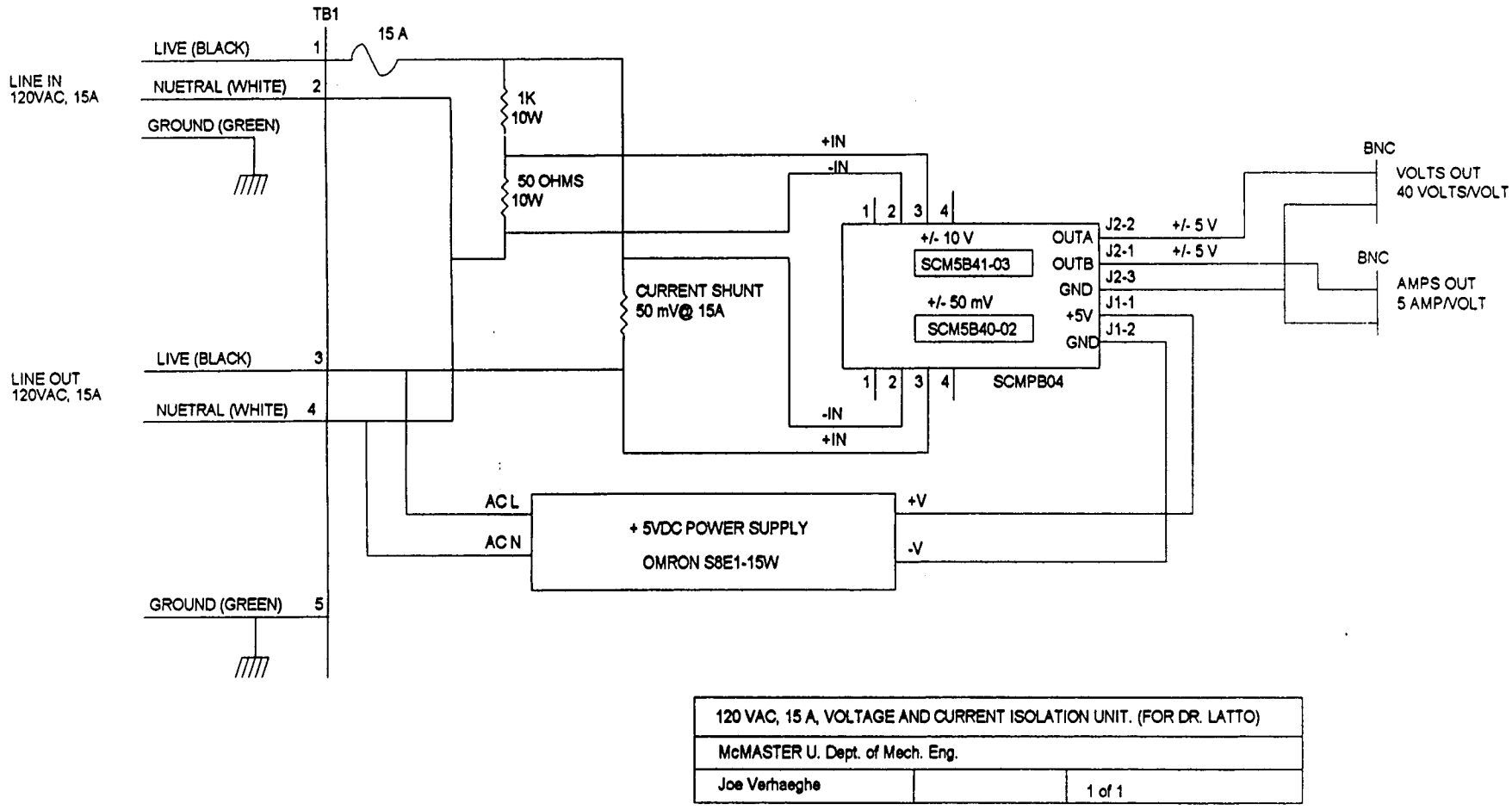

Figure 3.5.2. Power Measurement Unit Schematic

CHAPTER 4

EXPERIMENTS AND RESULTS ANALYSIS

4.1. EXPERIMENT SETUP

The objective of this research was primarily to investigate the effects of slurry concentration on the force and power consumption required by an orifice plate type vortex ring generator. The experiments were run with 10 different diameters of generator plate in 5 different concentrations of water/$CaCO_3$ slurry at 3 different plate oscillating frequencies. The primary variables are presented in Table 4.1.1.

Generator plate (ϕD x ϕd)
15" x 10" (38.1cm x 25.4cm)
15" x 7.5" (38.1cm x 18cm)
12" x 7" (30.48cm x 17.78cm)
12" x 8" (30.48cm x 20.32cm)
9" x 4.5" (22.86cm x 11.43cm)
9" x 5.25" (22.86cm x 13.34cm)
9" x 6" (22.86cm x 15.24cm)
6" x 4" (15.24cm x 10.16cm)
6" x 3" (15.24cm x 7.62cm)
6" x 3.5" (15.24cm x 8.89cm)

Slurry conc. (volume %)
19.80
11.00
7.94
4.24
2.12

Generator plate frequency (Hz)
1
1.5
2

Table 4.1.1. Experimental Setup Data

The experimental setup was such to provide sufficient data for performance analysis. Data that were collected during each test run were:

- displacement, measured by the displacement transducer mounted on the system;
- force, measured by the output from the load cell mounted on the drive rod and
- power consumed by system, by "visual" averaging from the wattmeter.

The signals were processed and recorded using LabTech Notebook version 5.1 data acquisition software.

A frequency inverter was used to control the drive motor and therefore the oscillating frequency of the generator plate. However, the sensitivity of the displacement transducer limited the maximum chosen oscillating frequency to 2 Hz. It was found that the signal was distorted above this value of 2 Hz, see Graph 4.1.1. and consequently, for convenience three oscillating frequencies of the generator plate of 1, 1.5 and 2 Hz were investigated.

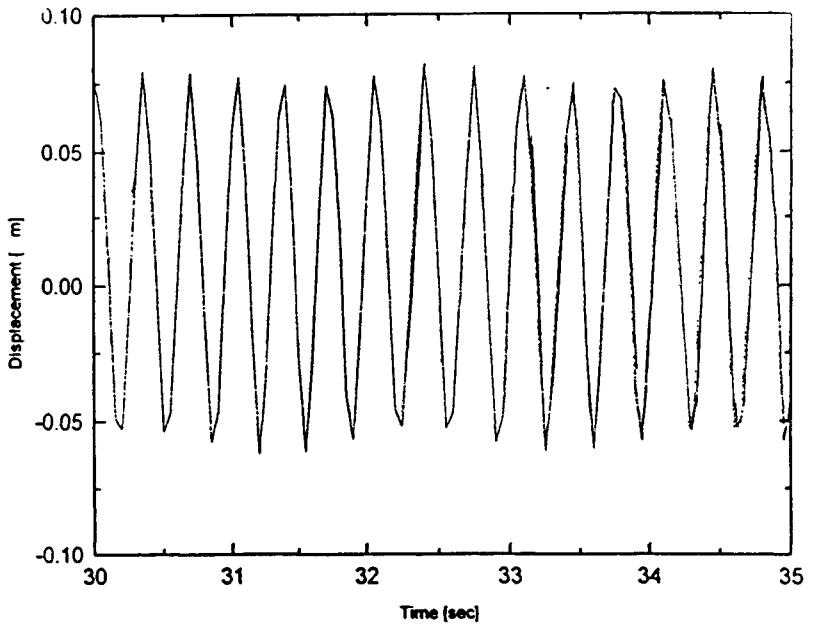

Graph 4.1.1. Signal distortion from displacement transducer for generator plate oscillating frequency of 3 Hz

As mentioned before, Latto recommended that ξ should be in the range $0.5 \leq \xi \leq 3.5$ with an optimal value 2.8. However this may only be true for certain displacement profiles of a vortex ring generator plate.

In general, when a plate moves down on the downstroke, a relatively low pressure field is created behind the plate and relatively high pressure field exists in front of the plate. This pressure distribution results in the generation of vortex ring on downstroke.

When the plate suddenly stops, as in case of trapezoidal displacement profile, fluid that travels behind the plate continues moving and encounters the plate. Because of the new relatively high pressure field created behind the plate,

flow passes through the orifice to create a secondary vortex ring. It is therefore expected that for trapezoidal displacement profile, four vortex rings are generated per cycle of the plate as shown in Figure 4.1.1.

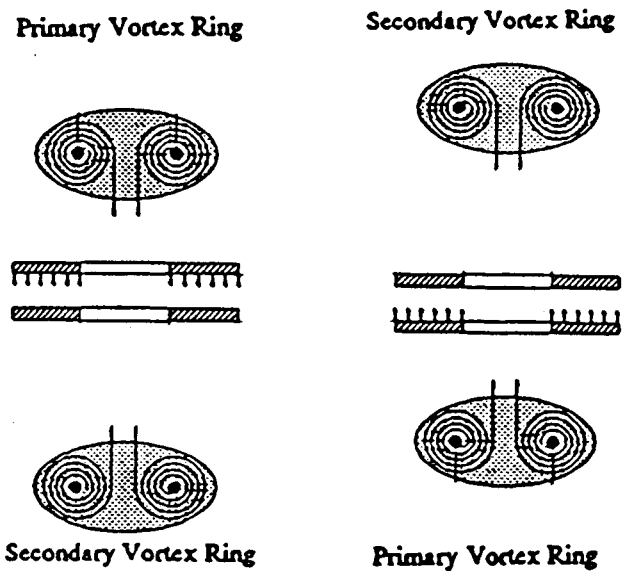

Figure 4.1.1. Vortex ring generation for the trapezoidal displacement profile

In the present case, the motion of generator plate is sinusoidal and the generator plate slows down relatively slowly. It is hypothesized that a very weak secondary vortex ring may be created and may combine with a primary ring. Therefore, it may be assumed that only two vortex rings are created per cycle when the generator plate moves in sinusoidal manner and for these experiments an optimal ξ would be 2.8/2=1.4. However, this has not been proven quantitatively.

Ideally ξ should be kept constant for various disk diameters. However it is difficult to comply with this criteria when D/d is reduced. This is because as D/d reduces, required stroke s becomes excessively large for most of the systems need to be considered. For this reason it was decided to keep stroke constant and thus vary ξ. The system design allowed maximum stroke of 5" (12.5 cm).

Using equation

$$\xi = \frac{s}{d}\left(\frac{D}{d}\right)^2 \tag{4.1.1}$$

the following table was developed for specific operating conditions:

generator plate (ϕD x ϕd)	ξ	generator plate (ϕD x ϕd)	ξ
15" x 10" (38.1cm x 25.4cm)	1.13	9" x 5.25" (22.86cm x 13.34cm)	2.80
15" x 7.5" (38.1cm x 18cm)	2.67	9" x 6" (22.86cm x 15.24cm)	1.88
12" x 7" (30.48cm x 17.78cm)	1.10	6" x 4" (15.24cm x 10.16cm)	2.81
12" x 8" (30.48cm x 20.32cm)	1.4	6" x 3" (15.24cm x 7.62cm)	6.67
9" x 4.5" (22.86cm x 11.43cm)	4.44	6" x 3.5" (15.24cm x 8.89cm)	4.20

Table 4.1.2. Generator Plate ξ

From the data in Table 4.1.2. it could be concluded that for an ξ opt of 1.4 a generator plate with diameter D of 12" (30.48 cm) and an orifice diameter of 8" (20.32 cm) and a stroke of 5" (12.5 cm) would give the best mixing results.

For a particular D/d ratio the s vs. d relation plot is easily obtained. In the case of D/d=1.5, this relation is presented in Graph 4.1.2. Using equation (4.1.1) and substituting ξ=1.4 and D/d=1.5 the simple function is derived: s=0.622d.

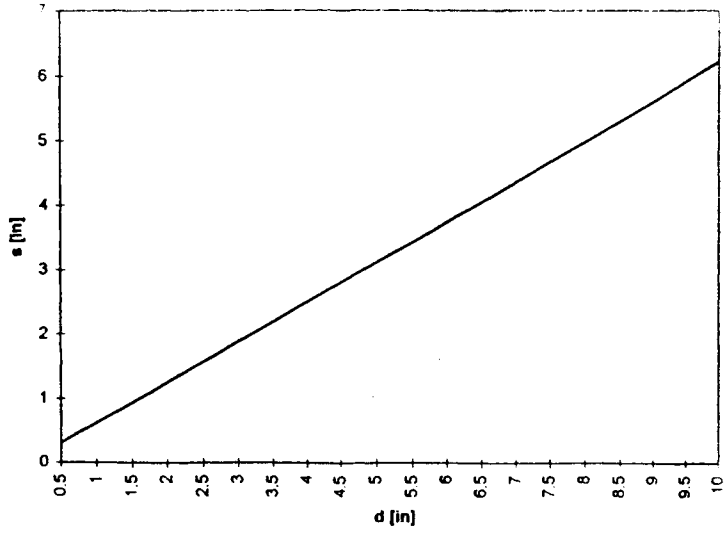

Graph 4.1.2. s versus d for D/d=1.5 and ξ=1.4.

Graph 4.1.2. presents the optimal stroke for given d for ξ=1.4 and for available generator plates for this experiment with D/d=1.5, the optimal stroke was calculated and is presented in Table 4.1.3.

ϕ15" x ϕ10" (38.1cm x 25.4cm)	s_{opt}=6.22" (15.80 cm)
ϕ9" x ϕ6" (22.86cm x 15.24cm)	s_{opt}=3.73" (9.47 cm)
ϕ6" x ϕ4" (15.24cm x 10.16cm)	s_{opt}=2.49" (6.32 cm)

Table 4.1.3. Optimal stroke for D/d=1.5 generator plates

4.2. MEASUREMENT SETUP

In order to eliminate the drag effects of the bearings and drive elements, the system including the generator plates was first run freely, "in the air", to obtain the system behavior characteristics and record inertial forces and frictional losses. Typical data are presented in Graphs 4.2.1 through 4.2.2. When graphically analyzing the force on the generator plate on low operating frequency it was noted that generated signal contained some noise that can be explained as being due to the sensitivity of load cell, friction in the mechanism, and vibration of generator plate at the lowest and the highest point of a cycle, when it changes direction of movement. At higher running oscillating frequencies these signals were dampened.

The next step in the experiments was to obtain data when the vortex ring generator was immersed in water and then in the $CaCO_3$ slurry. Each size of generator plate was run at three different oscillating frequencies in 5 different slurry concentrations. The total force reading was plotted and compared with force data obtained by running generator plates in "free air" at three different oscillating frequencies. Previously recorded force data, which included inertial forces and frictional loses of the mechanism were then subtracted from force reading obtained by running the system in the slurry. The resultant force was consequently the drag force due to a given slurry. The average drag force Fd was analyzed and used to calculate all relevant parameters.

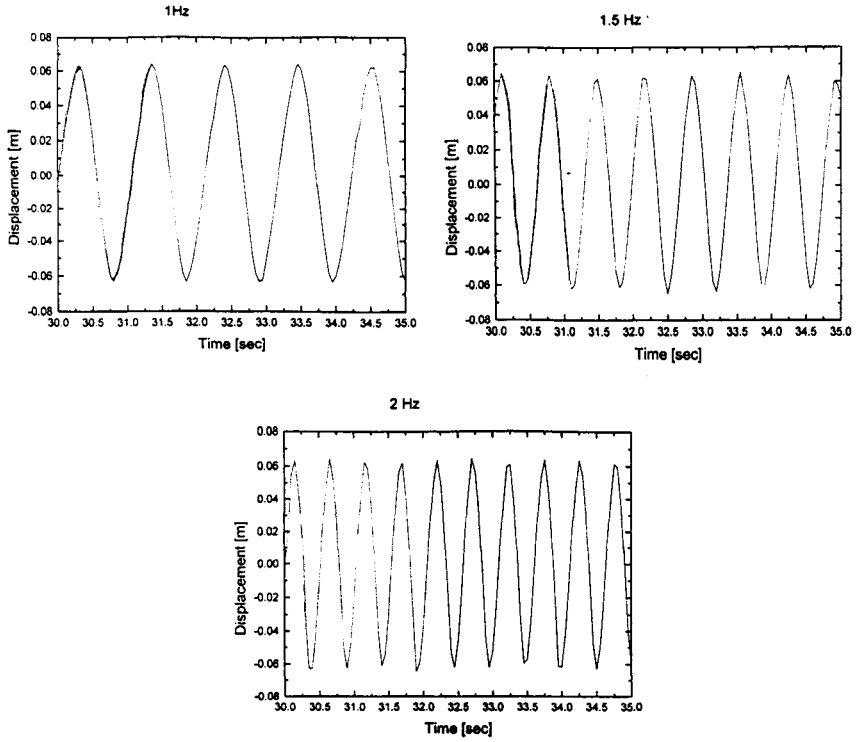

Graph 4.2.1. Displacement Profile

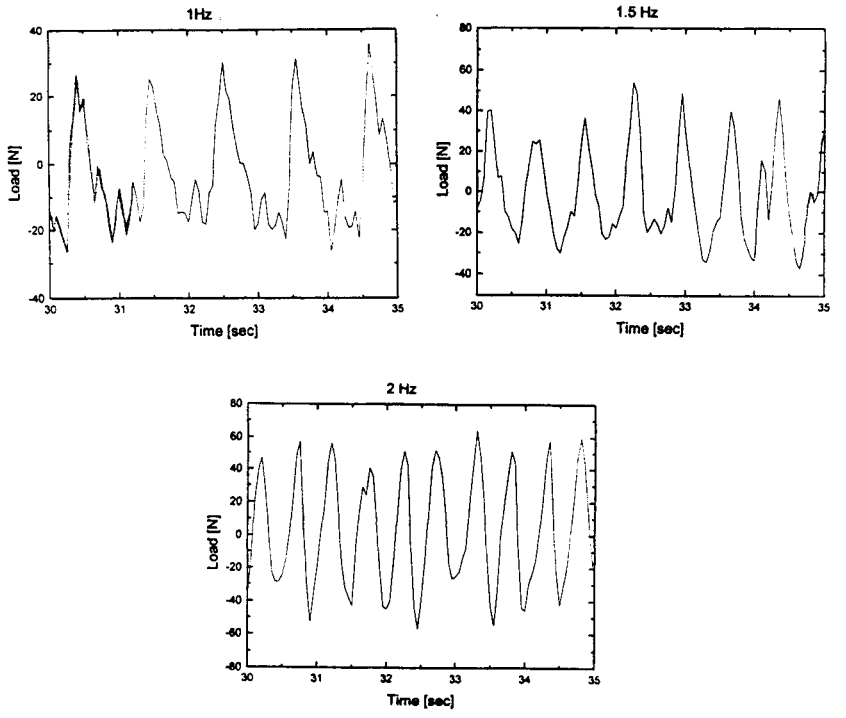

Graph 4.2.2. Load Profile

A given slurry concentration was mixed for 10 minutes before each test to ensure homogeneity of the slurry for all of the test runs for a given concentration. After each test, a sample of slurry was collected in order to measure the concentration. To determine the concentration of a given slurry, a given volume of the slurry was weighed. Each sample was measured three times and the average was used to determine concentration. The concentration was calculated using following equation:

$\rho_T m_T = \rho_T m_1 + \rho_T m_2$

$\rho_T m_T = \rho_T \rho_1 V_1 + \rho_T \rho_2 V_2$

$\rho_T m_T = \rho_T \rho_1 x V_T + \rho_T \rho_2 y V_T$

$\rho_T = x\rho_{H2O} + y\rho_{CaCO3}$

$\rho_T = (1-y)\rho_{H2O} + y\rho_{CaCO3}$

$$y = 1 - \frac{\rho_{CaCO_3} - \rho_T}{\rho_{CaCO_3} - \rho_{H_2O}};$$ volume concentration of $CaCO_3$ in slurry

V_T=const.=250mL sample volume

ρ_{H2O}=970.68 kg/m^3 for given atmospheric conditions

ρ_{CaCO3}=2000 kg/m^3

Concentration 1: m_{T1}=293.62 g ρ_{T1}=1174.48 kg/m^3 y_1=0.1980

Concentration 2: m_{T2}=270.97 g ρ_{T2}=1083.88 kg/m^3 y_2=0.1100

Concentration 3: m_{T3}=263.10 g ρ_{T3}=1052.40 kg/m^3 y_3=0.0794

Concentration 4: m_{T4}=253.57 g ρ_{T4}=1014.28 kg/m^3 y_4=0.0424

Concentration 5: m_{T5}=248.13 g ρ_{T5}=992.52 kg/m^3 y_5=0.0212

4.3. ANALYSIS OF VISCOSITY MEASUREMENTS

The viscosity was measured using a "Wells-Brookfield" synchro-lectric viscometer model LVF. Each measurement shaft has a designated viscosity coefficient corresponding to a rotational speed. The viscosity thus measured is a product of the instrument reading and appropriate shaft coefficient (see Appendix B). The resulting data are presented in Graphs 4.3.1 and 4.3.2.

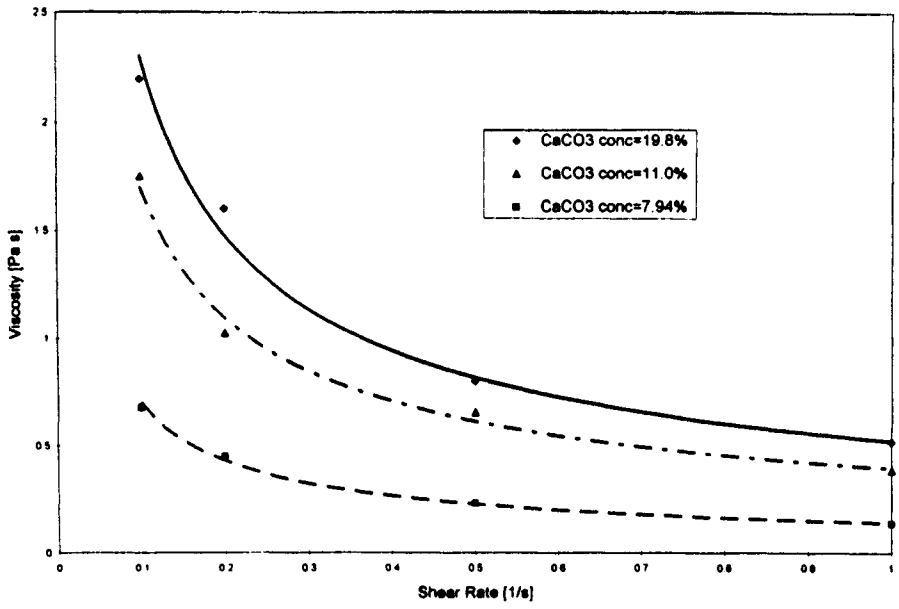

Graph 4.3.1 Viscosity vs. Shear Rate for 19.8%, 11.0% and 7.94% concentrations of $CaCO_3$ in slurry

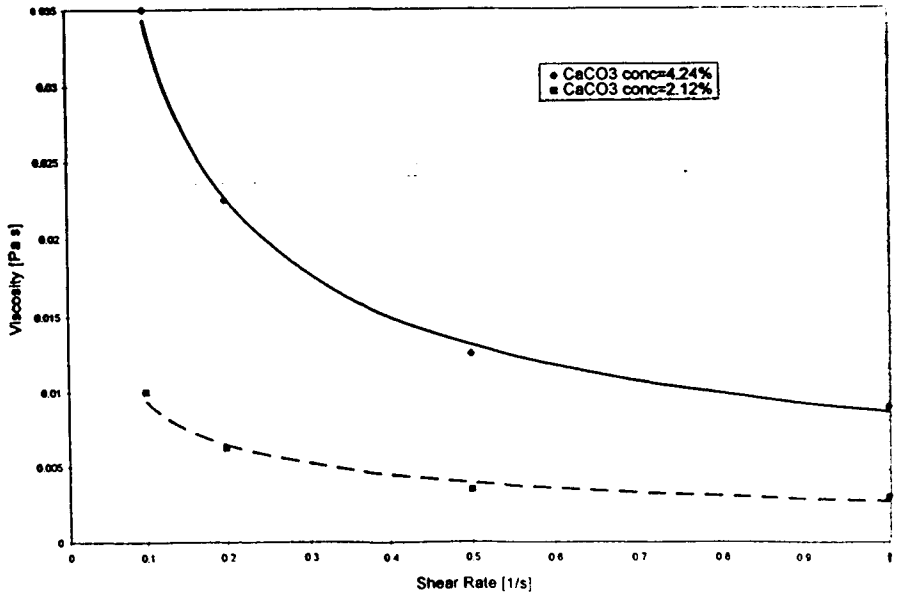

Graph 4.3.2 Viscosity vs. Shear Rate for 4.24% and 2.12% concentrations of CaCO3 in slurry

From Graphs 4.3.1 and 4.3.2 it can be seen that the $CaCO_3$ slurries used are shear thinning.

Graphs 4.3.3 through 4.3.12 present flow curves of the shear rate versus the shear stress and the viscosity versus the shear stress for aqueous $CaCO_3$ slurry and given concentrations. Comparing the $CaCO_3$ data with that for a Bingham Plastic Graph 4.3.13., it is apparent that it exhibits similar characteristics. The flow curve is characterized by a rate of shear that is linearly dependent on the shear stress above some given yield value τ_o. When the ordinate is shifted to τ_o, the viscosity defined by Newton's Law is called the plastic viscosity, μ'. The rheological equation of state for this material is:

$$\tau - \tau_o = -\mu' \frac{du}{dx}$$

The plastic viscosity value μ' was used to calculate a representative Reynolds number (Re) when considering the drag data.

Some of the materials that can be approximated by this equation are suspensions of thorium dioxide, clay, and talc, some paints, printing inks, toothpaste, and drilling muds. In order to overcome the required yield stress τ_o these materials may require higher power input to initiate mixing.

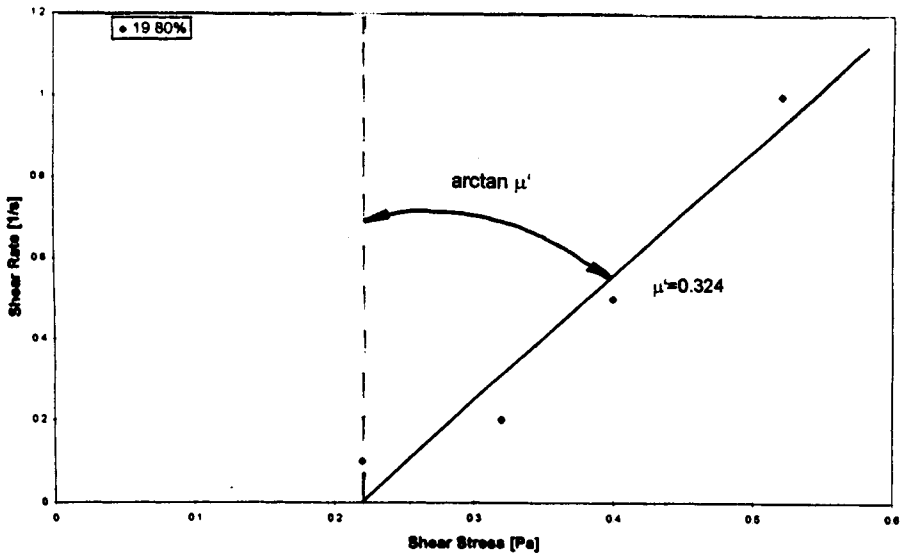

Graph 4.3.3. Shear Rate vs. Shear Stress for 19.8% concentration of $CaCO_3$ in slurry

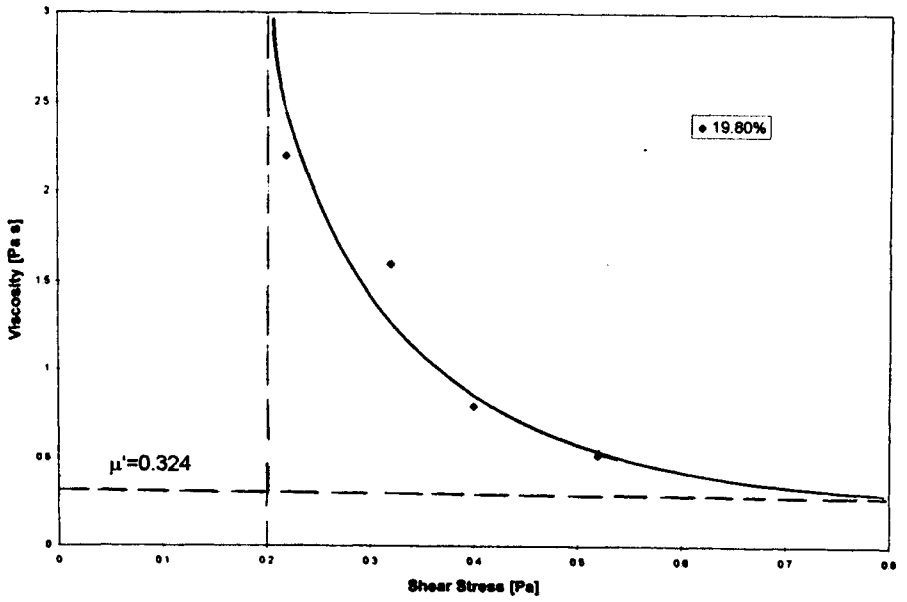

Graph 4.3.4. Viscosity vs. Shear Stress for 19.8% concentration of $CaCO_3$ in slurry

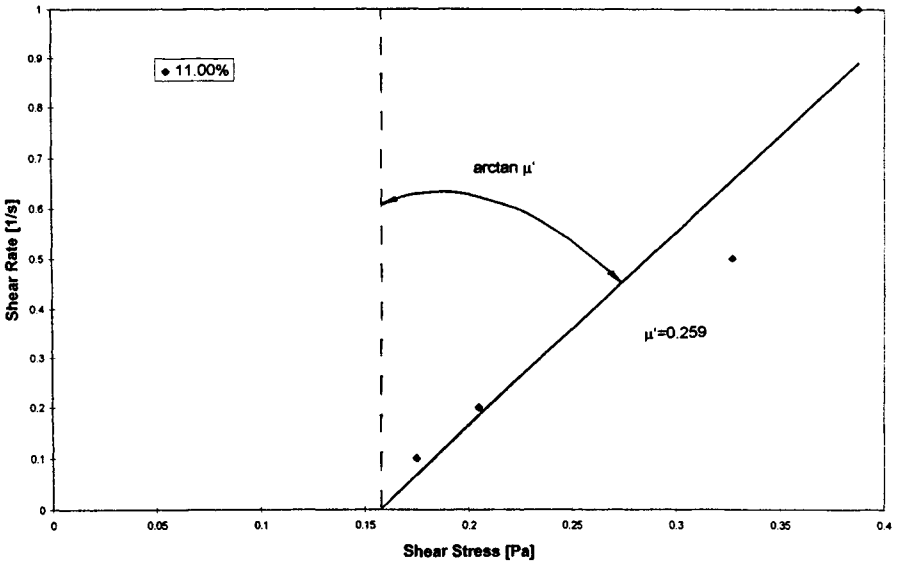

Graph 4.3.5. Shear Rate vs. Shear Stress for 11% concentration of $CaCO_3$ in slurry

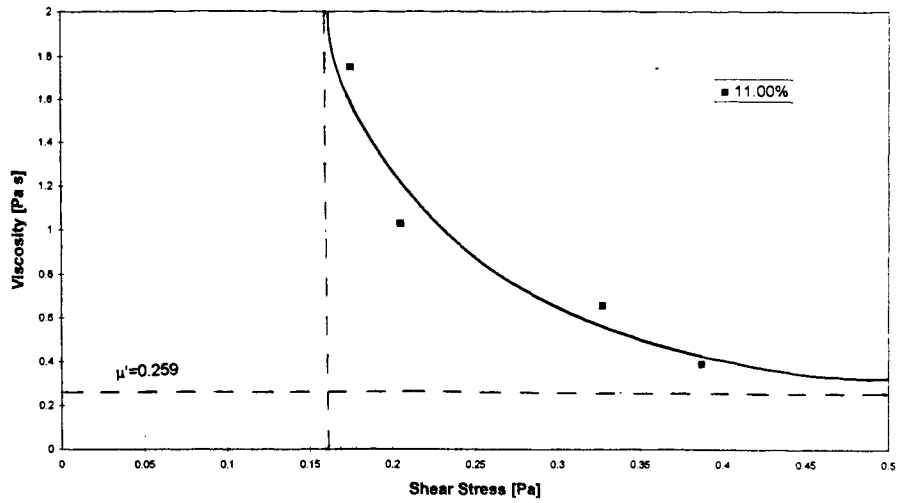

Graph 4.3.6. Viscosity vs. Shear Stress for 11.0% concentration of $CaCO_3$ in slurry

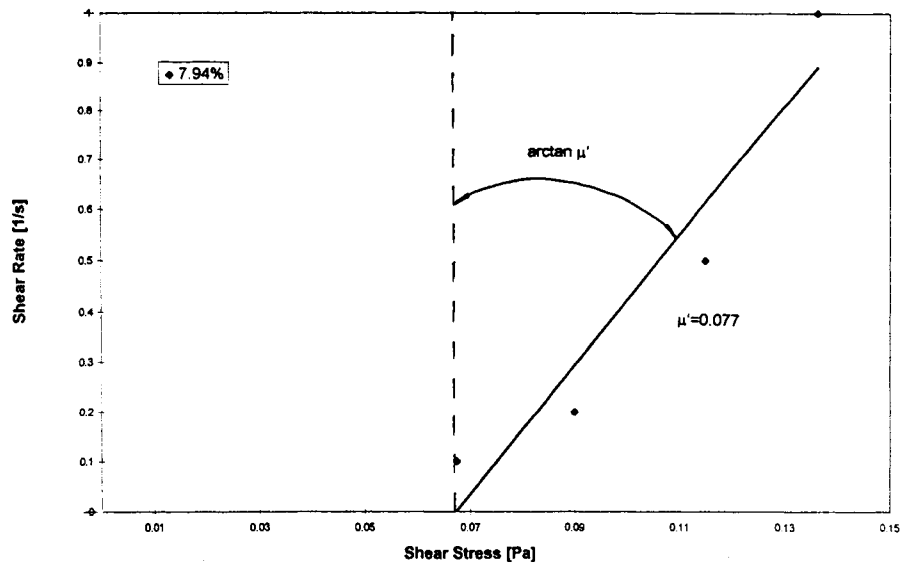

Graph 4.3.7. Shear Rate vs. Shear Stress for 7.94% concentration of $CaCO_3$ in slurry

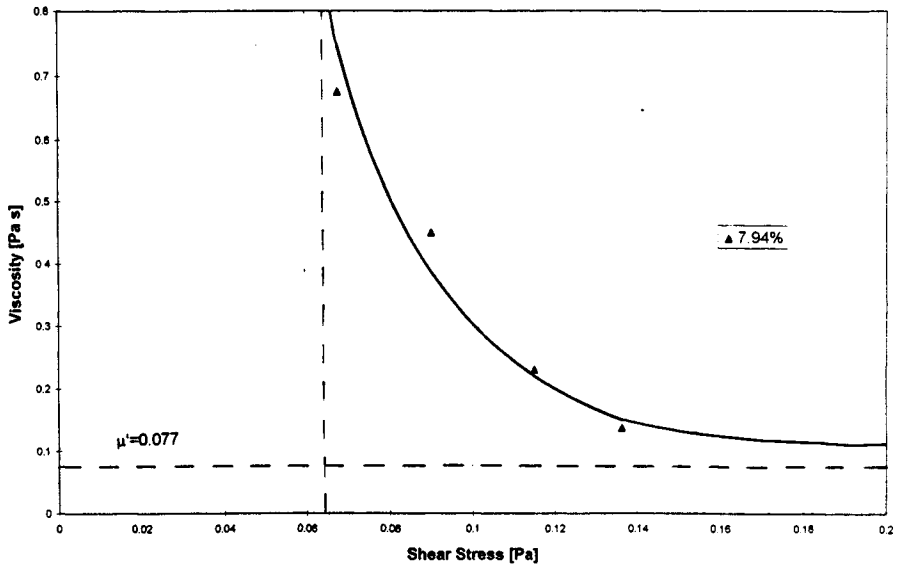

Graph 4.3.8. Viscosity vs. Shear Stress for 7.94% concentration of $CaCO_3$ in slurry

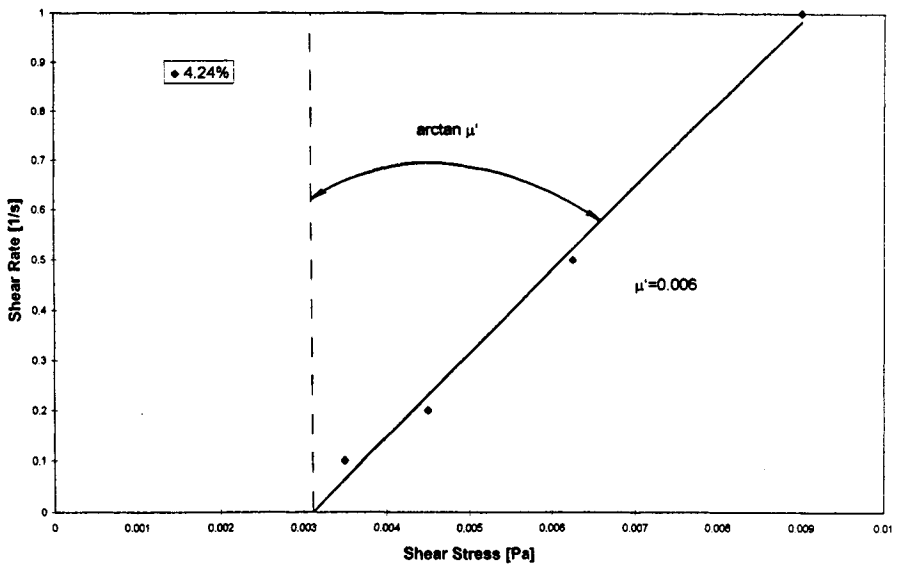

Graph 4.3.9. Shear Rate vs. Shear Stress for 4.24% concentration of $CaCO_3$ in slurry

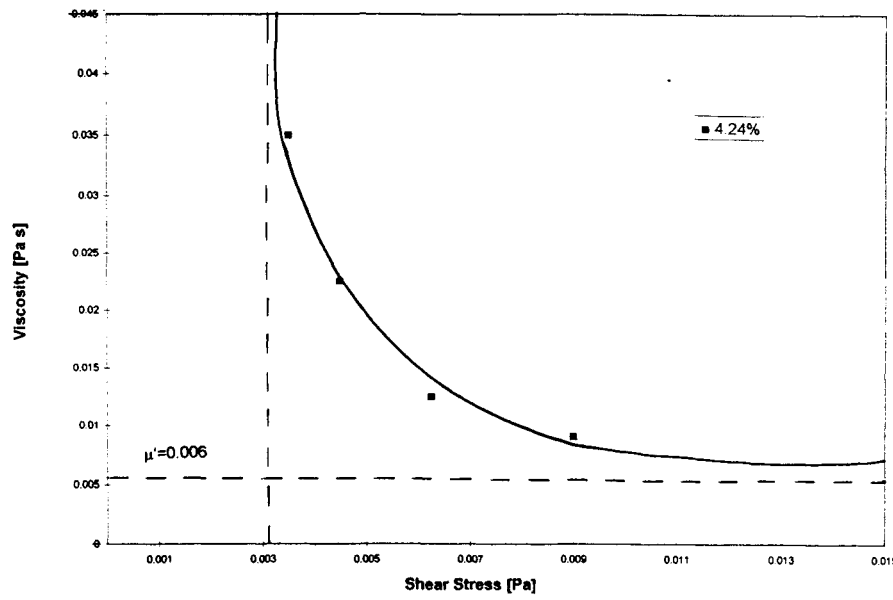

Graph 4.3.10. Viscosity vs. Shear Stress for 4.24% concentration of $CaCO_3$ in slurry

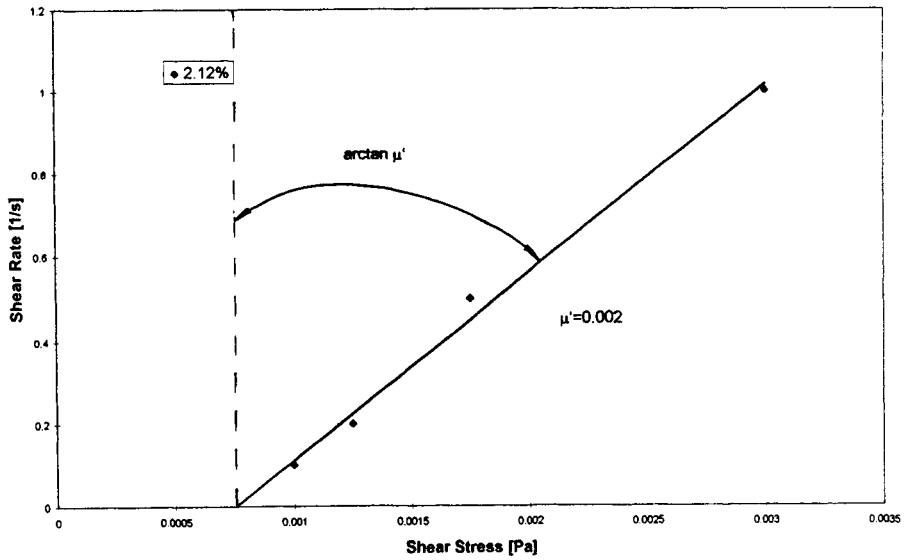

Graph 4.3.11. Shear Rate vs. Shear Stress for 2.12% concentration of $CaCO_3$ in slurry

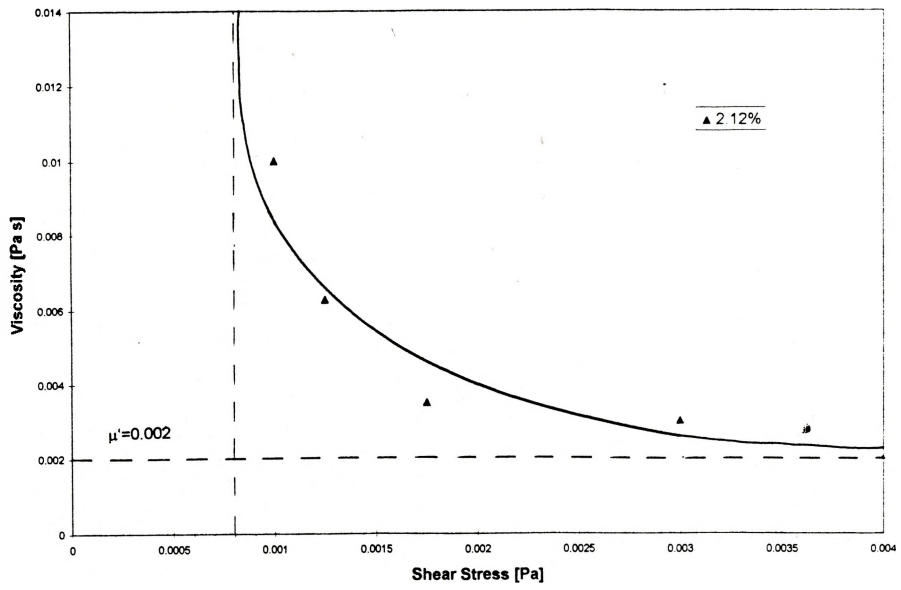

Graph 4.3.12. Viscosity vs. Shear Stress for 2.12% concentration of $CaCO_3$ in slurry

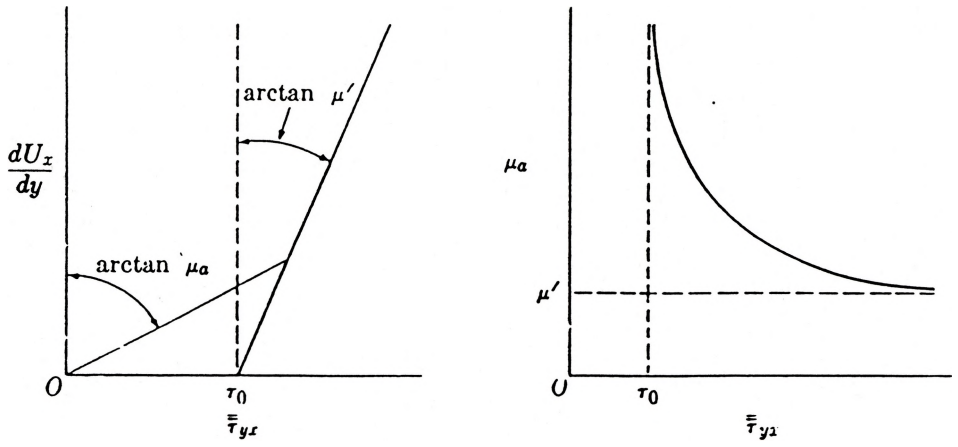

Graph 4.3.13. Flow Curves for Bingham Plastic

Graph 4.3.14. represents plastic viscosity μ' vs. $CaCO_3$ concentration in slurry, measured during experiments.

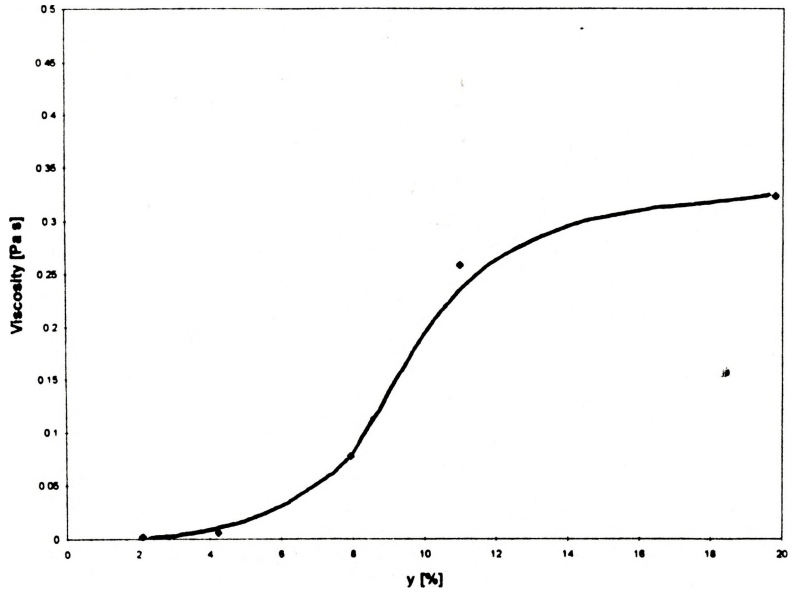

Graph 4.3.14. Plastic viscosity μ' vs. y [%] $CaCO_3$ concentration in slurry

4.4. ANALYSIS OF DRAG FORCE MEASUREMENTS

The drag force Fd was measured and plotted with respect to the slurry concentrations for each generator plate size and oscillating frequency (Graphs 4.4.1. through 4.4.10.). It was noted that the concentration had little effect on drag force for a given oscillating frequency and generator plate size for various concentrations. This was especially the case for the larger generator plates and at higher oscillating frequencies, where the fluctuation of data was smaller than the data fluctuation for the smaller generator plates. This could be explained by the output error and sensitivity of the load cell on the smaller loads.

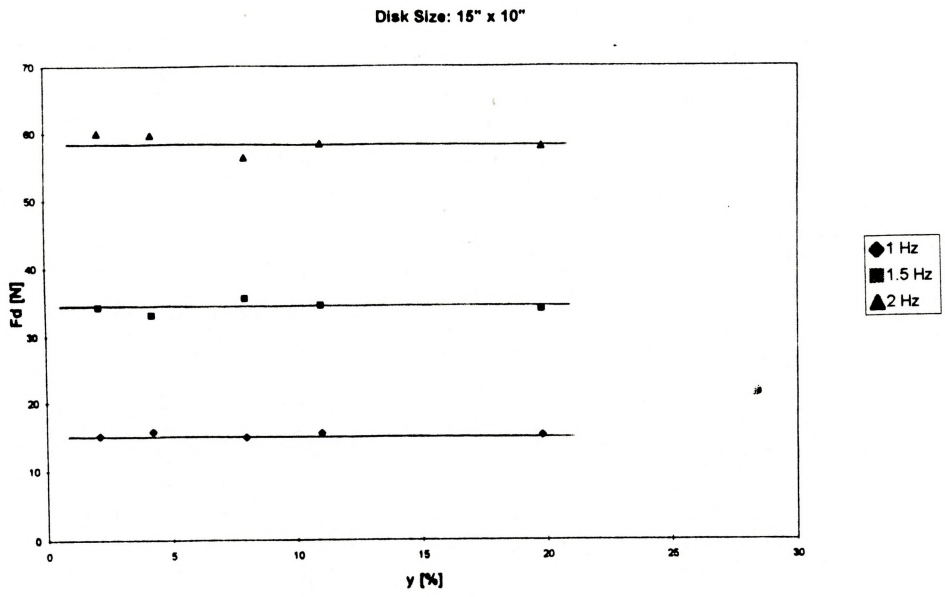

Graph 4.4.1. Drag Force Fd vs. concentration for given oscillating frequency for disk ϕ15"xϕ10" (38.1cm x 25.4cm)

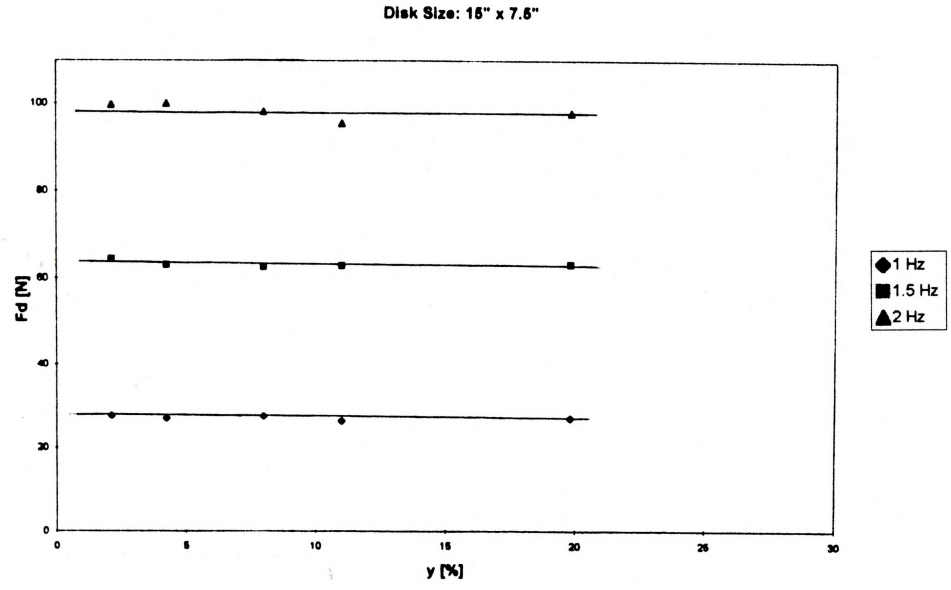

Graph 4.4.2. Drag Force Fd vs. concentration for given oscillating frequency for disk ϕ15"xϕ7.5" (38.1cm x 18cm)

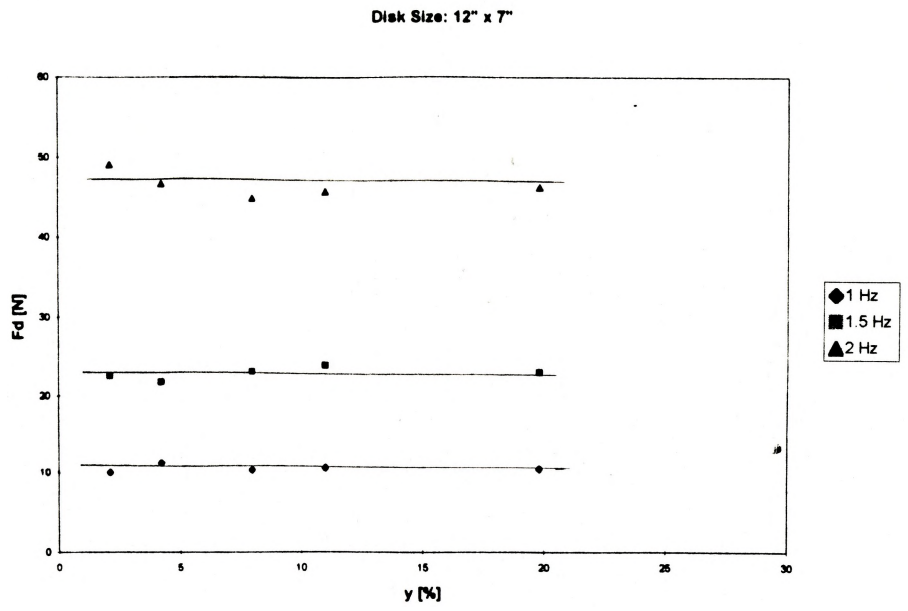

Graph 4.4.3. Drag Force Fd vs. concentration for given oscillating frequency for disk ϕ12"xϕ7" (30.48cm x 17.78cm)

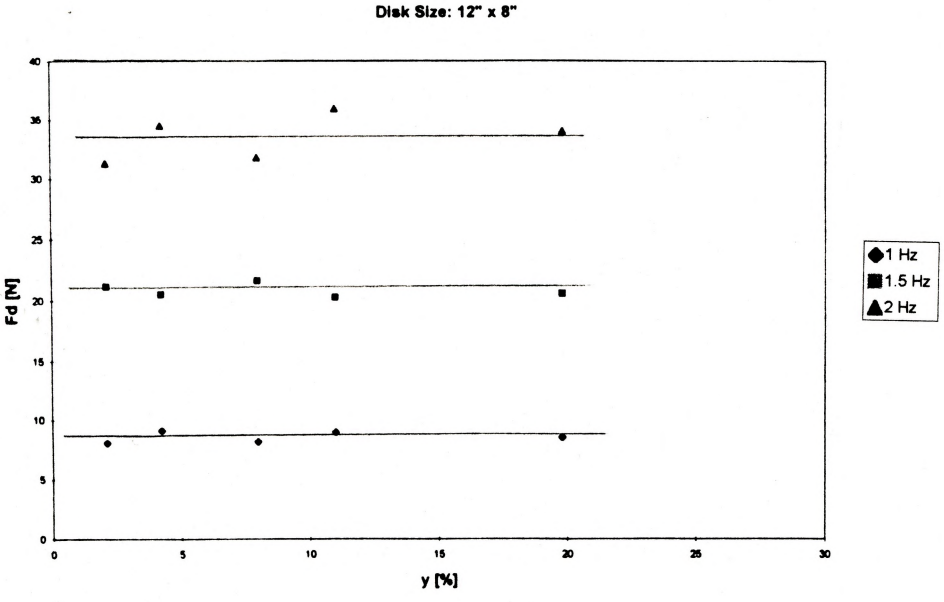

Graph 4.4.4. Drag Force Fd vs. concentration for given oscillating frequency for disk ϕ12"xϕ8" (30.48cm x 20.32cm)

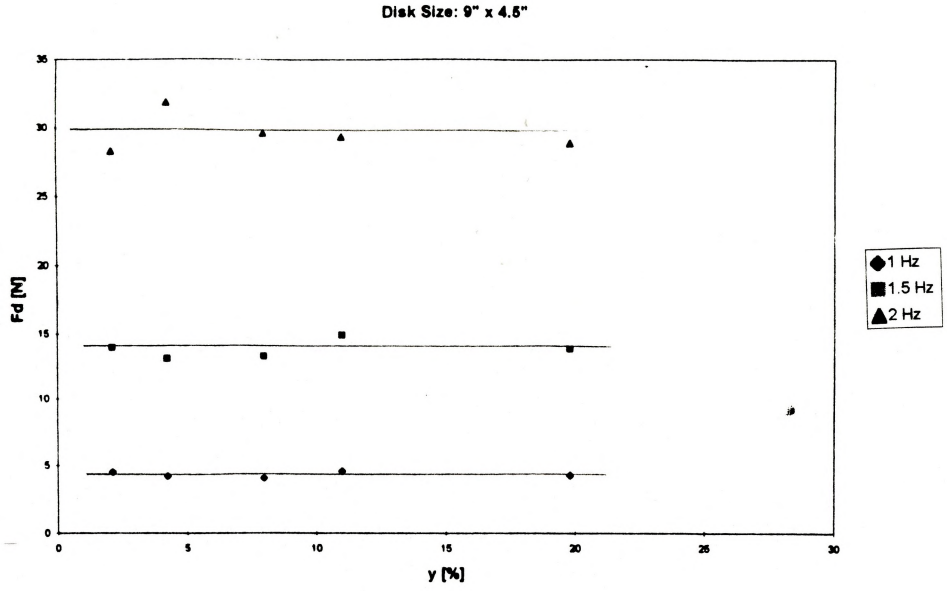

Graph 4.4.5. Drag Force Fd vs. concentration for given oscillating frequency for disk ϕ9"xϕ4.5" (22.86cm x 11.43cm)

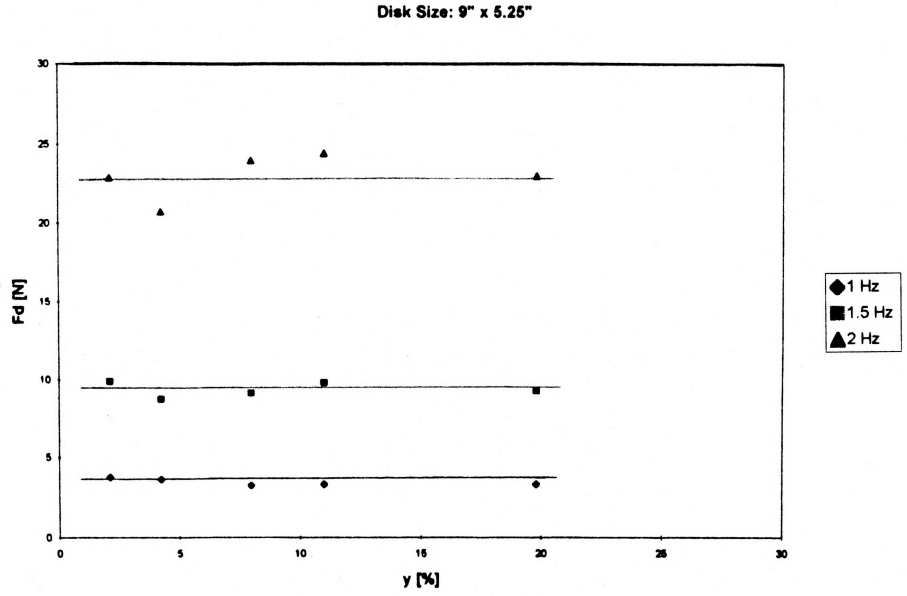

Graph 4.4.6. Drag Force Fd vs. concentration for given oscillating frequency for disk ϕ9"xϕ5.25" (22.86cm x 13.43cm)

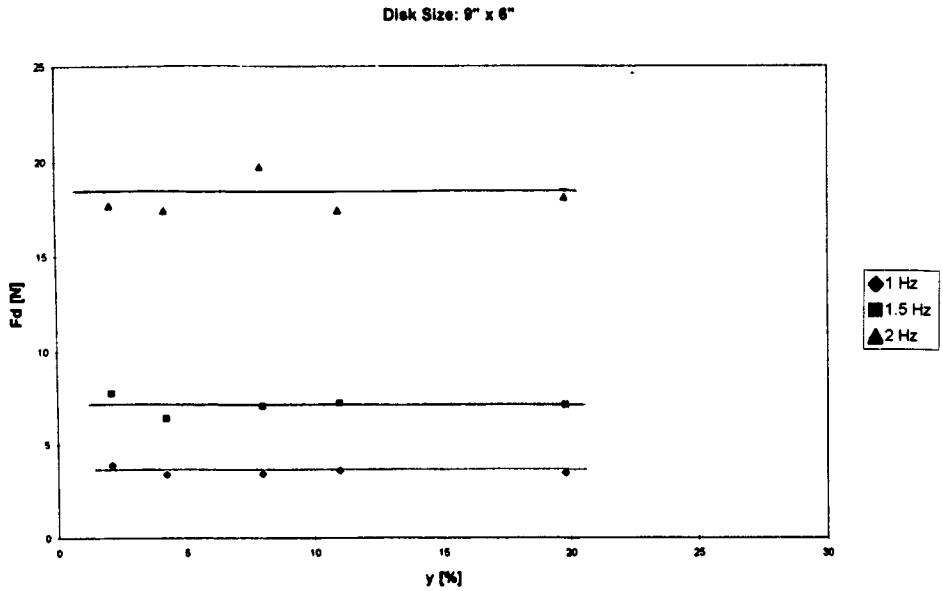

Graph 4.4.7. Drag Force Fd vs. concentration for given oscillating frequency for disk ϕ9"xϕ6" (22.86cm x 15.24cm)

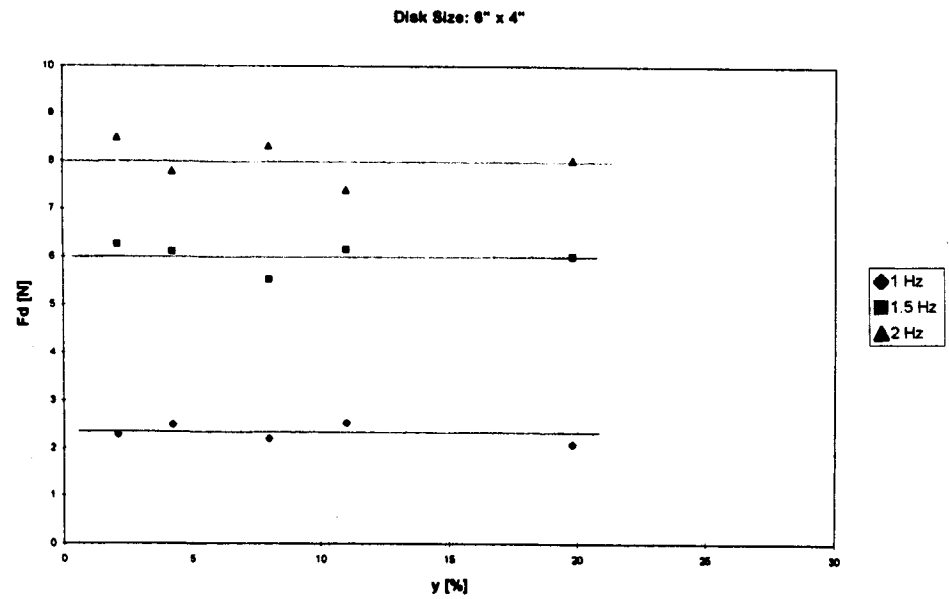

Graph 4.4.8. Drag Force Fd vs. concentration for given oscillating frequency for disk ϕ6"xϕ4" (15.24cm x 10.16cm)

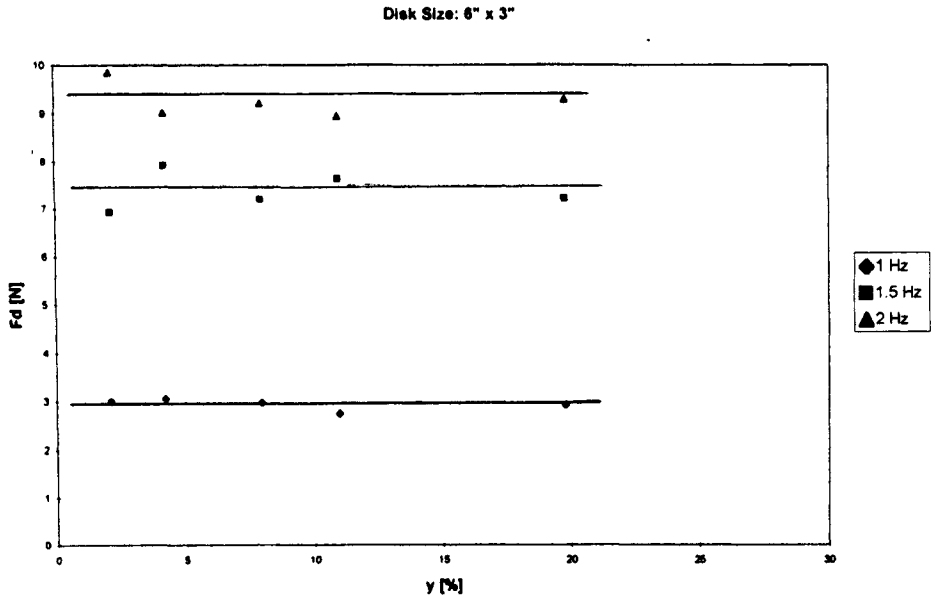

Graph 4.4.9. Drag Force Fd vs. concentration for given oscillating frequency for disk ϕ6"xϕ3" (15.24cm x 7.62cm)

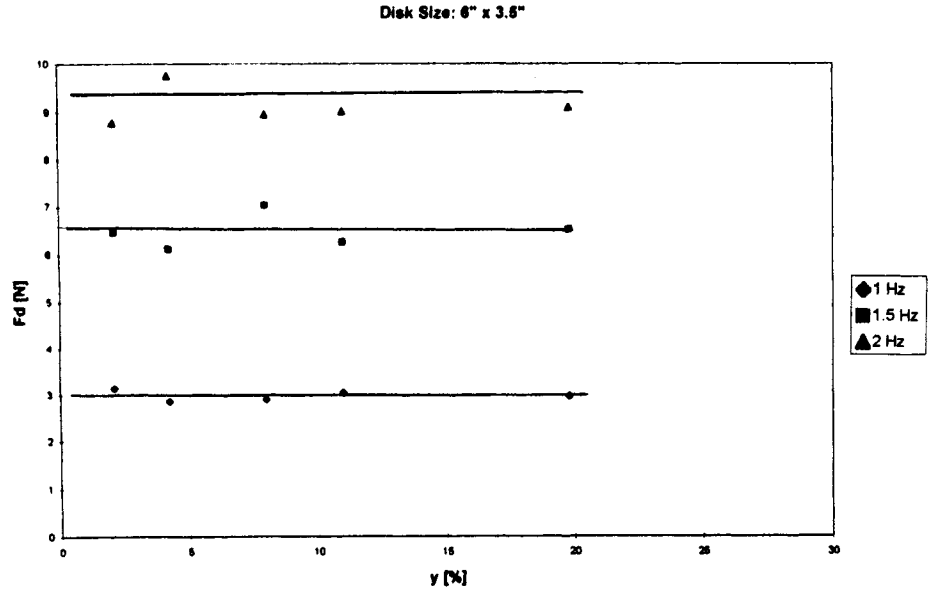

Graph 4.4.10. Drag Force Fd vs. concentration for given oscillating frequency for disk ϕ6"xϕ3.5" (15.24cm x 8.89cm)

The collected data were also used to determine the effect of the orifice diameter size d on the drag force for given D/d ratios and different oscillating frequencies. The resulting data are presented in Graphs 4.4.11. through 4.4.13. As expected, the drag force was smaller for smaller areas of generator plate. Fd was not simple function of the generator plate area for given oscillating frequency, since flow around plate creates complex pressure field, which, in turn, defines Fd.

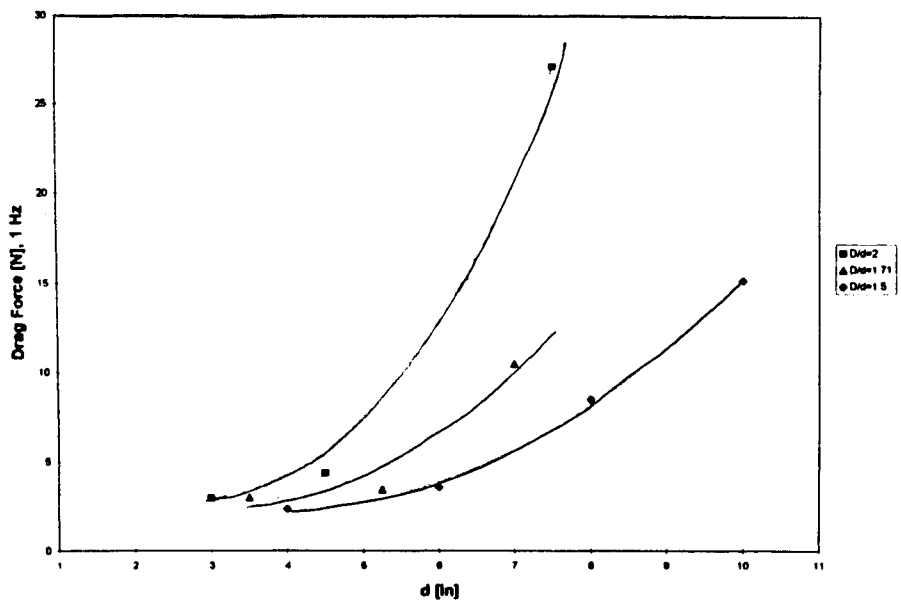

Graph 4.4.11. Drag Force Fd vs. d for different D/d ratios for generator plate oscillating frequency of 1 Hz

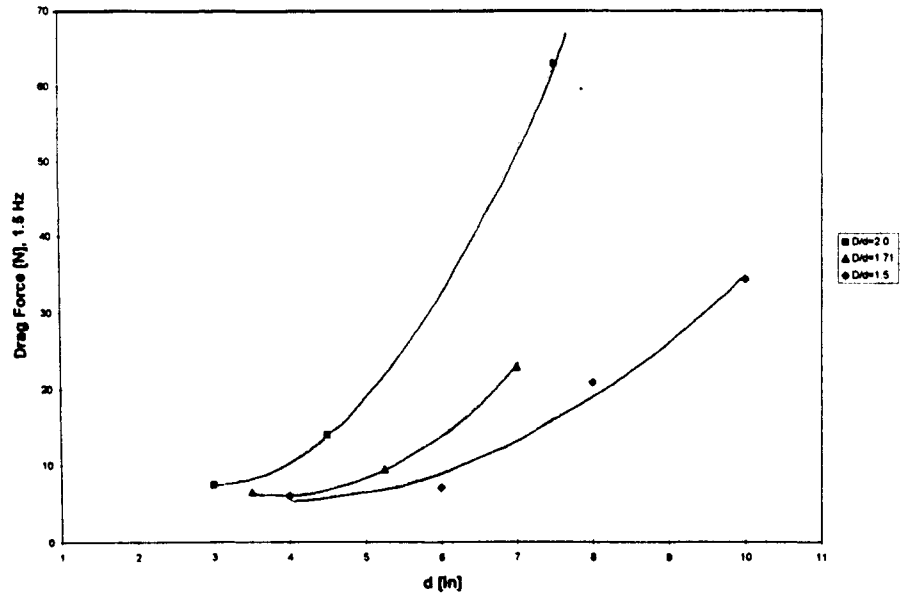

Graph 4.4.12. Drag Force Fd vs. d for different D/d ratios for generator plate oscillating frequency of 1.5 Hz

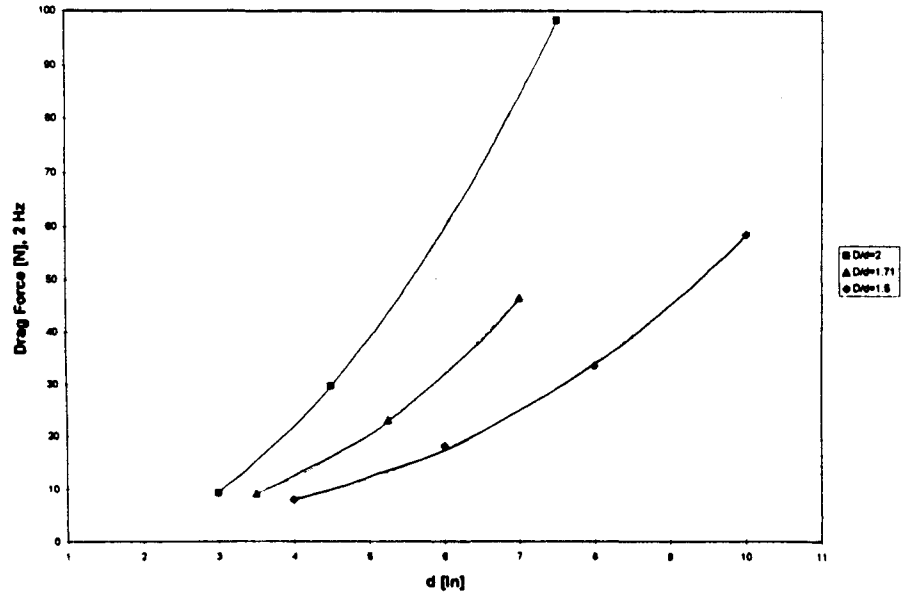

Graph 4.4.13. Drag Force Fd vs. d for different D/d ratios for generator plate oscillating frequency of 2 Hz

The drag force data obtained for water (Graphs 4.4.14 through 4.4.16) did not differ significantly to the $CaCO_3$ slurry (Graphs 4.4.11 through 4.4.13). This confirms the previous statement that within the range of concentrations used the concentration of the slurry appeared to have no significant affect on the drag force.

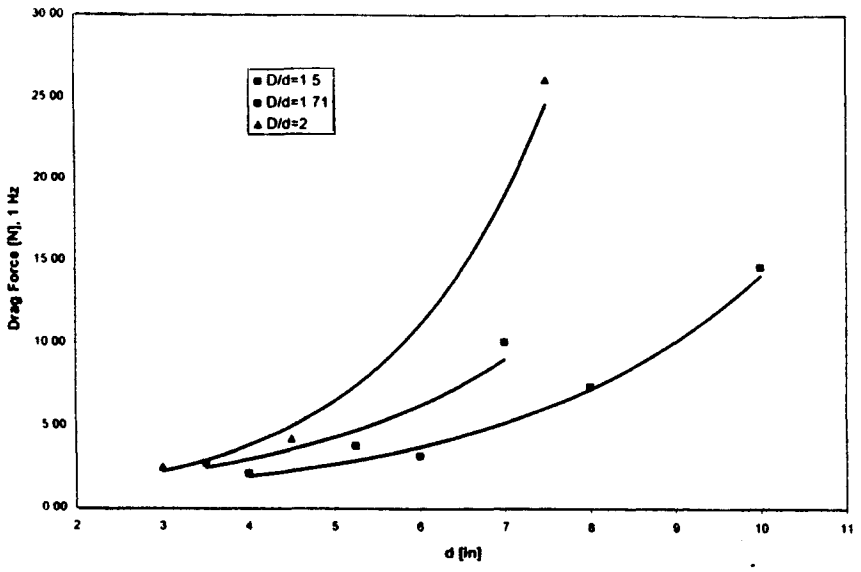

Graph 4.4.14. Drag Force Fd vs. d for different D/d ratios for generator plate oscillating frequency of 1 Hz (water)

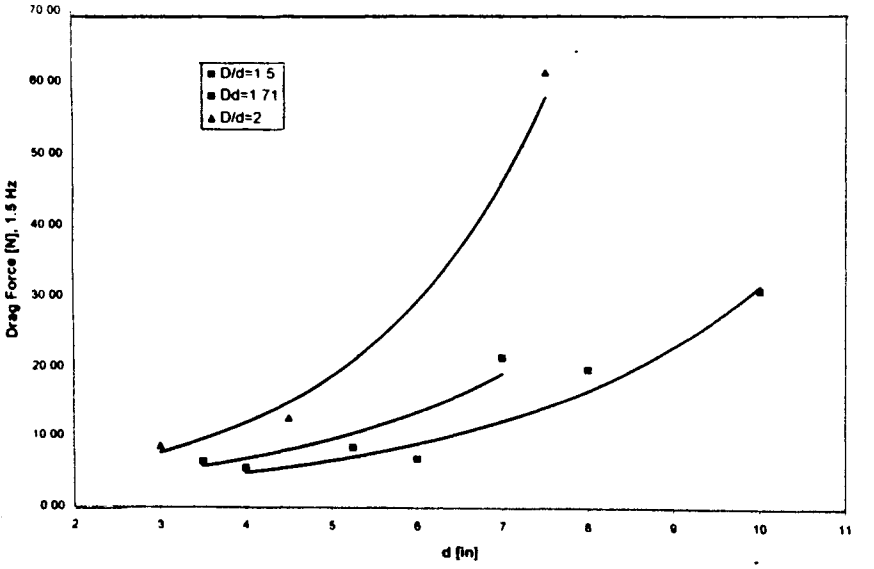

Graph 4.4.15. Drag Force Fd vs. d for different D/d ratios for generator plate oscillating frequency of 1.5 Hz (water)

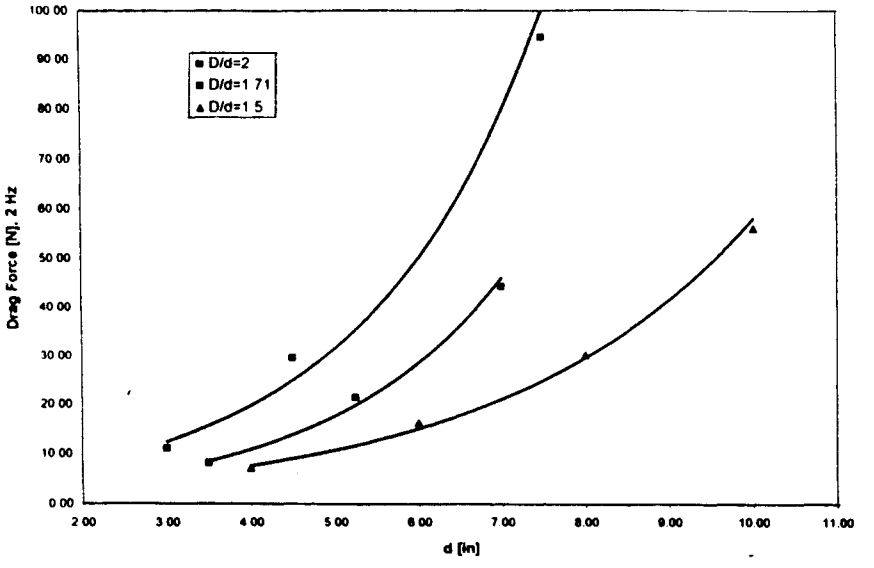

Graph 4.4.16. Drag Force Fd vs. d for different D/d ratios for generator plate oscillating frequency of 2 Hz (water)

The collected data were organized and arranged to obtain the relationship between the drag force Fd and the generator plate operating frequency and the orifice diameter d for given D/d ratio. The results are presented in Graphs 4.4.17. through 4.4.19.

It was noted that as the orifice diameter increases the Fd vs. oscillating frequency curve becomes steeper.

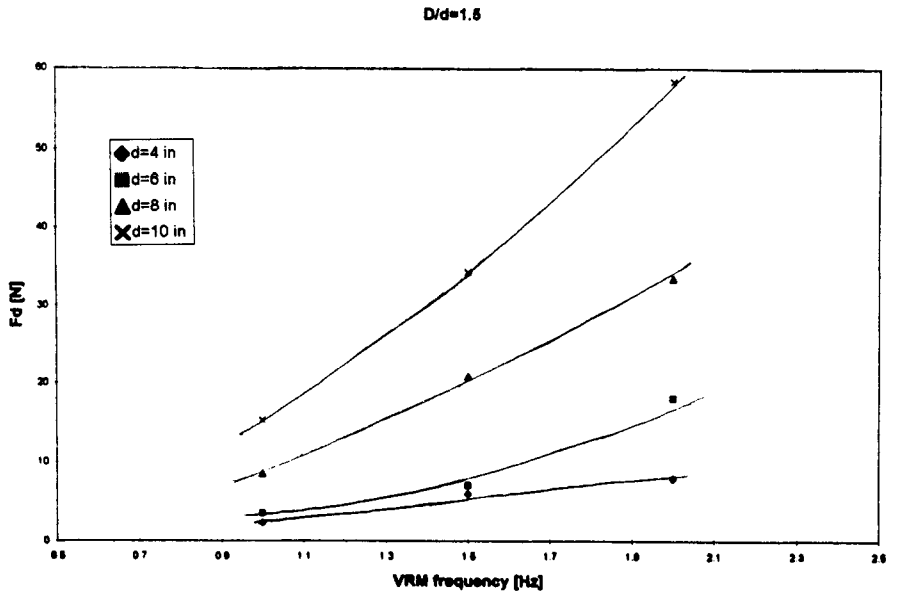

Graph 4.4.17. Drag Force Fd vs. oscillating frequency of generator plate for different d of generator plate for D/d=1.5

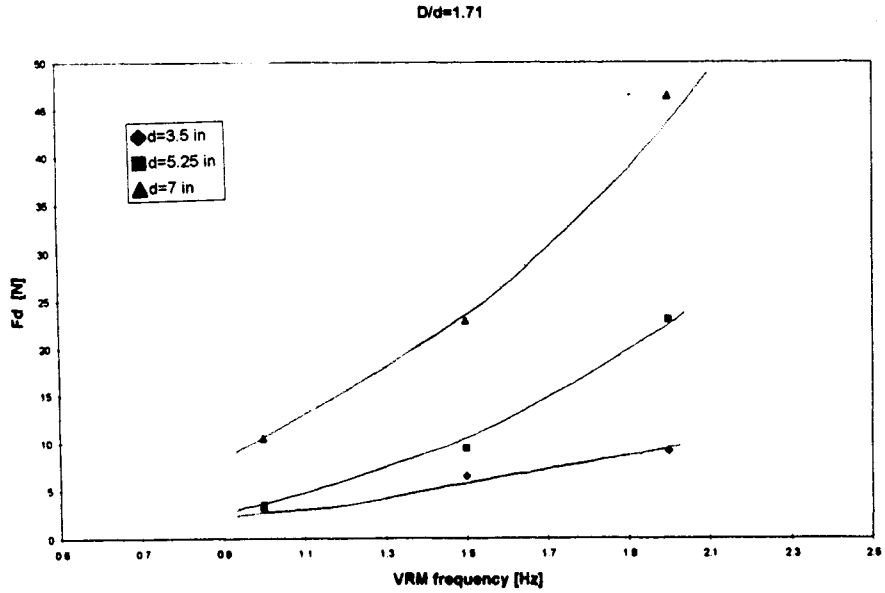

Graph 4.4.18. Drag Force Fd vs. oscillating frequency of generator plate for different d of generator plate for D/d=1.71

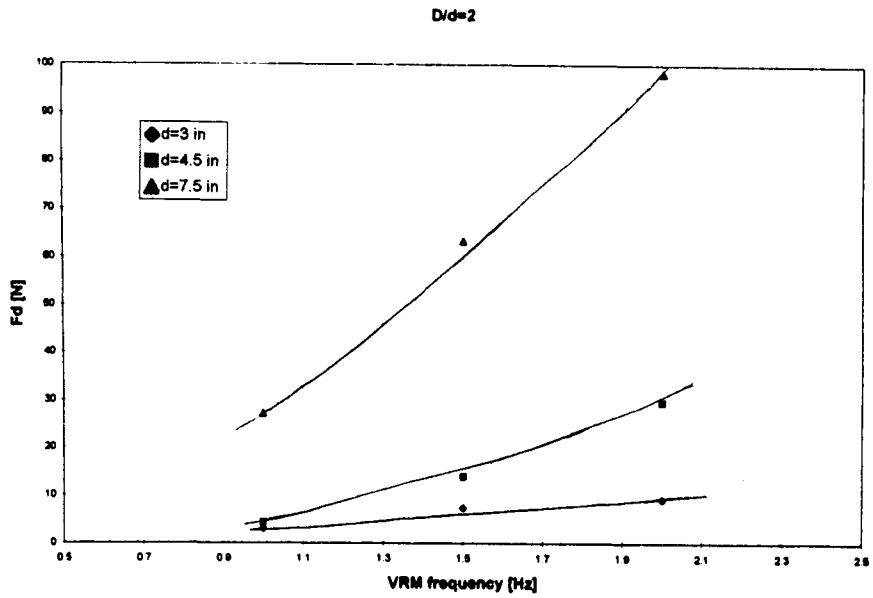

Graph 4.4.19. Drag Force Fd vs. oscillating frequency of generator plate for different d of generator plate for D/d=2

4.5. ANALYSIS OF DRAG DATA

Since the drag force was not significantly affected by the concentration of $CaCO_3$ slurry for a given oscillating frequency, it could be concluded that Cd, for a given generator plate size and oscillating frequency, was only a function of density of the slurry. A typical curve Cd vs. concentration is presented in Graph 4.5.1.

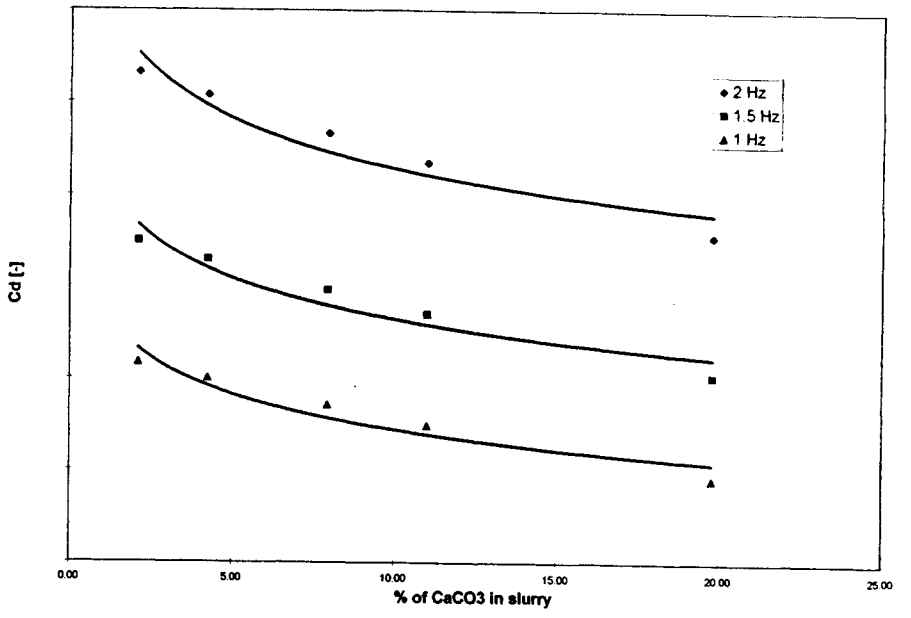

Graph 4.5.1. Cd vs. concentration for a disk (typical)

In order to generalize the data, the drag coefficient was plotted against the Re number, shown in Graphs 4.5.2. through 4.5.6. Graphs for given D/d ratios and different slurry concentrations.

The Reynolds number was defined by formula $Re=\rho vd/\mu'$. The orifice diameter d was chosen as the characteristic dimension, since it is one of the major parameters in formation of the vortex rings, and also a primary geometrical characteristic of the generator plate.

As previously stated, at the lower oscillating frequencies there was a larger error in the smaller disks loads reading, which was amplified and resulted in a bigger scatter in the Cd vs. Re curves for small Re numbers.

It can be observed that all curves had the same trend for larger Re numbers, that is, the drag coefficient increased as D/d increased and approached the same narrow range of Cd for same D/d ratio for different concentrations of slurry. Namely, for D/d=2 $Cd\approx13$-14, for D/d=1.71 $Cd\approx12$-13 and for D/d=1.5 $Cd\approx10$-11. This could be useful while sizing the drive shaft, in a way that if sizing were done for the region of Re numbers where Cd was constant for D/d=2 , the shaft would be sufficient for a range of concentrations, flow characteristics and smaller D/d ratios. However, the effect of vibration of the shaft should also be considered.

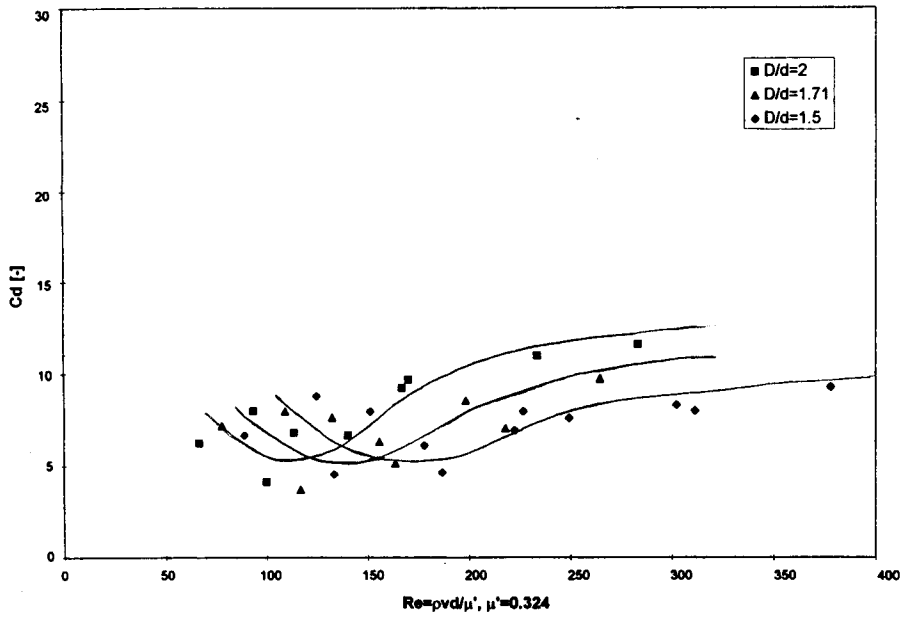

Graph 4.5.2. Drag Coefficient Cd vs. Re Number for different D/d ratios of vortex generator disks for 19.8% concentration of $CaCO_3$ in slurry (μ'=0.324 Pa s)

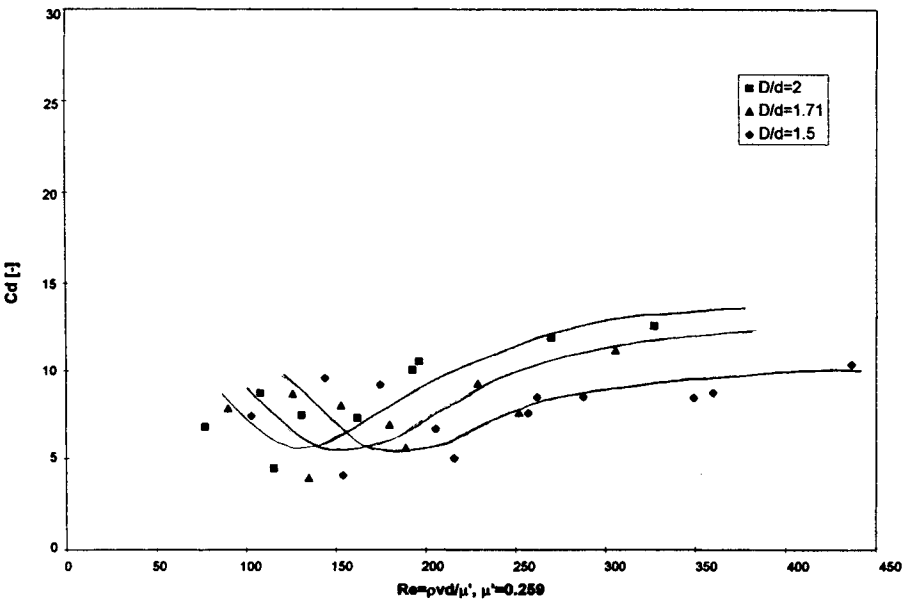

Graph 4.5.3. Drag Coefficient Cd vs. Re Number for different D/d ratios of vortex generator disks for 11% concentration of CaCO3 in slurry (μ'=0.259 Pas)

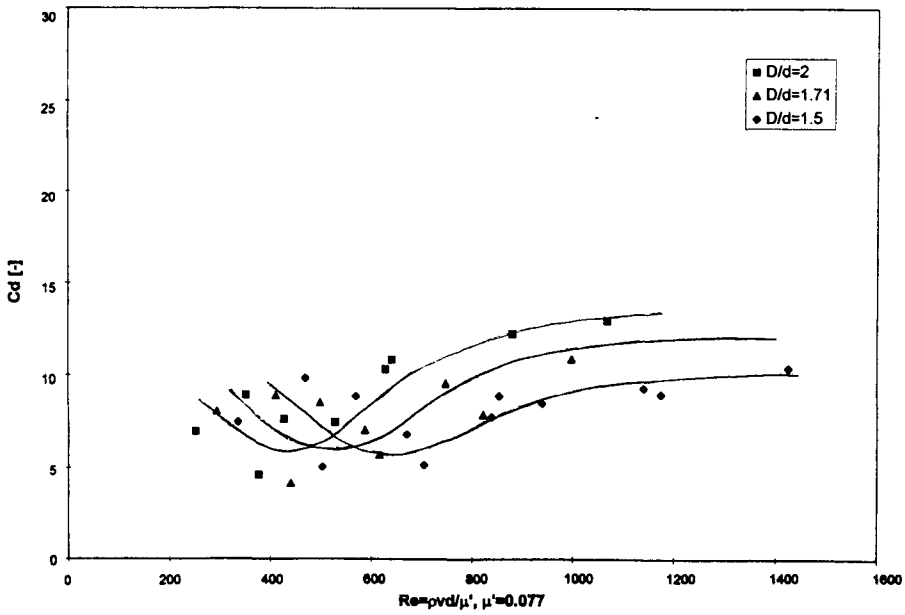

Graph 4.5.4. Drag Coefficient Cd vs. Re Number for different D/d ratios of vortex generator disks for 7.94% concentration of CaCO3 in slurry (μ'=0.077 Pas)

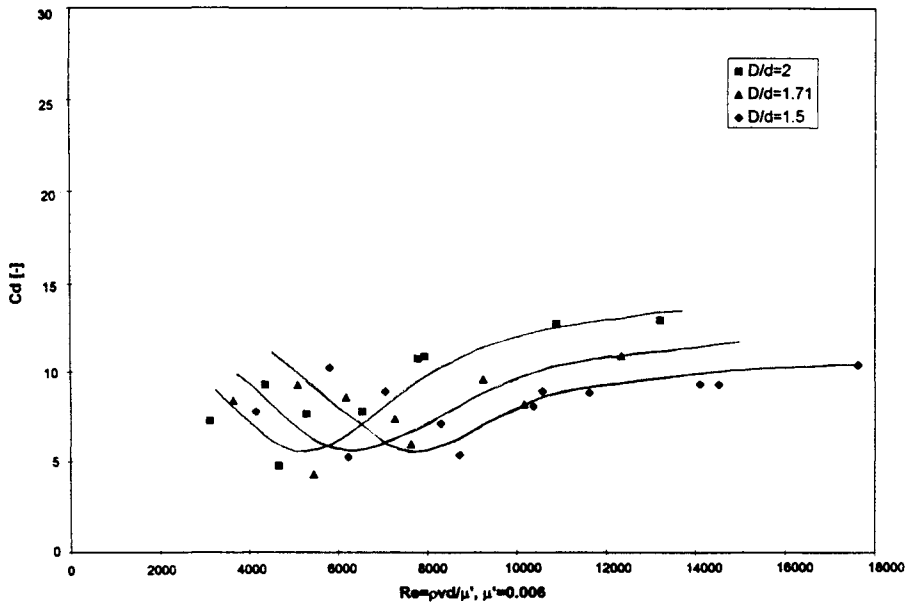

Graph 4.5.5. Drag Coefficient Cd vs. Re Number for different D/d ratios of vortex generator disks for 4.24% concentration of CaCO3 in slurry (μ'=0.006 Pa s)

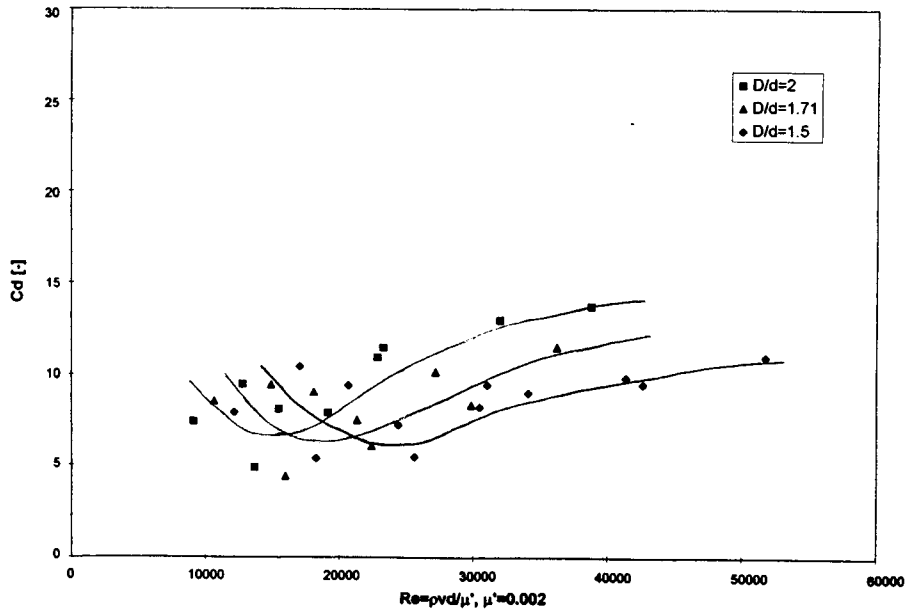

Graph 4.5.6. Drag Coefficient Cd vs. Re Number for different D/d ratios of vortex generator disks for 2.12% concentration of CaCO3 in slurry (μ'=0.002 Pa s)

4.6. ANALYSIS OF POWER MEASUREMENTS

As previously mentioned, the majority of published research refer to rotary mixers and there is only limited information available on vortex ring mixers, mostly due to their only recent introduction. One of the most common characteristics for different types of rotary mixers described in the literature, is the Power Number (Np). This dimensionless group is presented by the following equation (Sterbachek and Tausk):

$$Np=\Delta p/\rho v^2 \qquad 4.6.1.$$

The power number expresses power relations in the system and is important for determining the power input.

The Power number may be also written in the form:

$$Np = Fd/\rho v^2 A \qquad 4.6.2.$$

A plot of Np vs. Re number for different $CaCO_3$ slurry concentrations for given D/d ratio is presented in Graphs 4.6.1. through 4.6.3.

Extensive data on different types of rotary mixers can be found in literature and some of the experimental data includes effects of different slurries. Plot of Power number vs. Re number for a turbine impeller under non-baffled and baffled condition in $CaCO_3$ and $MgCO_3$ slurries is presented in Graphs 4.6.4. and 4.6.5. respectively (Nagata).

There is some similarity between the nature of the Np vs. Re curve in Graphs 4.6.1. through 4.6.3. compared with the Np vs. Re curve in Graph 4.6.5. found in the literature. However, no direct comparison should be made since Graph 4.6.5. refers to different flow characteristics, that is, constant speed and simpler geometry.

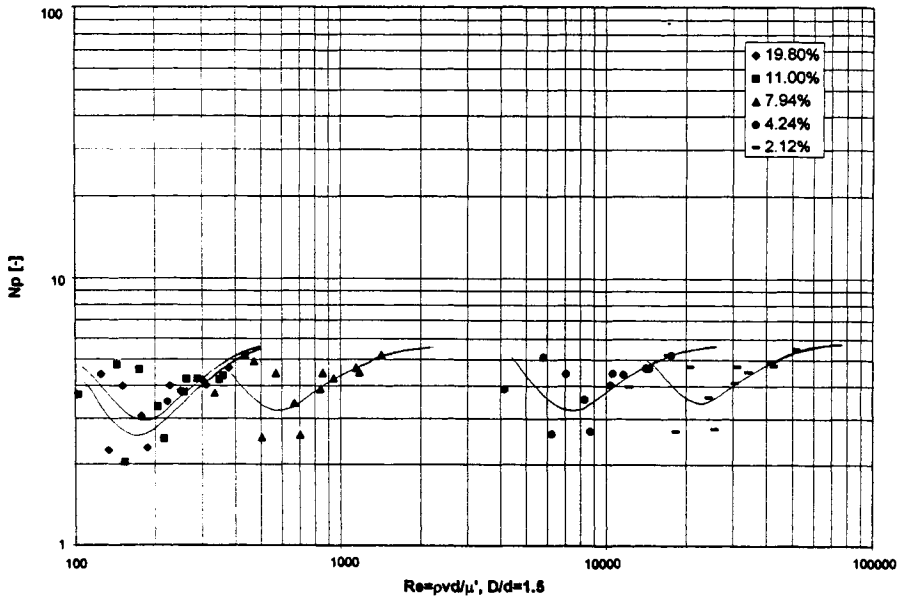

Graph 4.6.1. Power number Np vs. Re Number for different concentrations of $CaCO_3$ in slurry for D/d=1.5

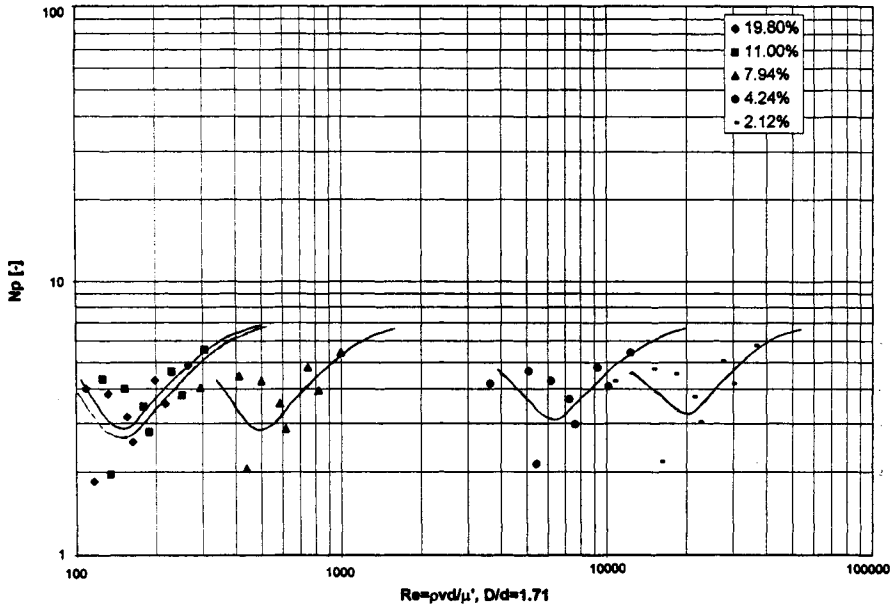

Graph 4.6.2. Power number Np vs. Re Number for different concentrations of CaCO3 in slurry for D/d=1.71

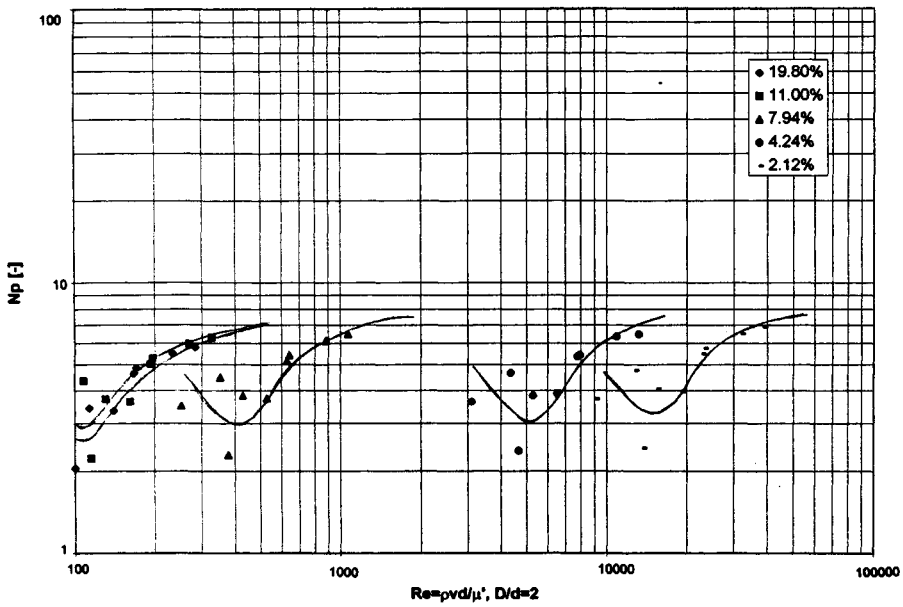

Graph 4.6.3. Power number Np vs. Re Number for different concentrations of CaCO3 in slurry for D/d=2

	Disper-soid	Medium	V%				
+	—	Machine oil	0	□	$CaCO_3$	Water	32.1
○	$MgCO_3$	Machine oil	6.77	◇	$CaCO_3$	Water	29.8
△	$MgCO_3$	Machine oil	7.96	⊕	TiO_2	Water	26.3
▽	$MgCO_3$	Machine oil	8.65	●	$MgCO_3$	Water	10.0
×	$MgCO_3$	Machine oil	48.9	○	$MgCO_3$	Water	12.8

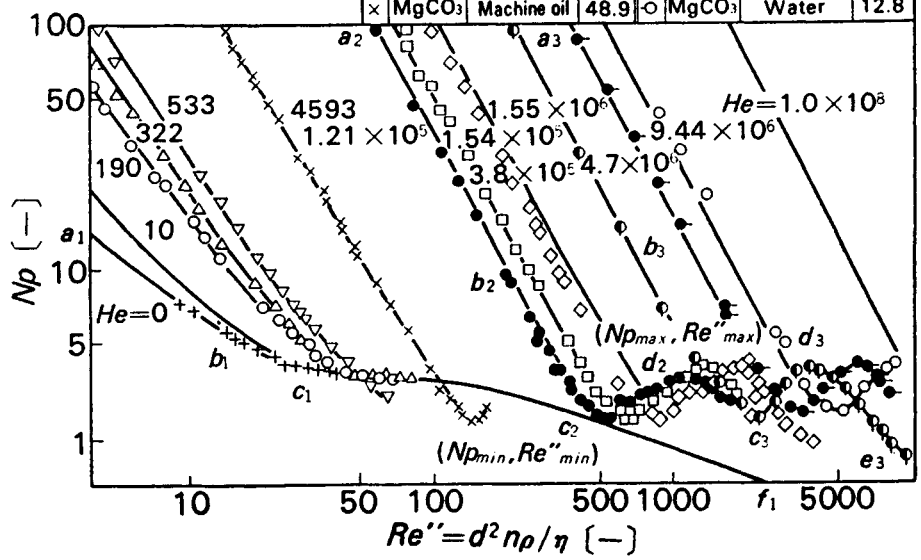

Graph 4.6.4. Power number vs. Re number for turbine impellers under non-baffled conditions for $CaCO_3$ (Nagata)

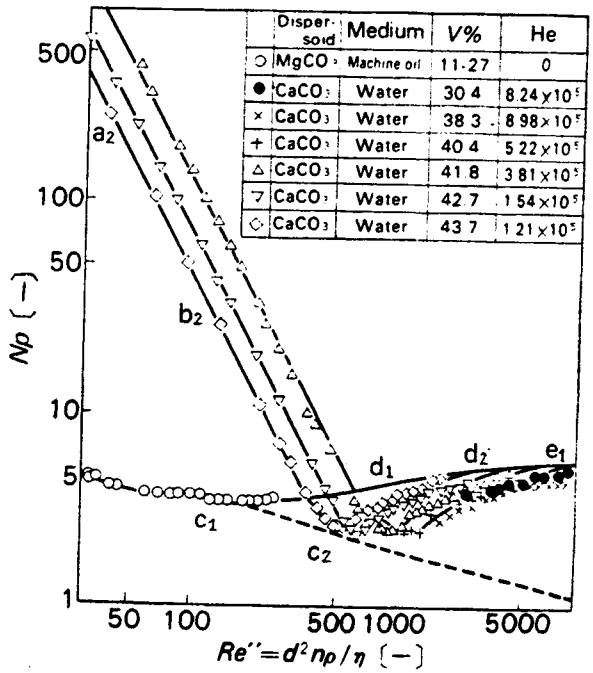

Graph 4.6.5. Power number vs. Re number for turbine impellers under baffled conditions for $CaCO_3$ (Nagata)

Analyzing Np vs. Re curves for given D/d ratio following could be observed:

For higher Re numbers Np vs. Re tends to approach the constant value for all concentrations, for the same D/d ratio. Therefore with a constant geometry and oscillating frequencies of the generator plate any change in viscosity requires same power input. This means it is possible to use an electric motor sized for any condition in the given range of Re numbers without risking overloading of the drive motor. The opposite situation occurs for the Re numbers where Np vs. Re curve has minimum. Consequently a VRM with an electric

motor sized for the minimum operating condition will overload if it departs from minimum condition.

The power that was required was also calculated using an EXCEL 5.1 spreadsheet using following formula:

$$P = F_d * v \qquad 4.6.3.$$

Velocity v is calculated as:

$$v = \frac{d\delta}{dt} = \frac{\delta_2 - \delta_1}{t_2 - t_1} \qquad 4.6.4.$$

where δ_i is the displacement taken as data provided from displacement transducer.

The calculated values are presented in Appendix A. When analyzing power consumed by the mixing process and comparing it to the total power consumed by the mixing system, it can be seen that the power ranges from 1% of total power for the smallest generator plate running at 1 Hz, to 19% of total power for the largest generator plate running at 2 Hz.

The power consumption was calculated using the drag force. The drag force was not significantly affected by the level of slurry concentration and therefore neither was the power consumption (Graph 4.6.6.).

The most contributing factors for power consumption were the generator plate size and the oscillating frequency that were used. A plot power vs. oscillating frequency of the generator plate for different orifice diameter for given D/d ratio is presented on Graphs 4.6.7. through 4.6.9. These graphs would be useful for optimizing the mixing process when used in conjunction with the mixing time and quality of mixing.

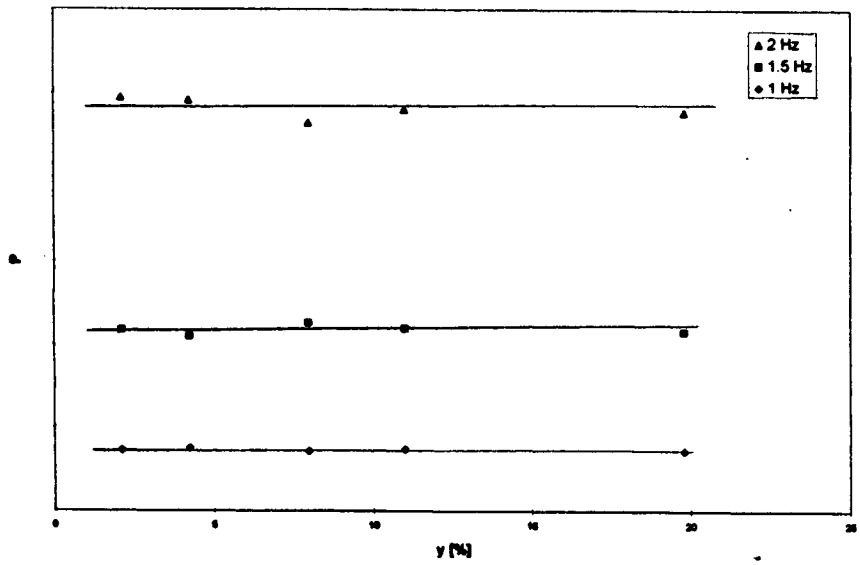

Graph 4.6.6. Power P vs. concentration for given oscillating frequency (typical)

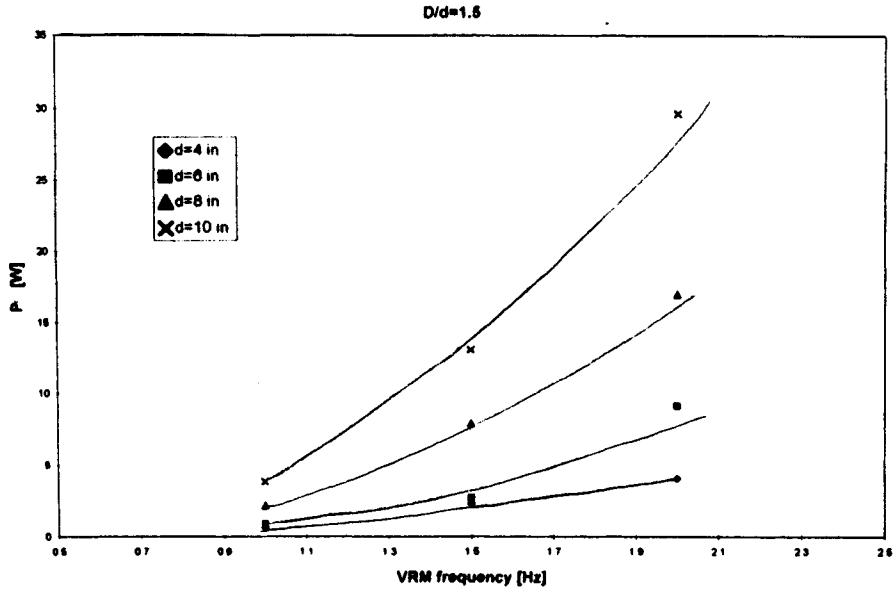

Graph 4.6.7. Power vs. oscillating frequency of the generator plate for different orifice diameters d for D/d=1.5

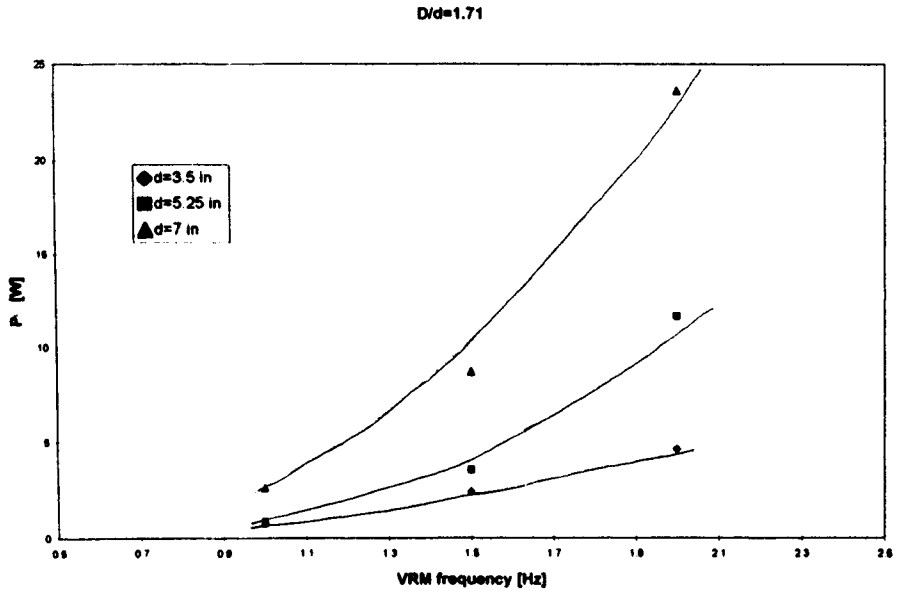

Graph 4.6.8. Power vs. oscillating frequency of the generator plate for different orifice diameters d for D/d=1.71

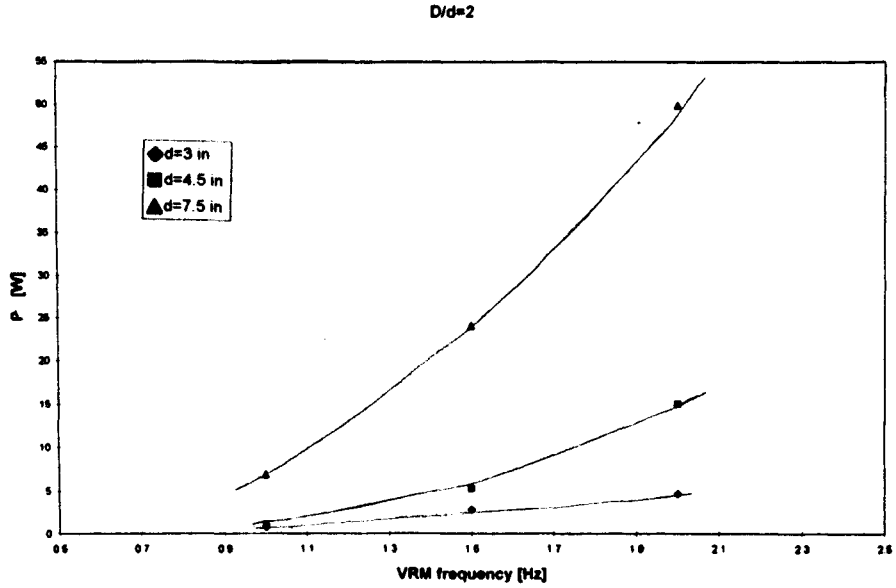

Graph 4.6.9. Power vs. oscillating frequency of the generator plate for different orifice diameters d for D/d=2

CHAPTER 5

CONCLUSIONS

A system for analysis of drag force and power consumption for an AC motor driven vortex ring mixing mechanism was developed.

Ten sizes of vortex ring generator plates were tested at three oscillating frequencies of generator plate in five aqueous $CaCO_3$ slurry concentrations. Collected data included displacement, force, concentration, viscosity and power measurements. The results of the study can be summarized as follows:

Firstly, rheology analysis revealed that tested $CaCO_3$ slurry exhibits Bingham plastic properties with shear thinning. Thus, the power requirement for a VRM may be higher for initiation of mixing for this type of slurry.

Secondly, it was concluded that the drag force and the power consumption appeared to be primarily a function of the generator plate outside diameter to orifice diameter ratio (D/d) and its oscillating frequency. Both drag force and power consumption increased as D/d ratio and oscillating frequency increased.

Thirdly, the $CaCO_3$ slurry concentrations tested in this study did not have any significant affect on the either the drag force or power consumption, but may have an affect on the power requirement during start-up, as previously stated.

Fourthly, for a particular mixing system the major efficiency penalty is in losses within drive system and only a fraction of the energy supplied, as high as 19%, is being transferred to the fluid being mixed.

Furthermore, the drag coefficient increased with increasing D/d ratio for larger Re numbers and approached narrow range of Cd for the same D/d ratio as the Re number increased. This range was the same for all five $CaCO_3$ concentrations investigated.

The nature of the Np vs. Re curve for the VRM used in the experiments was found to be similar to the Np vs. Re curve for the turbine impeller under the baffled condition. However, due to the more complex geometry and oscillating motion of the VRM, no direct comparison could be made.

Lastly, the drive system used in these experiments appears to be acceptable for the mixing of slurries having a yield stress, since it is capable of varying the power that is put in a mixture.

CHAPTER 6

RECOMMENDATIONS

This study showed that for a particular mixing system the major efficiency penalty is in losses within drive system and only a fraction of the energy supplied, as high as 19%, is being transferred to the fluid being mixed. It is therefore recommended that the design of the drive system be reviewed in order to asses the major areas of energy losses and a way of controlling them.

In order to reduce overhang load on a reducer output shaft, a coupler can be redesigned to stiffen the link between flywheel and output shaft as shown in Figure 6.1. Also, Scotch Yoke mechanism could be used as alternative to the currently used mechanism.

A problem that could occur during industrial application of this mixing system is related to the drive shaft length. With longer shafts there is tendency to bend caused by drag force which exaggerates unbalanced forces on the generator plate. Possible solution to this problem is to use the supporting structure for the shaft or to employ a conical shaped vortex ring generator.

Since this study showed that for the $CaCO_3$ slurry concentrations, drag force and power consumption were mainly affected by the size of the generator plate and its oscillating frequency, it is recommended that future research include mixing time and quality of mixing along with drag force and power measurements. Experiments may be applied to some frequently used industrial mixtures for determining the best combination of parameters. Eventually, with a design of highly efficient mixing mechanism different shapes of generator plates could be tested in order to reduce drag force.

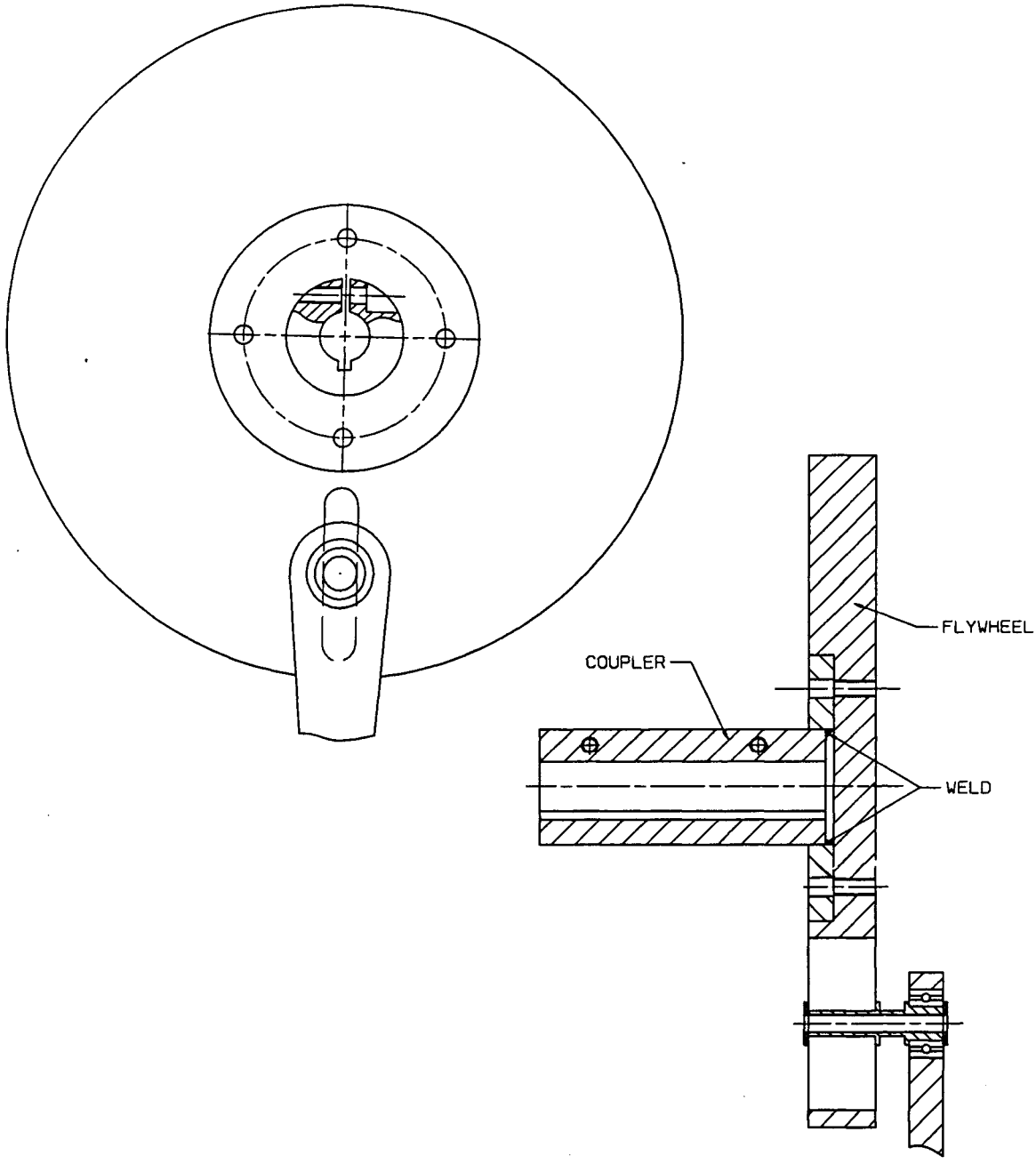

Figure 6.1. Mechanism Improvement - Coupler Redesign

REFERENCES

Ahmad S., "Mixing of stratified liquids using rotary mixers", M.Eng. Thesis, (1985), McMaster University.

Baird M.H.I., Rama Rao, N.V. and Stonestreet, P., "Power Dissipation and Holdup in a Gassed Reciprocating Baffle-Plate Column", Trans.Inst.Chemical Engineering, (1996), Vol. 74.

Baird M.H.I., Rama Rao, N.V. and Latto, B. "Liquid-Liquid Extraction Using Vortex Rings in a Batch Cell", Trans.Inst.Chemical Engineering, (1992), Vol. 70.

Baird, M.H.I., Rohatgi, A. and Wairegi, T., "Mixing effects and hydrodynamics of vortex ring", The Canadian J. of Chemical Engineering, (1979), Vol. 57, p. 19-26.

Bickford, John H., "Mechanisms for Intermittent Motion", (1972), The Industrial Press Inc, New York.

Borwankar, P. S., "Adaptive Learning Control of Pneumatic Drive Cyliders for Vortex Ring Mixers", Master Degree, (1996), McMaster University.

Brodkey, R. S., "The Phenomena of Fluid Motions", (1967), Addison-Wesley Publishing Company, Reading, Massachusetts

Cowie, Alexander, "Kinematics And Design of Mechanisms", (1961), International Textbook Company, Scranton, Pennsylvania

Didden, N., "On the Formation of Vortex Rings: Rolling and Production of Circulation", J. Appl. Math. Phys., (1979), Vol. 30, p. 101-116.

Glezer, A., "The Formation of Vortex Rings", Phys. Fluids, (1988), Vol. 31, p. 3532-3542

Kozic, Dj., Vasiljevic, B. And Bekavac, V., "Prirucnik za Termodinamiku", (1987), Masinski Fakultet Univerziteta u Beogradu.

Harnby, N., Edwards, M. F., Nienow, A. W., "Mixing in the Process Industries", (1985), Butterworts, London, England

Hua F., "Numerical simulation and experimental study of vortex ring behavior", Ph.D. dissertation, (1994), McMaster University.

Irdmusa J.Z. and Garris C.A., "Influence of initial and boundary conditions on vortex ring development", AIAA, (1987), Vol. 25.

Jensen, Preben W., "Cam Design and Manufacture", (1965), New York

Jones, Franklin D, "Ingenious Mechanisms: Vol. I-III", (1957), The Industrial Press Inc, New York.

Kamerman, P., Anderson, I., Lindley, C., Osfolk, P. and Taylor, J., "Drive Mechanism for Vortex Ring Mixer", Design Project, (1995), McMaster University

Kojovic, Milica, "An Experimental Study of the Effects of Generator Displacement Profile on Vortex Ring Mixing", Master Degree, (1997), McMaster University

Latto, B., "New mixer for slurries and stratified fluid", 12 th International conference on slurry technology, (1987).

Latto, B., "Novel vortex ring mixers for slurries and stratified liquids", Proceeding of the 14th International conference on coal and slurry technology association, (1989).

Latto, B., "Vortex Ring Mixers for Slurries and Controlled Addition of Gasses and Liquids", Proceeding of the 17th International conference on coal utilization and slurry technologies, (1992).

Latto B., Ho S.K., Hua F., "Vortex Ring Propagation in Stratified Fluids" , J. Fluid mechanics , (1994)

Latto, B., Papple, M.L.C., Shoukri M., Baird, M.H.I., "Mixing of thermally stratified fluids by injecting a series of vortex rings-a numerical simulation", Transaction of institution of chemical engineers, (1990), Vol.68.

Latto B., Baird M.H.I., Papple M.C.I., Shoukri M., "Numerical simulation of the transport of vortex rings in an initially stratified fluid", Chemical Engineering Communication, (1991), Vol. 103.

Linden, P.F., "The interaction of a vortex ring with a sharp density interface: a model for turbulent entrainment", J. Fluid Mechanics, (1973), Vol.60.

Maxworthy, T., "Turbulent vortex ring", J. Fluid Mechanics, (1974), Vol.64.

Maxworthy, T., "Some experimental studies of vortex rings", J. Fluid Mechanics, (1977), Vol.81.

Metzner, A. B., and Otto, R. E., "Agitation of Non-Newtonian Fluids", (1957), Al. Ch. E. J. 3. 3.

Nagata, S., "Mixing Principles and Applications", (1975), Halsted Press, New York.

Olson, M. Reuben and Wright, J. Steven, "Essentials of Engineering Fluid Mechanics", (1990), Harper & Row, Publishers, New York.

Perrons, R., "Vortex Rings Mixers: An Numerical Study of Ring Properties", Baccalaureate Thesis, (1995), McMaster University.

Peters, R. M., "Speed Variation With Elliptical Wheels", (1974), The Institution of Mechanical Engineers.

Stapleton, G., "Numerical Simulation of Vortex Rings", Baccalaureate Thesis, (1996), McMaster University.

Sterbacek, Z. And Tausk, P., (1965), "Mixing in the Chemical Industry", Pergamon Press, New York

Walker, J. D. A., Smith, C. R. Cerra, A. W. and Doligalski, "Impact of a Vortex Ring on a Wall", J. F. Mech., (1987), Vol. 181, pp. 99-140.

Wang, J., "A Numerical Simulation and Experimental Study of Vortex Rings", Master Degree, (1999), McMaster University.

APPENDIX A
POWER CONSUMPTION

Disk (ϕD x ϕd)	Disk speed (Hz)	Drag Force Power Pd (W)	Percentage of Total Power (%)	Total Power (W)
15" x 10" (38.1cm x 25.4cm)	1	3.63	5.2	70
	1.5	11.57	11.6	100
	2	24.62	16.4	150
15" x 7.5" (38.1cm x 18cm)	1	6.57	8.2	80
	1.5	21.51	16.5	130
	2	40.41	18.8	215
12" x 7" (30.48cm x 17.78cm)	1	2.53	3.6	70
	1.5	7.65	8.5	90
	2	19.13	15.0	127.5
12" x 8" (30.48cm x 20.32cm)	1	2.06	3.1	67.5
	1.5	7.23	8.5	85
	2	13.72	11.9	115
9" x 4.5" (22.86cm x 11.43cm)	1	1.05	1.6	67.5
	1.5	4.68	5.7	82.5
	2	12.23	11.4	107.5
9" x 5.25" (22.86cm x 13.34cm)	1	0.81	1.2	67.5
	1.5	3.17	4	80
	2	9.45	9.2	102.5
9" x 6" (22.86cm x 15.24cm)	1	0.71	1.1	65
	1.5	2.40	3.1	77.5
	2	7.41	7.6	97.5
6" x 4" (15.24cm x 10.16cm)	1	0.57	1.0	62.5
	1.5	2.03	2.8	72.5
	2	3.29	3.7	90
6" x 3" (15.24cm x 7.62cm)	1	0.86	1.4	62.5
	1.5	2.51	3.5	72.5
	2	3.81	4.1	92.5
6" x 3.5" (15.24cm x 8.89cm)	1	0.72	1.1	65
	1.5	2.18	2.9	75
	2	3.75	4.2	90

Stroke length s=5" (127 cm)

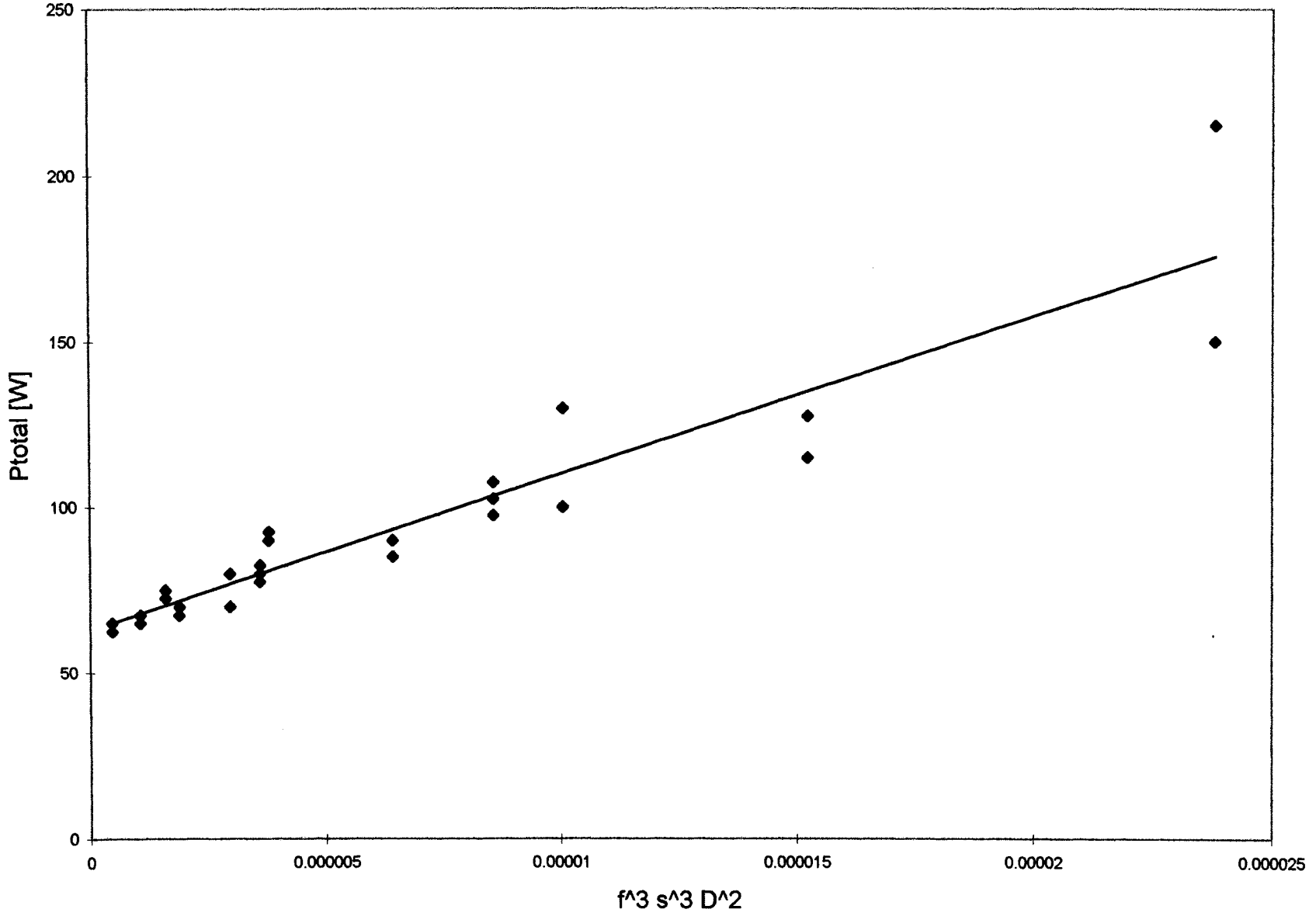
250
200
150
100
50
0
Ptotal [W]
0
0.000005
0.00001
0.000015
0.00002
0.000025
f^3 s^3 D^2

APPENDIX B

"WELLS-BROOKFIELD" SINCHRO-LECTRIC VISCOMETER MODEL LVF MEASUREMENT PROCEDURES

RANGE TABLES

SPEED RPM	MODEL RVT-C/P				MODEL HAT-C/P				MODEL HBT-C/P			
	1.565° cone		0.8° cone		1.565° cone		0.8° cone		1.565° cone		0.8° cone	
	range cps	rate sec^{-1}	range cps	rate sec^{-1}	range cps	rate sec^{-1}	range cps	rate sec^{-1}	range cps	rate sec^{-1}	range cps	rate sec^{-1}
100	64	384.00	32.7	750.00	128	384.00	65.45	750.00	512	384.00	261.8	750.00
50	128	192.00	65.4	375.00	256	192.00	130.90	375.00	1,024	192.00	523.6	375.00
20	320	76.80	163.5	150.00	640	76.80	327.25	150.00	2,560	76.80	1,309.0	150.00
10	640	38.40	327.0	75.00	1,280	38.40	654.50	75.00	5,120	38.40	2,618.0	75.00
5	1,280	19.20	654.0	37.50	2,560	19.20	1,309.00	37.50	10,240	19.20	5,236.0	37.50
2.5	2,560	9.60	1,308.0	18.75	5,120	9.60	2,618.00	18.75	20,480	9.60	10,472.0	18.75
1.0	6,400	3.84	3,270.0	7.50	12,800	3.84	6,545.00	7.50	51,200	3.84	26,180.00	7.50
0.5	12,800	1.92	6,540.0	3.75	25,600	1.92	13,090.00	3.75	102,400	1.92	52,360.00	3.75

SPEED RPM	MODEL LVT-C/P			
	1.565° cone		0.8° cone	
	range cps	rate sec^{-1}	range cps	rate sec^{-1}
60	10	230.00	5.14	450.00
30	20	115.00	10.28	225.00
12	50	46.00	25.70	90.00
6	100	23.00	51.40	45.00
3	200	11.50	102.80	22.50
1.5	400	5.75	205.60	11.25
0.6	1,000	2.30	514.00	4.50
0.3	2,000	1.15	1,028.00	2.25

EASILY CONVERTS FOR USE AS A STANDARD VISCOMETER

The Micro Viscometer will accept standard Brookfield Viscometer spindles. Simply unscrew micrometer adjusting ring and replace with modified guard leg (necessary for LV and RV series only). Use of lab stand extension is suggested.

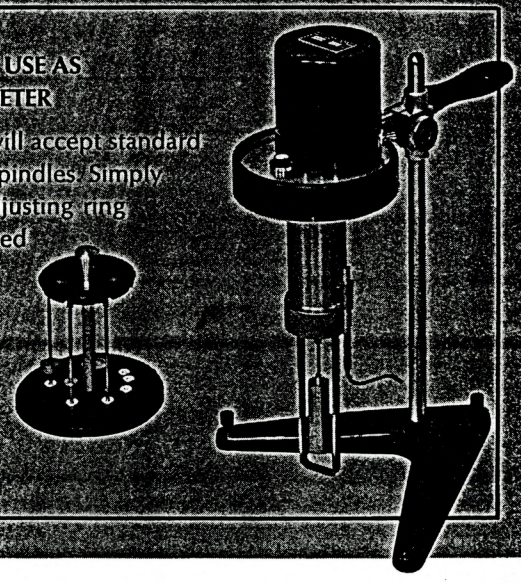

CUSTOMER SERVICE

Brookfield is the world's leading manufacturer of viscosity measuring and controlling instruments. With over 40 years of experience we have the technical know-how to help solve your problems. Please feel free to ask our assistance in selecting the most appropriate model Viscometer or in the most effective use of your present equipment.

BROOKFIELD

BROOKFIELD ENGINEERING LABORATORIES, INC.
240 Cushing Street, Stoughton, Massachusetts 02072
Cable Address: Brookfield U.S.A. Telephone: (617) 344-4310 Telex: 924-497

Brookfield FACTOR FINDER

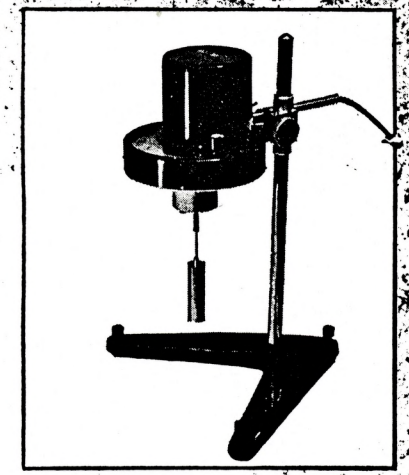

VISCOMETER MODEL

SPINDLE NUMBER

SPEED RPM

FACTOR

M = 1100

INSTRUCTIONS

To convert Viscometer dial reading to centipoise, adjust slide to expose Viscometer model and spindle number being used. Multiply reading noted on Viscometer 0-100 scale by factor given beside RPM at which measurement is being made. EXAMPLE: An LVT Viscometer with #1 spindle at 3 RPM, reading 25 on Viscometer 0-100 scale, gives a viscosity 25 x 20 = 500 cps.

NOTE: All Brookfield Viscometer models are included (2 models on either side of slide) with the first two letters of each model series shown, i.e. "LV" applies to LVO, LVF, or LVT models.

Full scale viscosity range for any Viscometer speed and spindle combination is equal to factor x 100. For those who wish to avoid multiplication by the more difficult factors, a direct reading viscosity chart has been included on the reverse side.

For complete information about Laboratory Indicating, Recording, and Process Control Viscometers write

BROOKFIELD ENGINEERING LABORATORIES, Inc., Stoughton, Mass., U.S.A.

RV 1		RV 2		RV 3		RV 4		RV 5		RV 6		RV 7		LV 1		LV 2		LV 3		LV 4
.5	200	.5	800	.5	2M	.5	4M	.5	8M	.5	20M	.5	80M	.3	200	.3	1M	.3	4M	.3	20M
1	100	1	400	1	1M	1	2M	1	4M	1	10M	1	40M	.6	100	.6	500	.6	2M	.6	10M
2	50	2	200	2	500	2	1M	2	2M	2	5M	2	20M	1.5	40	1.5	200	1.5	800	1.5	4M
2.5	40	2.5	160	2.5	400	2.5	800	2.5	1.6M	2.5	4M	2.5	16M	3	20	3	100	3	400	3	2M
4	25	4	100	4	250	4	500	4	1M	4	2.5M	4	10M	6	10	6	50	6	200	6	1M
5	20	5	80	5	200	5	400	5	800	5	2M	5	8M	12	5	12	25	12	100	12	500
10	10	10	40	10	100	10	200	10	400	10	1M	10	4M	30	2	30	10	30	40	30	200
20	5	20	20	20	50	20	100	20	200	20	500	20	2M	60	1	60	5	60	20	60	100
50	2	50	8	50	20	50	40	50	80	50	200	50	800								
100	1	100	4	100	10	100	20	100	40	100	100	100	400								

INSTRUCTIONS FOR USING CHART BELOW:

In the seven sets of scales below a viscosity scale is directly above a 0-100 scale. Obtain Factor for Viscometer model, spindle and speed being used as outlined on reverse side. Select appropriate scale below by associating the first one, two or three digits of the factor with the number shown at either end of scale. Place reading noted on Viscometer 0-100 scale on 0-100 scale selected below. Read viscosity directly above. Locate decimal point by comparing with full scale viscosity range of Viscometer model, spindle and speed being used.

EXAMPLE: An RVT Viscometer with #3 spindle at 50 RPM has a factor of 80. Select scale 8. If Viscometer 0-100 scale reading is 46.2, viscosity is 3700 cps.

Brookfield FACTOR FINDER

APPENDIX C
TECHNICAL SPECIFICATIONS

MODEL 60001 S-BEAM LOAD CELL

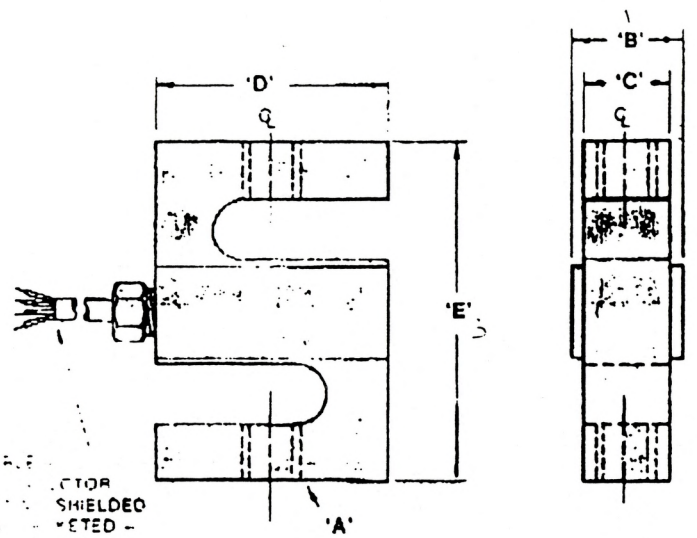

Capacity	A Thread*	B	C	D	E
25/200	1/4-28	.65	.50	2.00	2.50
250/300	3/8-24	.75	.50	2.00	3.00
500/1.5K	1/2-20	1.00	.75	2.00	3.00
2K/4K	1/2-20	1.25	1.00	2.00	3.00
5K	3/4-16	1.25	1.00	3.00	4.25
7.5/10K	3/4-16	1.25	1.00	3.50	4.75
15K	1"-14	1.50	1.25	4.00	5.50
20K	1 1/4-12	2.25	2.00	5.00	7.00

*UNF-2B

Wiring: Tension (+)
Red: +Input
Black: -Input
Green: +Output
White: -Output

SENSORTRONICS specializes in supplying original equipment manufacturers in the Electronic Weighing Systems Industry. Standard configurations and specifications may be altered to meet specific customer requirements on quantity orders. Please contact the factory regarding changes in performance and/or dimensional specifications, as required.

SENSORTRONICS manufactures many load cell configurations and companion equipment, such as weighmeters and junction/summing boxes. Literature on our complete product line is available upon request.

Represented by:

JTERTECHNOLOGY INC.
carsdale Road Don Mills ON M3B 2R2
)RONTO AREA (416) 445-5500

SENSORS TRANSDUCERS
SIGNAL CONDITIONERS
DIGITAL INDICATORS
DATA ACQUISITION

real (514) 683-0930 Ottawa (613) 723-1828
ipeg (204) 896-2037 Calgary (403) 266-7511
Vancouver (604) 270-9538

Other Areas 1-800-465-1600

SENSORTRONICS
Our people make the difference.

MODEL 60001 S-BEAM LOAD CELL

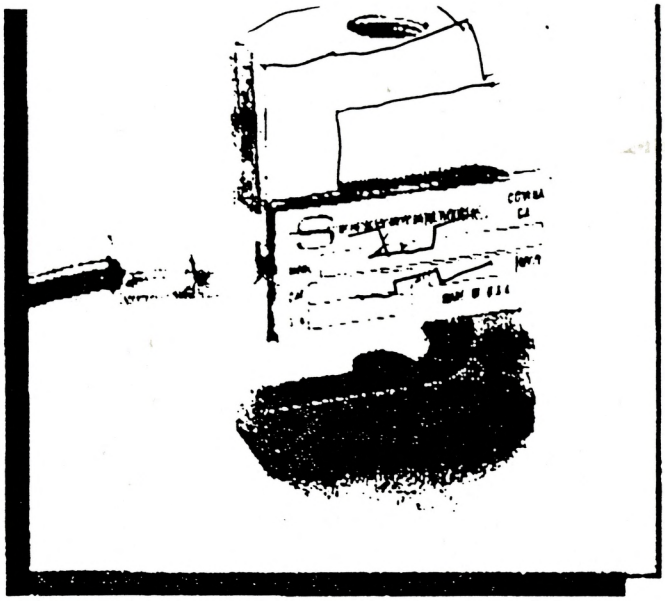

DESCRIPTION:

The Model 60001 is a versatile load cell readily adaptable to tension loading situations. Designed for single or multiple load cell applications, the 60001 is well suited to scale conversions, tank/bin/hopper installations and general purpose requirements.

The 60001 is constructed of high quality alloy tool steel to provide maximum protection against [illegible] impact loads. Each unit is electroless nickel plated for outstanding corrosion resistance. It also features multi-redundant environmental seals to guard against moisture ingression and temperature effects. As an option, the stainless steel model is available as Model 60050.

All Model 60001 Load Cells are Factory Mutual System Approved for use in Class I, II, and III; Division 1 and 2, Group A thru G hazardous locations.

FEATURES:

- Expanded range of capacities
- Integral loading brackets
- Stainless steel (Model 60050)
- Complete environmental protection
- Factory Mutual System Approved
- Exceeds NIST Handbook 44 requirements
- NTEP certified [illegible] available for class III [illegible] and class IIL [illegible]

PERFORMANCE SPECIFICATIONS:

UP to 2K = $322.

Rated Capacities (lbs.):	25, 50, 100, 150, 200, 250, 300, 500, 750, 1K, 1.5K, 2K, 2.5K, 3K, 5K, 10K, 15K and 20K
Safe Overload:	150% FS
Full Scale Output (FS):	3 MV/V (nominal)
Rated Excitation:	10 VDC (15 V maximum)
Zero Balance:	±1% FS
Non-Linearity:	<0.03% FS
Hysteresis:	<0.02% FS
Non-Repeatability:	<0.01% FS
Operating Temperature Range:	0°F to 150°F
Temperature Effect	
Output:	<0.0008% of reading/°F
Zero:	<0.0015% FS/°F
Bridge Resistance:	350 ohms (nominal)
Material and Finish:	Tool steel, electroless nickel plated

NTEP CERTIFIED LOAD CELLS AVAILABLE

Factory Mutual System Approved

SENSORTRONICS

Our people make the difference.

APPENDIX D

CRITICAL FORCE, STATIC DEFLECTION AND FREQUENCY OF VIBRATION FOR A DRIVE SHAFT

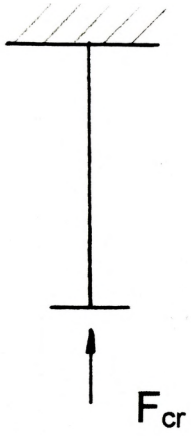

Critical Force for a Drive Shaft:

$$F_{cr} = \frac{\pi^2 EI_{min}}{4l^2}$$

F_{cr} - critical force [N];

$E = 210x10^9$ [N/m^2] - Young's modulus for steel;

$I_{min} = 0.05d^4 = 6.58x10^{-10}$ m^4 - minimal moment of inertia, d=0.01905 m;

$l = 0.72$ m - length of a drive shaft

$F_{cr} = 657.69$ N

Frequency of Vibration for a Given Static Deflection δ_{st} of a Drive shaft:

$$f = \frac{1}{2\pi}\sqrt{\frac{g}{\delta_{st}}}$$

δ_{st} [mm]	f [Hz]
5	7.05
10	4.98
15	4.07
20	3.52